UNIVERSITY OF COPENHAGEN
FACULTY OF SCIENCE

PhD Thesis

Bacteria, mosquitoes and beyond

Some studies on spatial and environmental ecology

Miguel Garrido Zornoza

Supervisors
Jan O. Haerter & Namiko Mitarai

This thesis has been submitted to the PhD School of
The Faculty of Science, University of Copenhagen
August 30, 2024

Miguel Garrido Zornoza

Bacteria, mosquitoes and beyond

PhD Thesis, August 30, 2024

Supervisors: Jan O. Haerter & Namiko Mitarai

University of Copenhagen

Faculty of Sciences

The Niels Bohr Institute

Blegdamsvej 17

2100 Copenhagen

The Niels Bohr Institute (photo from Miguel Garrido Zornoza)

If life seems jolly rotten
There's something you've forgotten
And that's to laugh and smile and dance and sing
When you're feeling in the dumps
Don't be silly chumps
Just purse your lips and whistle, that's the thing
And ...

Always look on the bright side of life, Eric Idle

The birds they sang
At the break of day
Start again
I heard them say
Don't dwell on what has passed away
Or what is yet to be
Ah, the wars they will be fought again
The holy dove, she will be caught again
Bought and sold, and bought again
The dove is never free
Ring the bells that still can ring
Forget your perfect offering
There is a crack, a crack in everything
That's how the light gets in

Anthem, Leonard Cohen

Preface

Thesis structure

This thesis is written as a compendium of independent research projects. These projects deal with different biological systems and their dependence on distinct atmospheric features. The overarching theme of the work presented here could be though as "*spatial environmental ecology*" and, contrary to the classical format, its content was developed as exploratory research, namely without a pre-defined hypothesis. After all, does research require one?

Concretely, this thesis is structured in three independent parts, partly developed in two different institutes. The first two parts, chapters 2 and 3, contain a short synopsis followed by a more extensive and detailed development in the form of a manuscript. The reader is thus left with the choice to select depth based on curiosity. The third part, chapter 4, is written in the style of a short monograph. This thesis is written using nosism and Oxford spelling. References within manuscripts are not contained in the final *Bibliography* section but within the manuscript itself.

Acknowledgements

To my family and friends. Mireia, Albert and Irene, trench buddies at NBI. To the CELS survivors and the wonderful group at the *Naturhistoriske* museum. Special mention to Adrian M. Tompkins and Cyril Caminade, the Earth System Physics group in ICTP and Namiko and Bente, for the always cheerful help. To Jan O. Haerter, who financed my PhD, making it possible. To my cold-nosed *rillettes*-devourer CAI.

Cheers

Abstract

Part 1: Microorganisms are ubiquitous in Nature and constitute key pieces in global energy and nutrient cycles. An important yet insufficiently understood interplay is that constituted by bacteria and their most common predator, the bacteriophages (short: phages). In this study we investigate predation, competition and diversity in a phage-bacteria spatially structured ecosystem shaped by intermittent biomass dispersal. Predatory dynamics between a single phage species and its bacterial host are characterized as a function of the dispersal parameters. Competition among phages is then studied by considering the presence of a secondary and less competitive phage species preying on the same bacterial host. The study reveals that the environmental context, in the form of habitat connectivity, significantly impacts the competitive outcome, allowing the "weaker" phage to coexist or even dominate under certain conditions. This research provides insights into the ecological complexity and potential coexistence mechanisms in microbial communities, underlining the role of environmental factors, such as dispersal, in shaping microbial diversity.

Part 2: The Asian tiger mosquito, *Aedes albopictus*, is known for its status as invasive species and capable vector of diseases such as dengue, Zika and chikungunya. Originating from southeast Asia, this species has spread worldwide due to globalization, adapting to various climates. Our research uses a climate-aware dynamical model to analyse the mosquito's life cycle and distribution in Italy, from 1980 to 2023. The study's objectives include calibrating and validating the model with field data, understanding the mosquito's geographical distribution and activity duration, and assessing the impact of heatwaves on its population dynamics. Simulated mosquito hotspots coincide with highly populated areas like Rome and Milan, with climate change

extending the mosquito's activity season, especially in the southern Italian coastal regions. The model's predictive capabilities have the potential to help guide public health interventions and improve surveillance and risk assessment of mosquitoes and, with further model development effort, mosquito-borne diseases.

Part 3: The mosquito *Anopheles gambiae s.s.* is a major vector of malaria in sub-Saharan Africa. As an ectothermic arthropod, its life cycle is susceptible to local climate variables, the magnitude of which change at a wide range of time scales, from sub-daily to seasonal and decadal. Using a climate-aware dynamical model, we investigate how variations in daily air temperature affect mosquito population by performing a "knock out" experiment, where the daily variability in air temperature at two-metre height is suppressed. Preliminary results allow us to $i)$ estimate the seasonal effect of this variability and the regions where these effects will increase mosquito population and $ii)$ ascertain a net change in the vector activity duration driven by variability at daily time scale. Ultimately, this project aims to provide insight into the effects of climate change on malaria spread.

Dansk resumé

Del 1: Mikroorganismer er allestedsnærværende i naturen og udgør vigtige brikker i det globale energi- og næringsstofcyklus. Et vigtigt, men utilstrækkeligt forstået samspil er det, der udgøres af bakterier og deres mest almindelige rovdyr, bakteriofagerne (forkortet: fager). I dette studie undersøger vi prædation, konkurrence og diversitet i et rumligt struktureret økosystem mellem fager og bakterier, der er formet af periodisk spredning af biomasse. Rovdyrsdynamikken mellem en enkelt fagart og dens bakterielle vært karakteriseres som en funktion af spredningsparametrene. Konkurrence mellem fager undersøges derefter ved at overveje tilstedeværelsen af en sekundær og mindre konkurrencedygtig fagart, der jager på den samme bakterielle vært. Undersøgelsen viser, at den miljømæssige kontekst i form af habitatforbindelser har stor indflydelse på konkurrenceresultatet, så den »svagere« fag kan sameksistere eller endda dominere under visse forhold. Denne forskning giver indsigt i den økologiske kompleksitet og potentielle sameksistensmekanismer i mikrobielle samfund og understreger den rolle, som miljøfaktorer, såsom spredning, spiller i udformningen af mikrobiel mangfoldighed.

Del 2: Den asiatiske tigermyg, *Aedes albopictus*, er kendt for sin status som invasiv art og dygtig vektor for sygdomme som dengue, zika og chikungunya. Denne art stammer fra Sydøstasien og har spredt sig over hele verden på grund af globalisering og tilpasning til forskellige klimaer. Vores forskning bruger en klimabevidst dynamisk model til at analysere myggens livscyklus og udbredelse i Italien fra 1980 til 2023. Undersøgelsens mål omfatter kalibrering og validering af modellen med feltdata, forståelse af myggens geografiske fordeling og aktivitetsvarighed samt vurdering af varmebølgers indvirkning på dens populationsdynamik. Simulerede mygge-hotspots falder sammen med tætbefolkede områder som Rom og Milano, og klimaforandringerne forlænger

myggens aktivitetssæson, især i de syditalienske kystregioner. Modellens forudsigelsesevne har potentiale til at hjælpe med at guide folkesundhedsinterventioner og forbedre overvågning og risikovurdering af myg og, med yderligere modeludviklingsindsats, myggebårne sygdomme.

Del 3: Myggen *Anopheles gambiae s.s.* er en vigtig malariavektor i Afrika syd for Sahara. Som et ektotermt leddyr er dens livscyklus modtagelig for lokale klimavariabler, hvis størrelse ændrer sig på en lang række tidsskalaer, fra under daglig til sæsonbestemt og dekadisk. Ved hjælp af en klimabevidst dynamisk model undersøger vi, hvordan variationer i den daglige lufttemperatur påvirker myggebestanden ved at udføre et »knock out«-eksperiment, hvor den daglige variation i lufttemperaturen i to meters højde undertrykkes. Foreløbige resultater giver os mulighed for at $i)$ estimere den sæsonmæssige effekt af denne variation og de regioner, hvor disse effekter vil øge myggebestanden, og $ii)$ fastslå en nettoændring i vektoraktivitetens varighed drevet af variabilitet på daglig tidsskala. I sidste dette projeckt har til formål at give indsigt i klimaforandringernes indvirkning på spredning af malaria.

Contents

1 Introduction

Some thoughts on ecology

Even though the term *ecology* (from ancient Greek (*oîkos*) - house, habitation and (*-logía*) - the study of) was coined in 1866 by the German scientist Herman Haeckel [1], observations of ecological nature date back to the ancient Greeks. A clear example of this somewhat old discipline is Herodotus' description of mutualistic interactions between crocodiles and sandpipers [2]. A reflection of the status of the discipline comes from the change of concepts and nomenclature through time. A central concept that has helped shape the current ecological view is that of *ecosystem*, introduced by Arthur Tansley in 1935 [3]. In his own words

> *" Though the organisms may claim our primary interest, when we are trying to think fundamentally we cannot separate them from their special environment, with which they form one physical system. It is the systems so formed which, from the point of view of the ecologist, are the basic units of nature on the face of the earth ... there is constant interchange of the most various kinds within each system ... These ecosystems, as we may call them, are of the most various kinds and sizes ... Some of the systems are more isolated in nature, more autonomous, than others. They all show organisation, which is the inevitable result of the interactions and consequent mutual adjustment of their components ... The great regional climatic complexes of the world are important determinants of the primary terrestrial ecosystems, and they contribute parts (components) to the systems, just as do the soils and the organisms. In any fundamental consideration of the ecosystem it is arbitrary and misleading to abstract the climatic factors."*

This fragment underlines the inherent inter-connectedness of organisms and their physical surroundings. The "*constant interchange*" could now be viewed

as energy and nutrient cycles, shaped by distinct "social" interactions (*e.g.,* competition, mutualism, predation, parasitism) taking place in complex dynamic equilibria and permanently evolving by means of natural selection. Nowadays, according to the Ecological Society of America, ecology is "*the study of the relationships between living organisms, ..., and their physical environments*" [4].

Ecology is thus irremediably linked to the study of how species are distributed across space and time as a function of the environment (*Biogeography*), including the interactions of organisms with the atmosphere (*Biometeorology*) or, in other words, with the atmospheric conditions and its downstream products, such as rainfall. The work presented in this thesis revolves around the last and moves across spatial and temporal scales: from micrometer-sized interactions among bacteria and their most common parasites or predators, the bacteriophages, to regional and continental scales, where mosquito dynamics are affected by large environmental differences in near-surface air temperature and precipitation patterns.

Thesis scope

The **first part** of the thesis focuses on the behaviour of a model predator-prey system, composed of bacteriophages and bacteria, when this is let to disperse stochastically in a spatially structured habitat. The **second part** is a regional modelling study, comprising Italy, of the temporal dynamics and geographical distribution of the mosquito *Aedes albopictus*, vector of relevant arboviruses such as dengue (DENV) [5], Zika (ZIKV) [6] and chikungunya (CHIKV) [7]. We addressed the effect of climate change and short-term heatwave events on the behaviour of the mosquito. The **third** and last part focuses on the impact of climatic variability on the population of the mosquito *Anopheles gambiae s.s.*, one of the main malaria vectors in the African continent [8]. The modelling study takes place in a region of sub-Saharan Africa.

2

Dispersal-mediated competition and diversity in a phage-bacteria ecosystem

2.1 Synopsis

2.1.1 Introduction

Microorganisms are ubiquitous and numerically dominate in nature, with estimates of $\sim 10^{30}$ prokaryotes and $\sim 10^{31}$ viruses on Earth [9, 10]. A particularly relevant interplay is given by bacteria and their most common parasite or predator, the bacteriophages (short: phages, namely viruses that infect bacteria) [10–12]. These constitute key pieces in energy and nutrient cycles [12–28] and compose a complex ecological network [17, 29–31] still insufficiently understood. Mathematical models can aid to elucidate some potential parts of this network by studying factors that maintain microbial diversity in an isolated manner. For large-scale ecosystems these conceptual studies are frequently based on well-mixed models, with the competitive exclusion principle [32] as a theoretical corner stone, *e.g.,* [16, 17]. In the case of sessile organisms, when the habitat is spatially-structured and exclusion rules only apply locally, within the domain of individual habitats, a higher degree of global diversity has been conceptualized [33]. Metapopulation studies focusing on predator-prey and host-parasite interactions [34, 35] show that migration between habitats can both drive species to extinction and maintain global diversity by reintroducing locally extinct species from another habitat.

For the case of microorganisms and, in particular, phage-bacteria systems, the atmosphere can be considered as a vector that promotes their dispersal [36–38], with the potential to connect otherwise isolated surface habitats [39]. Aerosolization, dispersal and the subsequent deposition mechanisms vary greatly among species, *e.g.,* [40–44], with size, hydrophilic and nucleating properties affecting the transfer rates, and thus typical residence times, from surface to atmosphere and vice versa [39, 45]. This complex scenario yields a palette of simultaneous transport regimes, where biomass is passively carried around in both continuous and discrete manners.

In this chapter we study how the interplay between phages and bacteria is shaped by intermittent and wind-driven biomass transport in a spatially structured habitat.

2.1.2 Objectives

The objectives of this study are two-fold:

1.- Baseline dynamics: first, we start by studying whether this biomass transport regime pushes the system away from its well-mixed local behaviour and the resulting situation in the spatial system.

2.- Implications for competition and diversity: the observed departure from well-mixed conditions has the potential to affect the exclusion principle and, therefore, to have implications on the competitive and coexistence rules among the species present in the spatially structured habitat. We study this possibility by adding a second and, in principle, less fit phage that shares the same bacterial host and thus competes with the first for a common single resource, adhering to the exclusion principle.

2.1.3 Methods

A simple conceptual model was developed for this study. In the model, space is spatially structured as a lattice of $2N$ habitats. The lattice is arranged as two 1-dimensional layers each containing N points (Fig. 2.1a). In the lower layer

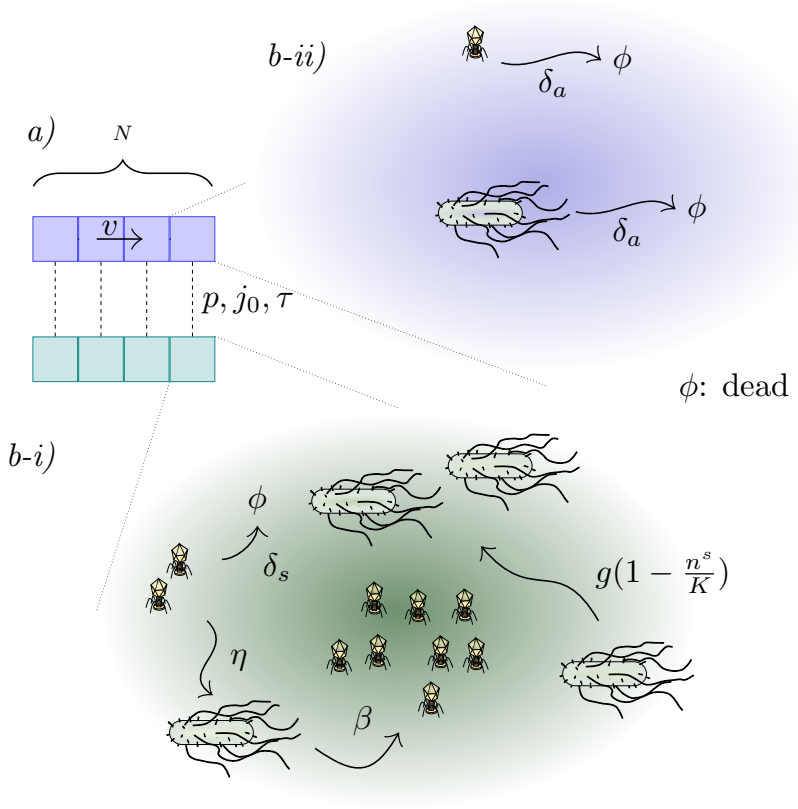

Figure 2.1: $a)$ Lattice of $2N$ discrete habitats $b)$ Reactions specific to the phage-bacteria system $i)$ Surface reactions $ii)$ Upper layer or "atmospheric" reactions.

lattice points represent surface habitats, whereas the upper layer aims to model an idealized atmosphere, where particles are horizontally advected across the lattice. In the surface layer biomass can only travel vertically and, consequently, migration from one habitat to another can only happen indirectly, via the upper layer. Since each layer represents a physically distinct environment, different reactions (r) can happen within: in the surface bacteria are allowed to grow (g) while being predated by phages (η) who multiply upon such event (β), but suffer from decay (δ_s) and thus need their host to survive (Fig. 2.1b-i); in the upper "atmospheric" layer microorganisms can only travel (v) and decay (δ_a), and thus this layer constitutes a transient habitat (Fig. 2.1b-ii).

Surface dynamics

In the model, phages and bacteria occupy a set of homogeneous and well-mixed surface habitats where coexistence rules are determined by the set of Lotka-Volterra equations [46]

$$\frac{dn_s}{dt} = gn_s\left(1 - \frac{n_s}{K}\right) - \eta n_s m_s \ , \tag{2.1}$$

$$\frac{dm_s}{dt} = (\beta - 1)\,\eta n_s m_s - \delta_s m_s \ . \tag{2.2}$$

Here, η is the adsorption rate, β is the phage burst size, δ_s is the phage's decay rate, g the bacterial growth rate and K the habitat's carrying capacity, specific to the environmental context. System ((2.1)-(2.2)) is globally stable and, upon perturbations, behaves as a stable spiral. This means biomass fluxes are likely to force the system into sustained oscillations, as observed in stable systems subject to demographic noise [47].

Dynamics in the upper layer

Species can be passively dispersed from one surface habitat to another via an upper layer, representing an idealized role of the atmosphere in biomass transport. When in this "atmospheric" layer, population densities follow the advection-reaction equation

$$\frac{\partial n_a}{\partial t} = -v\frac{\partial n_a}{\partial x} - \delta_a^n n_a \ , \tag{2.3}$$

$$\frac{\partial m_a}{\partial t} = -v\frac{\partial m_a}{\partial x} - \delta_a^m m_a \ . \tag{2.4}$$

Here, δ_a^m and δ_a^n are the respective phage and bacterial decay rates, of similar magnitude, and v is the horizontal advection velocity, taken constant for simplicity.

Vertical transport

As mentioned before, vertical biomass fluxes could be a composition of different transport mechanisms. As a conceptual study, however, we have the freedom to only describe those of interest in order to neatly study their role and associated emergent behaviour. If, for example, we were interested in the ecological implications of bacterial nucleation we could model vertical transport to be

asymmetric (particles are aerosolized at different rates than they are brought back to the surface by wet or dry deposition) characterized, perhaps, by a pronounced seasonality. We could then study species coexistence and spatial distribution as a function of their nucleating properties. In this study vertical transport is symmetric and stochastic. This comes from considering fluxes associated to turbulent eddies. In atmospheric models, sub-grid-scale turbulent transport is modelled as a diffusion equation, with mass travelling on average down the gradient. We here adopt this modelling framework. Furthermore, vertical transport is considered to be intermittent and triggered only when near-surface wind speed surpasses a given threshold. We do not model this explicitly, but encompass both the wind regime and the roughness of the surface over which the air moves in the parameter p, the probability of activating vertical transport. This is treated as a free parameter and the interplay between phages and bacteria is studied as a function of its value. Graphically, we can think of this vertical transport scheme as down-the-gradient fluxes trying to cross a door that will only be open with probability p.

Extinction threshold

Species' populations are described in terms of their densities and, as such, are not treated as individuals. This might drive the system to reach unrealistically low densities. To avoid this, a truncation is introduced and density values are set to *e.g.,* zero when a trajectory crosses a given density threshold. In this study we set the **extinction threshold** equal to one microorganism per grid point, *i.e.,*

$$\rho_{ext.} = \frac{1}{V} \, , \tag{2.5}$$

where $V = \Delta x^3$, with Δx being the linear extend of each surface and atmospheric habitat. We have **not** studied the sensitivity of our results with respect to this threshold value.

The introduction of the threshold imposes an upper bound to the distance biomass can be dispersed. This "*signal length*" is determined by how biomass is lost in the upper layer, and is thus determined by the vertical exchanges with surface habitats, as the signal is advected, and microorganism decays. In

this study we adopt an operational definition, independent on the first: we define the signal length, x^*, as the distance travelled by a biomass emission of magnitude K, when $p = 0$. The tendency equation,

$$\rho(t) = \rho(t_0) \cdot e^{-\delta_a t} = K \cdot e^{-\delta_a t} \ , \tag{2.6}$$

yields

$$t^* = -\frac{1}{\delta_a} \cdot ln\left(\frac{\rho_{ext.}}{K}\right) \ , \tag{2.7}$$

or, equivalently,

$$x^* = v \cdot t^* \ . \tag{2.8}$$

In turn,

$$x^* = L \cdot N \cdot \Delta x \ , \tag{2.9}$$

hence

$$L = -\frac{v}{\delta_a \cdot N \cdot \Delta x} \cdot ln\left(\frac{\rho_{ext.}}{K}\right) \ . \tag{2.10}$$

Here L stands for the fraction of the total system length, $N \cdot \Delta x$, travelled by the signal. In this study x^* is controlled by δ_a, which acts as a tuning parameter (Fig. 2.2). Spatial dynamics will reveal to be strongly dependent on the value of this parameter, which controls the connectivity between surface habitats. The downside of adopting this definition, and studying the system behaviour as a function of its value, is that we can only compare cases with equal p's.

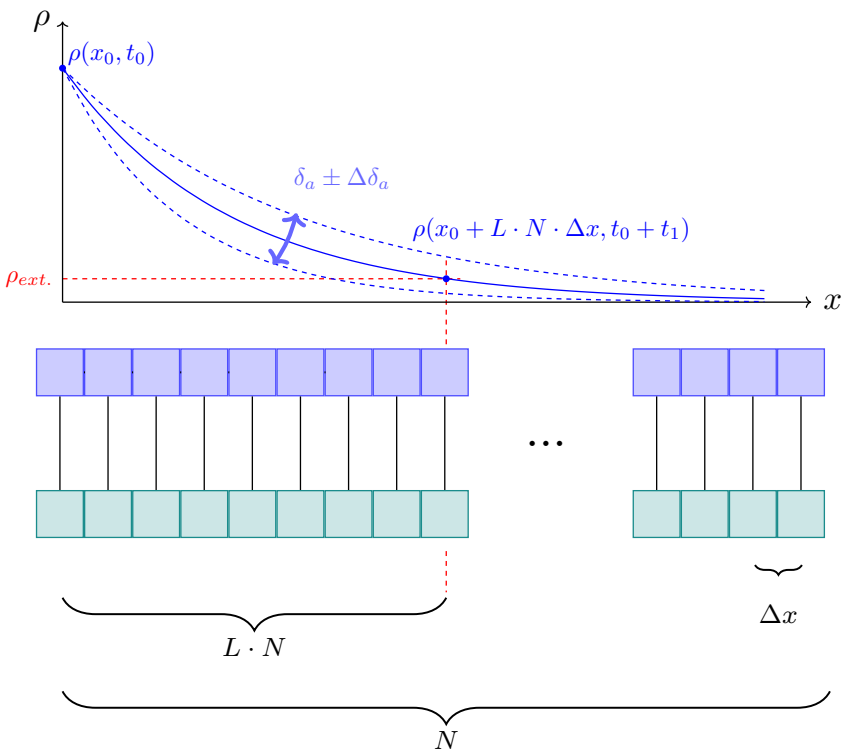

Figure 2.2: Schematic of the distance travelled by a biomass emission, ρ, as a function of the spatial and tuning parameters relevant to define the signal length, L.

2.1.4 Results

1.- Baseline dynamics: within the framework of the spatial model, single surface habitats undergo extinction and re-population events, both driven by biomass fluxes. Upon gain and loss of biomass, surface densities experience sustained oscillations which are at times amplified, pushing the system into the extinction threshold. Spatially, the system reaches a statistical steady state where the fraction of habitats occupied by both phages and bacteria, C (of coexistence), that occupied solely by bacteria, F (as in free), and the fraction of empty habitats, E, remain constant. Individual habitats are however permanently changing status and for this, the spatial steady state is "dynamical". Furthermore, the value of each fraction is found to be dependent on the phage-bacteria intrinsic parameters (Fig. 2.3), with potential implications for competition and diversity.

2.- Implications for competition and diversity: the consequences of these baseline dynamics on diversity are investigated by introducing a second and,

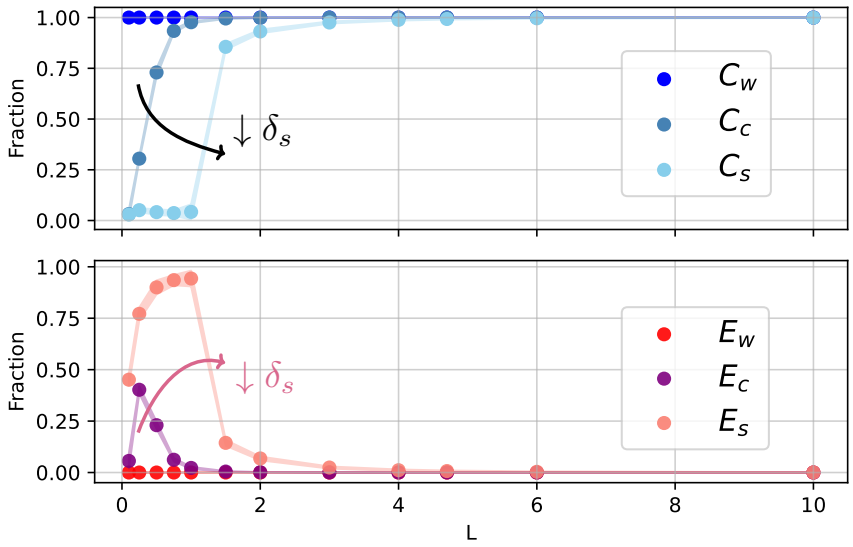

Figure 2.3: Fraction of habitats in a coexistence (up) and extinct (down) state as a function of the signal length, L, for three different phage's decay rate in the surface, δ_s. Each dots represents the steady-state values of independent simulations. (C_c, E_c) stands for the control case, (C_w, E_w) and (C_s, E_s) for two set of simulations performed with 10-fold increases and decreases in δ_s, respectively.

in principle, lesser phage in the spatial system. Our results show that, not only does the "weaker" phage manage to coexist but, in some biomass transport regimes, it dominates over the "stronger" competitor. This underlines that fitness is here dependent not only on their intrinsic parameters, but on the environmental context and that coexistence rules, as inferred from the exclusion principle, are dependent on the connectivity and stability of local surface habitats. Furthermore, the observed spatial coexistence affects the presence of the stronger phage in regions of the spatial system where the "weaker" phage is not present, creating new, indirect competitive dynamics.

2.1.5 Discussion

The conceptual model presented here is a strong tool to unveil potential links introduced by dispersal in the complex coexistence network composed by phages and bacteria. The framework is flexible and can be modified to further understand the ecological implications of asymmetric transport, driven by the empirically observed differences in aerosolization and deposition properties of diverse microorganisms, as well as to further understand the net role of intrinsic parameters in the global spatial context.

2.2 Manuscript

Title: "Stochastic microbial dispersal drives local extinction and global diversity"

Authors: Miguel Garrido Zornoza[1], Namiko Mitarai[1], Jan O. Haerter[1,2,3,4]

[1] The Niels Bohr Institute, University of Copenhagen, 2100 Copenhagen, Denmark

[2] Constructor University, Bremen, Germany

[3] Leibniz Centre for Tropical Marine Research, Bremen, Germany

[4] Department of Physics and Astronomy, University of Potsdam, Potsdam, Germany

My contribution: conceptualization, investigation, methodology, project administration, programming/software development, visualization, writing, review and editing.

Publication status: published in *The Royal Society Open Science*

Hyperlink: https://doi.org/10.1098/rsos.231301

ROYAL SOCIETY OPEN SCIENCE

royalsocietypublishing.org/journal/rsos

Research

Cite this article: Garrido Zornoza M, Mitarai N, Haerter JO. 2024 Stochastic microbial dispersal drives local extinction and global diversity. *R. Soc. Open Sci.* **11**: 231301.
https://doi.org/10.1098/rsos.231301

Received: 14 September 2023
Accepted: 20 February 2024

Subject Category:
Ecology, conservation, and global change biology

Subject Areas:
ecology, evolution

Keywords:
coexistence, dispersal, trade-off, stochastic, competition

Author for correspondence:
Miguel Garrido Zornoza
e-mail: mgarrizoraca@gmail.com

Stochastic microbial dispersal drives local extinction and global diversity

Miguel Garrido Zornoza[1], Namiko Mitarai[1] and Jan O. Haerter[1,2,3,4]

[1]The Niels Bohr Institute, University of Copenhagen, 2100 Copenhagen, Denmark
[2]Constructor University, Bremen, Germany
[3]Leibniz Centre for Tropical Marine Research, Bremen, Germany
[4]Department of Physics and Astronomy, University of Potsdam, Potsdam, Germany

MGZ, 0000-0001-5030-4537; NM, 0000-0003-0116-7606; JOH, 0000-0002-8617-3847

Airborne dispersal of microorganisms is a ubiquitous migration mechanism, allowing otherwise independent microbial habitats to interact via biomass exchange. Here, we study the ecological implications of such advective transport using a simple spatial model for bacteria–phage interactions: the population dynamics at each habitat are described by classical Lotka–Volterra equations; however, species populations are taken as integer, that is, a discrete, positive extinction threshold exists. Spatially, species can spread from habitat to habitat by stochastic airborne dispersal. In any given habitat, the spatial biomass exchange causes incessant population density oscillations, which, as a consequence, occasionally drive species to extinction. The balance between local extinction events and dispersal-induced migration allows species to persist globally, even though diversity would be depleted by competitive exclusion, locally. The disruptive effect of biomass dispersal thus acts to increase microbial diversity, allowing system-scale coexistence of multiple species that would not coexist locally.

1. Introduction

Microbes are involved in global nutrient and energy cycles and constitute a key functional group in the ocean's food web [1–3]. For example, half of the oxygen in the atmosphere is generated by photosynthetic bacteria [2]. There are a total of $\sim 10^{30}$ prokaryotes on Earth [4], of which $\sim 10^{29}$ are oceanic bacteria [4]

THE ROYAL SOCIETY PUBLISHING

permanently hunted down by bacteriophages (short: 'phages', i.e. viruses that infect bacteria), which constitute their most common 'predator', or parasite [5–7]. Indeed, studies point to the ubiquity of viral infections [5,8], for example, 20–30% of marine bacteria are believed to be infected at any given time by phages [5]. Beyond regulating their host's population and community structure [9–12], and despite their lack of metabolism, viruses also influence energy and nutrient cycles by modifying the microbial metabolism [7,13–16] and by directly impacting microbial mortality [15,17–23].

However important, the interplay between phages and bacteria, reflected in the size and complexity of their ecological network [12,24–26], is still poorly characterized. Mathematical modelling is a strong tool to unveil possible mechanisms that maintain microbial diversity. When considering large-scale aquatic ecosystems (e.g. [11,12]), much work is based on well-mixed models, where the competitive exclusion principle [27] dominates the coexistence rules. However, when the habitat is spatially structured, these rules are altered and a higher degree of diversity is allowed [28]. Metapopulation studies of predator–prey and host–parasite systems [29,30] have shown that migration between habitats can support global coexistence by reintroducing locally extinct species from another habitat, but also trigger species extinction by provoking large-amplitude predator–prey oscillations.

In phage–bacteria systems, dispersal due to aerosol transport has the potential to cover vast distances [31,32], before returning to the surface via wet or dry deposition [33]. Indeed, models suggest $\sim 10^{24}$ particles containing bacteria to be emitted globally every year into the atmosphere [34] with residence times estimated to vary from days to weeks [34]. In this sense, we can consider the atmosphere as a vector that promotes microbial dispersal across otherwise spatially disconnected habitats [35], with the potential ability to impact an ecosystem's composition [28,35–37] despite the much lower advected concentration numbers as compared to surface populations [33,34,38,39].

In this work, the focus is on the atmosphere's role in biomass transport and its potential to shape microbial community structure, in particular, the predator–prey system composed of phages and bacteria. We view the atmosphere as a habitat where these microbes are carried around stochastically as sessile organisms and can only survive transiently, that is, do not replicate but suffer from decay. Passive dispersal thus provides a migration mechanism for these microorganisms, which are transported across the surface, considered to be physically homogeneous and spatially subdivided. Our goal is to understand the ecological implications of such a system. For this, we here develop a simple two-layer neutral dispersal [40] model. Within the framework of our model, we first address the baseline dynamics emergent from these dispersal-mediated stochastic biomass fluxes, which effectively connect surface habitats. Extinction within a given habitat as a result of stochastic migrations is shown to be of utmost importance in shaping community structure. Second, we study the implications of such dynamics on competition and diversity, focusing, for simplicity, on a two-phage system sharing a common bacterial host. We find biodiversity to self-organize, even under conditions where competitive exclusion would rule out coexistence.

2. Methods

2.1. Model concept

Our quasi-one-dimensional model consists of two coupled one-dimensional layers, or linear habitats (see figure 1*a*), each subdivided into N sites. In the lower layer, each of these sites constitutes a surface habitat, where basic chemical or physical nutrients are sufficiently available and species can replicate and interact. These discrete surface habitats are connected only by airborne dispersal via the upper layer. This layer, representing the atmosphere, is only relevant for directed advective transport, as well as decay, disregarding replication or predation processes. Microbes thus only spread passively. The exchange between the two layers is enabled through vertical stochastic population fluxes.

Our model is, therefore, a hybrid between a continuous formulation, taking place for replication and decay in the surface layer as well as transport within the atmospheric layer, and stochastic processes, which occur when biomass is transported vertically. Decay is possible in both layers and in practice likely more pronounced in the atmospheric layer due to UV radiation exposure there [41].

2.2. Model formulation

In both linear habitats, the spatial coordinate x is discretized into N positions $x_i = i\Delta x$, with the integer $i \in [0, N)$ and the spatial extent of each habitat Δx.

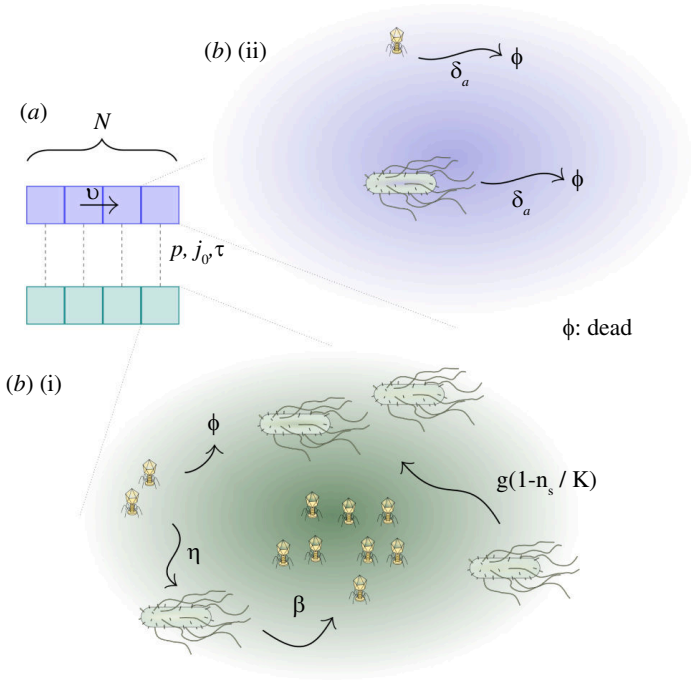

Figure 1. Schematic representation of the spatial model. (*a*) Two different types of biomass transport are modelled: continuous advective flow, v, in the upper layer and vertical stochastic transport, described with three parameters (p, j_0, τ), that allows particles to 'jump' across layers, effectively coupling them. (*b*) Bacteria undergo a layer-dependent palette of events. (i) When in the surface, they are exposed to phage predation (η), and have access to enough nutrients to grow logistically (g, K). (ii) As an aerosol, they avoid predation but are exposed to a much higher decay rate (δ_a), accounting for the more extreme conditions found in the atmosphere. Aerosolized phages follow an analogous behaviour, whereas when on the surface, they predate and multiply (η, β), as well as decay (δ_s), requiring the presence of the host to survive.

2.2.1. Surface dynamics

Within each grid box at a given discrete position x_i, the lower-layer (surface) bacterial and phage population densities, $n_s(x_i, t)$ and $m_s(x_i, t)$, respectively, are assumed to follow the set of Lotka–Volterra equations [42]

$$\frac{\mathrm{d}n_s}{\mathrm{d}t} = g n_s\left(1 - \frac{n_s}{K}\right) - \eta\, n_s m_s\,, \tag{2.1}$$

$$\frac{\mathrm{d}m_s}{\mathrm{d}t} = (\beta - 1)\eta n_s m_s - \delta_s m_s\,, \tag{2.2}$$

where we have dropped the explicit reference to spatial and temporal coordinates for simplified notation. In equations (2.1) and (2.2), η is the reaction kernel or the adsorption rate, and captures the reaction-limited nature of phage infection, that is, how often viruses can both find and infect their host; β is the phage replication number, typically referred to as burst size; δ_s the phage decay rate (see figure 1*b*(i) for a zoom into these local dynamics). Furthermore, in this predatory dynamics, we tacitly assume lytic [43] phages and well-mixed populations within each grid box. We thus ignore the high degree of spatial heterogeneity one could find in different environments [44–47] and its associated ecological impact [48,49]. We put the focus on bulk and large-scale behaviour, setting our scale of interest to a few metres.

The zeroth trophic level, representing basic chemical or physical energy sources, is not explicitly modelled. Instead, in equation (2.1), we assume bacteria follow logistic growth [50] with maximum growth rate g and a constant maximum carrying capacity, K. K is thereby specific to the environmental context of the system. We do not have an explicit bacteria decay term here because, in a deterministic system with species described in terms of population densities, the bacterial decay rate can be absorbed into the growth rate without loss of generality.

2.2.2. Dynamics in the upper layer

We assume the transport of bacteria and phages present in the upper layer to take place by passive advection following the atmospheric flow. The population densities will thus follow the advection-reaction equation, that is,

$$\frac{\partial n_a}{\partial t} = -v\frac{\partial n_a}{\partial x} - \delta_a^n n_a, \tag{2.3}$$

$$\frac{\partial m_a}{\partial t} = -v\frac{\partial m_a}{\partial x} - \delta_a^m m_a\,. \tag{2.4}$$

In contrast to the surface layer, here we consider explicit positive δ_a^n and δ_a^m, of similar magnitude, representing the respective bacterial and phage decay rates in the atmosphere (figure 1*b*(ii)). v is the horizontal advection velocity, which we have set constant for simplicity.

2.2.3. Vertical transport

Vertical transport is taken as a stochastic process. We build our parameterization of microorganism emissions on literature [51] based on an empirical dust emission formulation [52,53]. The key concept we take from this work is a critical threshold value for near-surface wind speed above which vertical transport is finite. As a threshold phenomenon, this wind-driven emission mechanism is considered to be intermittent. Conceptualizing, aerosolization events are taken as discrete on-/off-like processes that occur with some activation probability, p, a parameter that aims to capture the frequency with which the wind speed is above the given threshold. Since this threshold might depend on the type of terrain, a given value of p qualitatively encompasses both the wind regime in a given location as well as the roughness of the surface over which the air is moving. In our model, we treat p as a free parameter.

On top, we shall consider net vertical exchanges to be qualitatively similar to eddy-like mixing, and triggered by this critical threshold on wind speed. In turbulent eddies, often parameterized as down-the-gradient fluxes [54], downward fluxes are fully correlated with emission events since mass transport is modelled to act in a similar way to molecular diffusion, but at a much larger scale. Consequently, in our scheme, the net exchange of biomass across layers is not only intermittent but, when finite, proportional to the vertical density gradient in each particular column. The proportionality constant, or rate of exchange, j_0, is also taken as a free parameter.

The duration of these discrete events remains to be defined. In reality, their length is not necessarily fixed but, for simplicity, we here consider a constant exchange time scale, T. Consequently, when active, vertical transport will have a typical duration of $\tau \sim T$. This exchange is set to be independent among species, and of stochastic nature, that is, it will only happen with our probability, p. For simplicity, this is taken to be independent of the state of the system in the previous time interval.

2.2.4. Vertical transport algorithm

Biomass exchange between the two levels of a specific column is therefore temporally discontinuous or intermittent and regulated by the three free parameters (see figure 1*a*):

(1) p, the probability of having a particle flux between layers for a given duration;
(2) τ, the duration of this intermittent biomass exchange between layers;
(3) j_0, the rate at which these microbes are exchanged when vertical transport is active.

Summarizing, each location experiences biomass fluxes between same-column grid boxes with a frequency set by p. When this flux is active, particles are exchanged at a constant rate j_0 for a time τ. In practice, we evaluate the net intermittent bacterial and phage fluxes between layers, $j_n(x,t)$ and $j_m(x,t)$, respectively, with the following algorithm:

For each horizontal position x_i and each species separately, with $i \in [0, N)$, draw $\alpha \in U[0,1)$, then, during the time $t \to t+\tau$

— If $\alpha \leq p$, the downward and upward fluxes are set to $j^{down} = j_0 \cdot n_a(x_i, t)$ and $j^{up} = j_0 \cdot n_s(x_i, t)$, with the net flux being $j_n(x_i, t) = j^{up} - j^{down}$.
— If $\alpha > p$, there is no biomass exchange in column x_i, that is, $j_n(x_i, t) = 0$.

This allows for particle fluxes along the gradient, leading to discrete aerosolization or colonization events whose frequency, duration and magnitude are free parameters. The final system reads as

$$\frac{\partial n_s}{\partial t} = g n_s\left(1 - \frac{n_s}{K}\right) - \eta n_s m_s - j_n, \tag{2.5}$$

$$\frac{\partial m_s}{\partial t} = (\beta - 1)\eta n_s m_s - \delta_s m_s - j_m, \tag{2.6}$$

$$\frac{\partial n_a}{\partial t} = -v\frac{\partial n_a}{\partial x} - \delta_a^n n_a + j_n, \tag{2.7}$$

$$\frac{\partial m_a}{\partial t} = -v\frac{\partial m_a}{\partial x} - \delta_a^m m_a + j_m. \tag{2.8}$$

Parameter values for equations (2.5)–(2.8) can be found in table 1 (appendix A). For the simulation of this model, population densities are randomly initialized across the spatial system (see appendix A), which is solved with periodic boundary conditions.

2.2.5. Extinction threshold

Even though we work with population densities, we consider species populations to be integer numbers. For this, we manually introduce an extinction threshold equal to one individual per grid box, that is, $\rho_{ext} \equiv 1/V$, V being the volume of the box. Whenever a particular trajectory drops below ρ_{ext}, the species' population is immediately set to zero.

2.2.6. Main model assumptions

It is informative to briefly summarize the main model assumptions and limitations:

(1) Net vertical fluxes are proportional to vertical population density differences. Furthermore, vertical transport is considered to be completely uncorrelated among species, that is, each species undergoes vertical transport independently of the other species. The model can be extended to study the effect of correlated emissions/depositions among species.
(2) The frequency (p) and rate (j_0) of aerosolization or deposition events are assumed to be equal among species. This could be generalized to allow for the empirically observed species-specific parameters [55–59].

3. Results

3.1. Core dynamics

We now look at the emerging dynamics of such a system and the resulting ecological consequences. However, the full complexity of the spatial model is better understood in terms of the behaviour of its individual components.

3.1.1. Single column

Let us first focus on single surface grid-boxes in two different scenarios in order to decouple: (i) the effect of biomass loss to the upper layer (negative fluxes) and (ii) the effect of biomass gain from upstream sources into a populated habitat (positive fluxes).

3.1.1.1. Negative fluxes

Let us consider habitats to be completely disconnected from their neighbours, that is, once aerosolized, microbes are advected and lost. Vertical transport thus represents a net loss of surface biomass. We shall study the effect of these intermittent fluxes by looking at the deviation of the population densities with respect to some deterministic expectation. More concretely, for this, let us look at the limit where fluxes are continuous ($\tau \to 0$) and a fraction p of the time vertical transport is active. This limit yields the deterministic equations

$$\frac{\mathrm{d}n_s(t)}{\mathrm{d}t} = g n_s\left(1 - \frac{n_s}{K}\right) - \eta n_s m_s - p j_0 \cdot n_s\,, \tag{3.1}$$

$$\frac{\mathrm{d}m_s(t)}{\mathrm{d}t} = (\beta - 1)\eta n_s m_s - \delta_s m_s - p j_0 \cdot m_s\,. \tag{3.2}$$

It is known that systems (equation 2.1)–(equation 2.2) and (equation 3.1)–(equation 3.2) contain a globally stable coexistence fixed point [60] (appendix B). Further, upon small perturbations, their transient relaxation to the steady state can be described as a stable spiral (appendix C), that is, population density trajectories oscillate back to this coexistence fixed point. This yields a clear picture of the deterministic dynamics when habitats are nudged away from their steady state. In this frame, the study of discrete transport comes from comparing the behaviour of system (equation (3.1))–(equation (3.2)) against its stochastic counterpart—equations (equation (2.5)) and (equation (2.6)) with $j^{\mathrm{down}} = 0$—as we move between the well-mixed ($p \to 0$) scenario, where surface habitats are isolated, and the continuous flux ($p \to 1$) case. This is done by looking at the behaviour of both systems for different (p, j_0) values while keeping the product $pj_0 = \mathrm{const}$. Since the parameters p and j_0 appear as a product in (equation (3.1))–(equation (3.2)), they effectively behave as one, and any combination fulfilling this restriction is equivalent in the deterministic system, that is, it will result in the same dynamics. For convenience, let us now define an 'equivalent deterministic line' (EDL) as that where $pj_0 = \mathrm{const}$. If we move along an EDL, as we tend to either $p = 1$ or $p = 0$, both continuous and discrete scenarios converge, but, we will show that the behaviour is rather different for finite p owing to stochasticity in fluxes and the existence of the extinction threshold.

When subject to intermittent fluxes, stochastic effects appear: the original transient oscillatory relaxation to the coexistence fixed point is now substituted by trajectories which systematically show sustained oscillations and become unstable in some regions of the EDL. As seen in figure 2*a*,*b*(i) (right), the continuous case converges to the coexistence fixed point (n^{st}, m^{st}) from equations (B 3) and (B 4) whereas trajectories subject to intermittent biomass fluxes oscillate, eventually driving the system to extinction. We find two distinct types of extinction: (i) bacterial extinction, thus also causing parasite extinction; (ii) phage extinction and bacterial survival. Negative fluxes therefore open the possibility for coexistence among phages and bacteria (C), phage-free (F) and extinct (E) habitats, where neither species is present. In figure 2*a*,*b*(i) (left), we show the distinct explored phase space of each of the two types of extinction events. Given the stochastic nature of these fluxes, one particular realization might significantly differ from another. For this, the ensemble average of many independent repetitions is depicted in figure 2*a*,*b*(ii) (bottom). By counting the number of extinctions in time, figure 2*a*,*b*(ii) (top), we find the extinction rate to be exponentially distributed, and dependent on the pair (p, j_0). A broader analysis is represented in the (p, j_0) phase diagram of figure 3*a*, in which the region where these transitions take place is mapped out. We can define three distinctly different (p, j_0) regions. (i) A deterministically unstable region, where even in a phage-free environment logistic growth cannot sustain bacterial biomass loss to the upper layer. The system is therefore driven to extinction. This is a deterministic prediction (appendix D). The connected purple dots in figure 3*a* show the limit where a finite density fixed point is still feasible. (ii) A stable region with permanent coexistence among phages and bacteria. Discontinuous fluxes make the system oscillate incessantly. (iii) A stochastically unstable region where, depending on the manner biomass is lost, that is, the (p, j_0) pair, habitats with coexisting species transition either towards a phage-free state (dark blue diagonal) or an extinction of both phages and bacteria (white upper left, also in figure 3*a*). The border region between stable and extinct states shows a colour gradient reflecting the different extinction rates within the stochastically unstable region (a lower population average among independent habitats indicates the mixed presence of both extinct and populated habitats). This underlines the temporal aspect of the phase diagram, that is, for sufficiently long times, every habitat is susceptible to suffer from a concatenation of events that

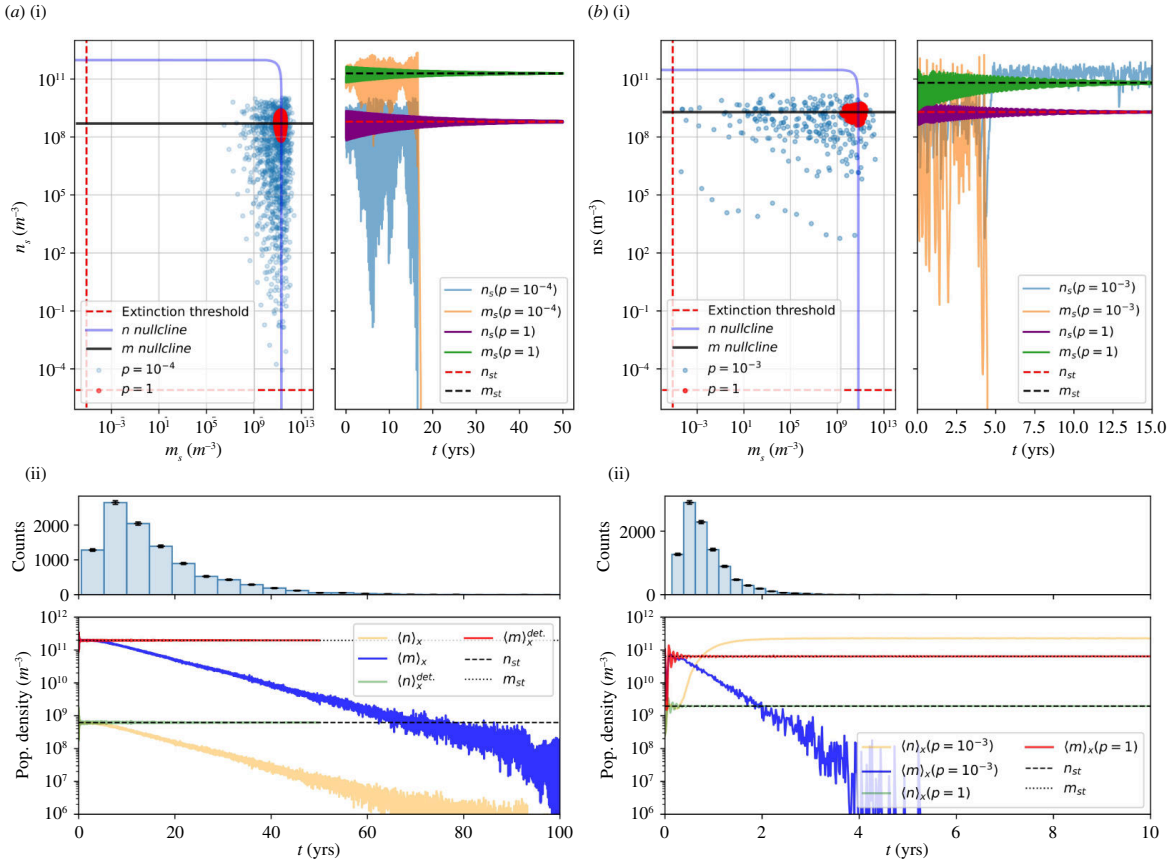

Figure 2. Negative fluxes. (*a*) (i) Right. Time series of phage and bacteria population densities for deterministic ($p = 1$) and stochastic ($p = 10^{-4}$) vertical transport cases along the same equivalent deterministic line, $p \cdot j_0 \cdot \tau = 1.6 \times 10^{-5}$. Here, the oscillations reach the bacterial extinction threshold, after which the phage population density decays to zero, as they need their host to survive. Left. Explored phase space of a $C \rightarrow E$ transition. (ii) Population density average of 10^3 and 10^4 independent surface habitats for the same deterministic ($p = 1$) and stochastic ($p = 10^{-4}$) transport cases, respectively. Decaying trajectories, corresponding to the stochastic case, are the result of individual extinction events, counted in the histogram above (shared time axis). (*b*) (i,ii) Analogously to the previous case, a $C \rightarrow F$ transition is shown ($p = 10^{-3}$) and compared to its deterministic limit ($p = 1$) in the $p \cdot j_0 \cdot \tau = 2 \times 10^{-4}$ equivalent deterministic line. Notice the decay time-scale difference with respect to the previous case. Here, decay events happen much faster.

drive it to extinction. As seen in the diagram (and previously explored in figure 2*a*,*b*(ii) (top)), this time scale is set by (p, j_0).

3.1.1.2. Positive fluxes

Next, we analyse the system's response against the stochastic migration of phages or bacteria into a habitat populated by either bacteria or both phages and bacteria. From the system (equation 3.1)–(equation 3.2) nullclines we can see that, when pushed beyond some critical trajectory (figure 3*b*, in blue), the system will deterministically cross the extinction threshold. The critical trajectory thus provides a conceptual basis to understand the migration dynamics in our system. For example, if the bacterial habitat is in its carrying capacity, K, any migration attempt on the phage's side will result in a complete deterministic depletion of the host (as seen from the phase portrait), thereby driving the full habitat to extinction. However, if the bacterial habitat has not yet reached the carrying capacity, it is possible for the parasite to successfully migrate, that is, push the trajectory into a region within the area encompassed by the critical trajectory. The transition $F \rightarrow C$ is thus conditional. Based on this discussion, we see that depending on the migrated population, a particular habitat can transition to any of the three possible states (except $E \rightarrow C$). This yields a more complex dynamical scenario as compared to the initial unique absorbing state (see figure 3*c*). Let us now look at the consequences of such a scenario in a connected system.

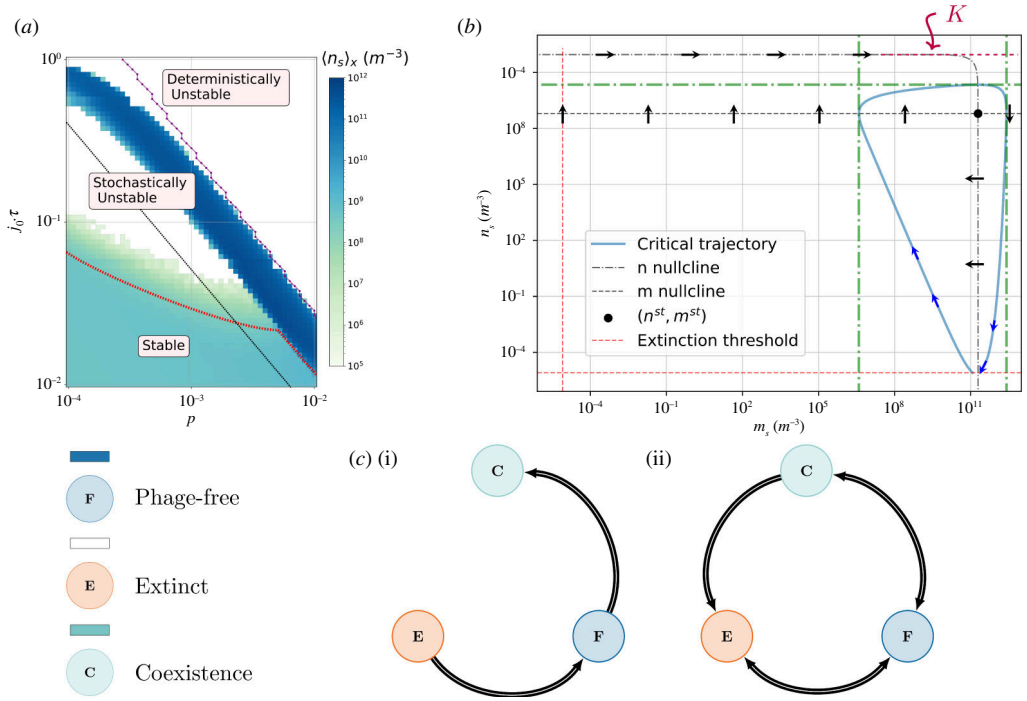

Figure 3. Single habitat dynamics. (*a*) Phase diagram of the single grid-box system. Each pixel represents the bacterial population average over 10^3 independent habitats at $t = 150$ years. Below, colours are matched to the corresponding state of the system: *C*, coexistence; *F*, phage-free; *E*, extinct. The black dashed line is an example equivalent deterministic line. (*b*) Positive flux framework imposed by the critical trajectory. Any migration event, or concatenation of migration events, must push the trajectory into the area encompassed by the critical trajectory, otherwise, the habitat is doomed to cross the extinction threshold. This limits, for example, the manner in which phages can migrate into a habitat populated by their host without driving that same habitat to extinction. (*c*) Available transitions of individual habitats. (i) Without an extinction threshold, a habitat can only undergo $E \rightarrow F$ bacteria-mediated transitions and $F \rightarrow C$ phage-mediated transitions. *C* is therefore an absorbing state. (ii) Diagram of new dynamical possibilities. These constitute the aggregate of negative and positive fluxes onto a system with a finite extinction threshold.

3.1.2. Multiple columns

3.1.2.1. Connectivity effect

We now focus on the (p, j_0) region of the phase diagram where coexistence states become extinct upon negative fluxes in the single column case, that is, $C \rightarrow E$ transitions (white zone in the stochastically unstable region). Let us study their collective behaviour by allowing a finite degree of connectivity, that is, biomass emissions will get advected a finite fraction of the system length, *L*, before decaying, and thus dynamically 'interact' with downstream locations. This length is defined in a simple way, to provide a clear operational definition (see explicit derivation in appendix F). In short, it gives the distance, x^*, an emitted flux of magnitude K would travel before its density reaches the extinction threshold, ρ_{ext}, if $p = 0$. This is, the only biomass loss in the upper layer comes from the decay component, δ_a. This scenario yields the relation

$$x^* = L \cdot N \cdot \Delta x = -\frac{v}{\delta_a} \cdot \ln\left(\frac{\rho_{ext}}{K}\right), \tag{3.3}$$

with N being the total system size. This length is effectively controlled with δ_a, which is chosen as a tuning parameter to modulate the system's connectivity. In figure 4, we show individual contiguous habitats of a connected system with $L = 0.5$. From this, we see that, when biomass is allowed to disperse, the spatial system simultaneously splits into the three possible states, thus surviving local extinctions. Locally, each habitat is susceptible to transition from one state to another while the global system self-organizes into a statistical steady state. Two examples are shown in figure 5*a*. Even though first neighbours are uncorrelated, the fraction of the spatial system belonging to either state is a function of the system's connectivity (*L*), figure 5*b*, reflecting the effect of dispersal distance for coexistence.

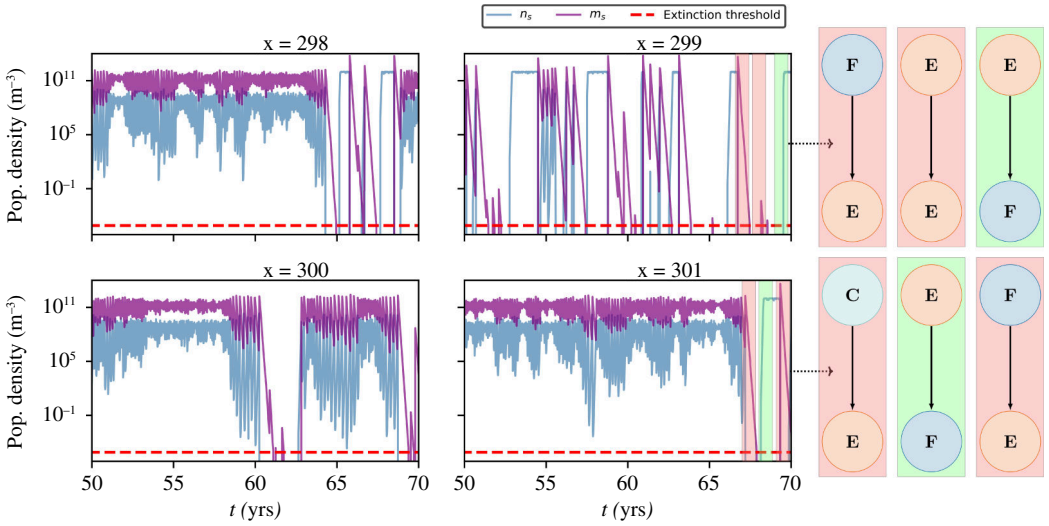

Figure 4. Connectivity effect. Time evolution of neighbouring surface habitats of a system with $N = 1000$ and $L = 0.5$. Here, $p = 10^{-4}$ and $j_0 = 6 \times 10^{-3}\ s^{-1}$. Different examples of extinction mechanisms are depicted to the right—for example, migration of the parasite, driving the system into the extinction threshold ($F \rightarrow E$, two cases shown); phages migrating into an empty habitat, thus causing them to decay ($E \rightarrow E$); bacteria migrating into empty habitats and colonizing them ($E \rightarrow F$, two cases shown); an unstable habitat upon negative fluxes ($C \rightarrow E$). For this particular spatial system, 93% of phage migrations into an F habitat resulted in extinction, reflecting the role of the critical trajectory introduced by the extinction threshold.

3.2. Implications for competition and diversity

The new dynamical possibilities (figure 3*c*(ii)) drive the spatial system towards a new set of steady states (figure 5*a*,*b*). Fundamentally, these configurations might not only depend on the biogeographic connectivity, L, but also on the system's response to biomass fluxes, that is, the way trajectories converge back to the coexistence fixed point. Since this response is set by the deterministic parameters $(g, \beta, \eta, \delta_s, K)$, these steady states might be sensitive to a change in, at least, one of them. Interestingly, these parameters are also a measure of fitness, or competitive ability. A higher competitive trait for the phage, such as a bigger burst size, β, or a lower decay rate in the surface layer, δ_s, might even be detrimental, since, by changing the system's convergence to the steady state, it could increase the chance of crossing the extinction threshold, and thus alter the habitat's longevity. This line of thought underlines the non-trivial effects intra-population variability might have on the spatially structured habitat, and the complexity of understanding the net role of intrinsic or system-specific parameters. We now look at the dynamical role intrinsic parameters have in the spatial steady states, and the implications for competition and diversity. For the latest, we focus on the simplest extension of our study, that is, we introduce an extra phage which infects the same host and thus represents a direct competitor.

3.2.1. Dynamical role of deterministic traits

Let us focus, for simplicity, on the aforementioned decay rate, δ_s. To understand the grounds of the conceptualized competition–longevity trade-off, we briefly go back to the system (equation 2.1)–(equation 2.2) and summarize the effect of δ_s in an isolated deterministic system.

First, from a linear stability analysis of system (equation 2.1)–(equation 2.2) (appendix C), we can show that the decay time scale of small perturbations, τ_{per}, is proportional to δ_s^{-1}. Systems with fitter viruses (smaller δ_s) will thus take longer to fall back into their steady-state population densities. This might allow future fluxes to further amplify an initial departure from the steady state.

Second, given the existence of an extinction threshold, the stability of coexistence states is also related to the amplitude of their oscillations. This happens to increase for lower values of δ_s (see appendix G). Consequently, the stability of the habitat decreases for systems with stronger (smaller δ_s) viruses.

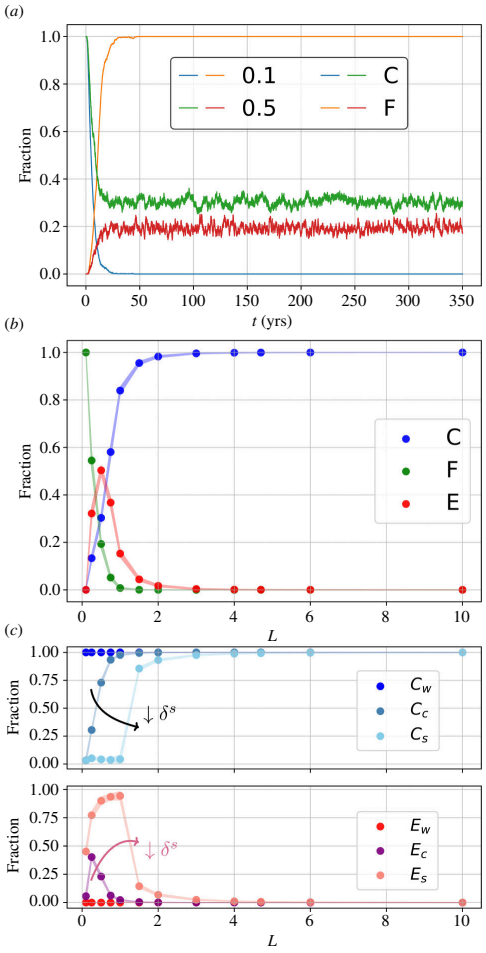

Figure 5. Steady states. (*a*) Relaxation to a steady state. Example trajectories for the $L = 0.1, 0.5$ cases for C and F fractions. Fluctuations correspond to transitions of individual habitats to a different state. (*b*) The fraction of columns in each state is a function of the system's connectivity, L. Here, trajectories are simulated for 350 years with periodic boundaries until a steady state is ensured. From this, we neglect the first 50 years and compute the mean. Scattered points are complemented with lines of width equal to $2 \cdot \sigma$, to exemplify the signal noise and thus the rate at which columns transition between states. (*c*) Steady-state dependence on the phage decay rate. Analogously to the previous case, we now show the steady-state C and E fractions in three spatial systems, each containing either the control (c), the weaker (w) or the stronger (s) phage.

3.2.2. Effect of phage decay rate in the spatial system

Having the effect of δ_s on local population dynamics in mind, let us now look at the behaviour of the connected system in the two distinct scenarios of increasing and reducing by 10-fold the phage decay rate in the surface, δ_s. A comparison between these two independent spatial systems and the one with untouched δ_s value (control) is depicted in figure 5*c*. We can see that, for any given value of the system's connectivity, L, the number of E habitats increases (decreases) for the stronger (weaker) phage case. A better competitive ability, having a clear local destabilizing effect, has detrimental effects on a spatial level. Intrinsic parameters thus clearly modify the spatial steady state and might therefore have an impact on global competition and diversity.

3.2.3. Competition of two phage types in a spatial system

Let us now evaluate direct competition among phages with distinct competitive abilities. Examining the effect of phage migration into an isolated C habitat populated by the competitor we see that, as expected, competitive exclusion applies and the stronger phage takes over (appendix E). In the following, we demonstrate that the full spatial model can allow the global coexistence of these competing phage species.

To study direct competition, we choose an arbitrarily small non-zero value of δ_s (the absolute zero would be biologically unfeasible) for the stronger phage, $\delta_s^{str\cdot}$. We then simulate the spatial system for a range of δ_s values for the weaker phage, δ_s^w, with $\delta_s^w \geq \delta_s^{str\cdot}$. This is initially done for a fixed (p, j_0)

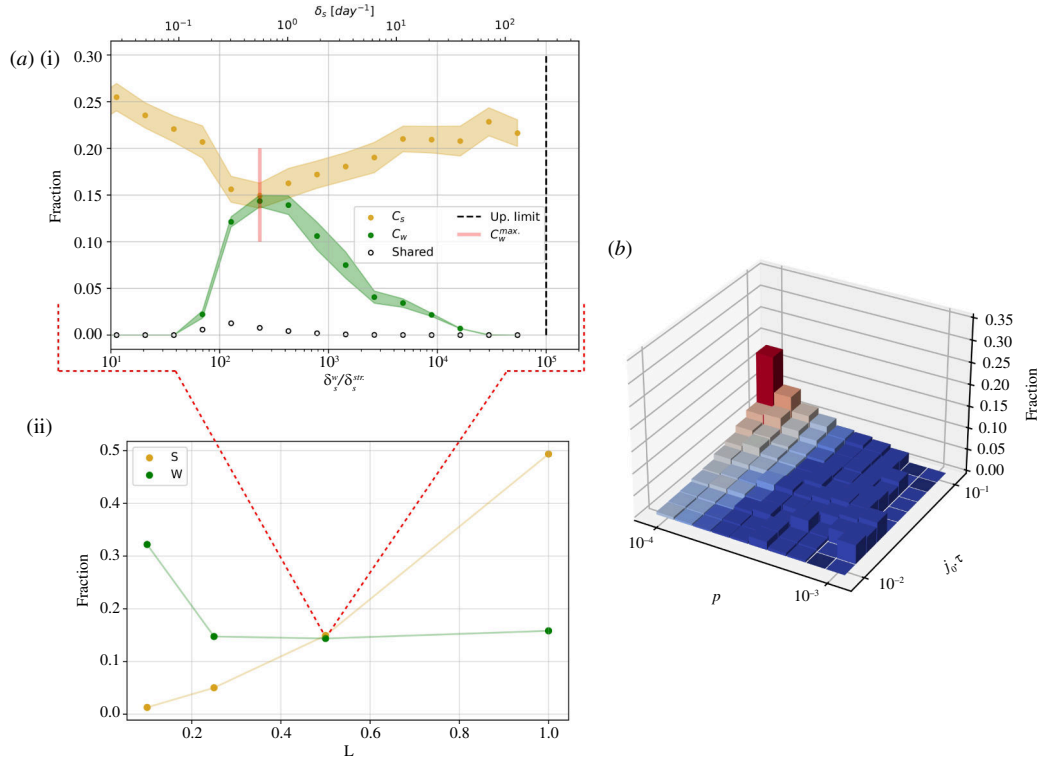

Figure 6. Direct competition of two phage types. (*a*) (i) For a fixed pair $(p, j_0) = (0.1, 3.2) \times 10^{-3}$, we compute the fraction of habitats occupied by the weaker phage strain in the steady state , C_w, for $\delta_s^w/\delta_s^{str.} \in [10^1\text{–}10^5]$. From this, we take $C_w^{max.} = \max(C_w)$. The black dashed line marks the upper deterministic limit for the feasibility of the coexistence fixed point. (ii) Analogous analysis for different system connectivities, L. A clear transition appears as a function of L, from a dominance of the stronger phage to a dominance of the weaker competitor. The low fraction of habitats shared by both phages (white scattered dots) points towards local competitive dynamics acting on a much faster time scale than habitat connectivity. (*b*) Effective fitness landscape. We systematically estimate the optimal δ_s value for the weaker phage strain for different (p, j_0) pairs for $L = 0.1$. This can be considered a measure of the effective fitness, as opposed to the intrinsic fitness, measured only from the deterministic parameters. Red shades indicate a dominance of the weaker strain, that is, a higher number of habitats occupied by it than its stronger competitor.

pair and different connectivities, L. In figure 6*a*(i), we show the ability of the weaker phage to coexist in the spatial system. This coexistence is only possible in a given range of δ_s^w values, establishing a limit to how similar the weaker competitor can be in order for coexistence to be achieved. We also find the existence of an optimal decay rate value that maximizes the fraction of occupied sites by the weaker competitor, to the detriment of the stronger. That is, even though competitive exclusion applies and competitive dynamics act on a much faster time scale than biomass transport (see figure 6*a*(i) white dots), the weaker phage indirectly affects the number of habitats where the stronger competitor is present, thus creating new competitive dynamics. Furthermore, we learn that not only does the intrinsically less fit strain manage to coexist in the spatial system, but, for low connectivities, it even dominates over its stronger competitor (figure 6*a*(ii)). Fitness is therefore not fully determined by the intrinsic deterministic parameters, but also by the biomass transport regime, and thus the aggregate context of the particular habitat.

In figure 6*b*, we calculate the weaker phage species' optimal decay rate for a given (p, j_0) region to illustrate this idea. This same exercise can be done for the rest of the system's intrinsic parameters, such as the phage's burst size, β, or the bacterial growth rate, g, in order to understand the role each parameter plays on a global scale.

4. Discussion

In our simple two-layer model, the predatory bacteria–phage system we study is subject to discrete, intermittent, wind-driven gain and loss of biomass corresponding to migrations from upwind habitats and local aerosolization events, respectively. The stochastic fluxes introduced by such gain and loss processes provoke sustained oscillations in the population densities, observed in otherwise stable

systems when subject to demographic noise [61]. These oscillations push individual habitats far from their coexistence fixed point, occasionally driving them to extinction. On a spatial level, the system reaches a new balance between local extinctions and dispersal-mediated migration, leaving a finite fraction of habitats either unpopulated or phage free. Overall, dispersal comes in as a source of instability as well as a driver for global microbial persistence in locally ephemeral habitats. Furthermore, these baseline dynamics are revealed to be crucial for microbial diversity. Even though competitive exclusion applies within individual habitats, conditions exist where, by persisting longer in local habitats, weaker phage strains manage to coexist in the spatial system and even dominate to the detriment of the stronger competitor, that is, indirectly reducing its presence in habitats where the first are not present.

In the framework of the model, inter-specific differentiation in competitive ability and its consequent change in habitat longevity is suggested to be important in allowing multi-species coexistence. This differentiation, however, seems to only be allowed if bounded, qualitatively aligning with the limiting similarity suggested by Tilman [28]. There are, however, a few elements linked to the particularities of the phage–bacteria system of study. (i) Whereas the limiting similarity concept suggests the existence of an upper bound to the fitness distance for species coexistence, we here observe that not only adjacent competitors (in our case the two phage species) are not allowed to be too close, but also too far from each other. We thus find that coexistence is allowed within a fitness interval, that is, there is also a lower bound to the fitness distance. (ii) Within this interval, there is an optimal fitness value, where the number of inhabited habitats by the weaker competitor is maximized. This is, however, not the highest possible value the competitor could have in order to coexist. This introduces the interesting idea of not having a clear evolutionary strategy for the weaker competitor. (iii) The spatial presence of the stronger phage decreases with the presence of the weaker counterpart, even though competitive exclusion applies and competitive dynamics work at a faster time scale than migration. In consequence, competition not only takes place locally, but also via the re-arrangement of the spatial structure.

In the atmosphere, the fate of a microorganism is related to the aerosolization, atmospheric processing and deposition circumstances, such as the drying conditions upon aerosolization or deposition [62], atmospheric temperature and humidity [63–65], salinity (osmostic pressure) [66,67], UV exposure [41] and nutrient availability [35]. All these traits likely represent environmental dispersal filters, a role supported by the suggested non-neutrality of dispersal [40,68–70], affecting the travel distance and survival rates, or the biogeographic connectivity. On top, we note that, despite comparably harsh conditions, the atmosphere has been proposed as a habitat where microorganisms can be metabolically active and grow [71–74] as well as contribute to physical [75–77] and chemical [78,79] transformations, potentially modifying cloud formation processes [76,77,80] and thereby affecting the hydrological cycle [81] and Earth's global energy budget. These are all mechanisms susceptible to affect system-specific parameters such as the typical dispersal distance or the growth rate in a species-dependent manner. Our case study thus constitutes a proof of concept of the role microbial dispersal can play for community longevity and diversity.

Ethics. This work did not require ethical approval from a human subject or animal welfare committee.

Data accessibility. The full spatial model can be found at https://github.com/Mgarrizor/ecology_paper, and has been archived in the Zenodo repository [82].

Declaration of AI use. We have not used AI-assisted technologies in creating this article.

Authors' contributions. M.G.Z.: conceptualization, investigation, methodology, project administration, software, visualization, writing—original draft, writing—review and editing; N.M.: conceptualization, funding acquisition, supervision, writing—review and editing; J.O.H.: conceptualization, funding acquisition, supervision, writing—review and editing.

All authors gave final approval for publication and agreed to be held accountable for the work performed therein.

Conflict of interest declaration. We declare we have no competing interests.

Funding. The authors gratefully acknowledge funding from the Novo Nordisk Foundation Interdisciplinary Synergy Program (grant no. NNF19OC0057374). J.O.H. acknowledges funding by a grant from the VILLUM Foundation (grant no. 13168) and the European Research Council (ERC) under the European Union's Horizon 2020 research and innovation programme (grant no. 771859). N.M. acknowledges funding by the Novo Nordisk Foundation NERD programme (NNF21OC0068775).

Appendix A. Simulation details

A.1. Transport scheme

For our choice of spatial length scale, $\Delta x = 50$ m, and typical diffusion coefficients for phages and bacteria (see caption in table 1), relevant timescales for crossing one habitat boundary are $\sim \Delta x^2/D = 10^8$–10^9 years and thus molecular diffusion can safely be neglected as a dominant transport mechanism. The choice of grid box size implicitly constrains the typical length scale of the phenomenon driving the vertical transport of biomass. We assume vertical transport events among neighbouring columns to be uncorrelated. In order for this assumption to hold the effective length over which a single mixing event takes place should not be bigger, or much smaller, than Δx. Turbulent eddies can vary greatly in size, from millimetres to hundreds of metres, suggesting that, in a more realistic setting, these compartments should be size distributed and their size should change in time. In this work, for simplicity, we assumed they are all of the same size.

A.2. Time step

In practice, we set τ to the numerical time-step when integrating (equation 2.5)–(equation 2.8). This is, $\tau = \Delta t$. With this, in the algorithm, for every time step, we allow for vertical exchange at each column with probability p. This choice reduces the dimensionality of the explored parameter space, since τ is kept fixed throughout the study.

A.3. Numerical scheme

Advection was in principle treated with a Lax–Wendroff scheme and a flux limiter correction to avoid spurious oscillations. However, in order to deal with 'delta-like' peaks from stochastic sources, which created density differences of up to $\sim 10^{12-14}$ in contiguous grid boxes, we decided to instead set the Courant number ($\equiv v \cdot \Delta t/\Delta x$) to unity, a trade-off that allowed us to better advect particles but constrained the time-step, and thus the numerical efficiency. For the time-stepping scheme, we used a fourth-order Runge–Kutta algorithm.

A.4. Initial density profile

The initial density profile of species X is selected by drawing uniformly distributed values from the interval $[0, X^{st})$, where X^{st} is the steady state calculated in equations (B 3) and (B 4).

Appendix B. Lyapunov stable

We here show that the averaged equations (equation 3.1)–(equation 3.2) contain a globally asymptotically stable coexistence fixed point. For clarity, we write population densities in units of the carrying capacity, K, that is, $x \equiv n \cdot K^{-1}$ and $y \equiv m \cdot K^{-1}$. By re-scaling the parameters accordingly, the equation reads as

$$\dot{x} = \tilde{g}x \cdot (1 - x) - \tilde{\eta}xy - \tilde{c}x\,, \tag{B 1}$$

$$\dot{y} = (\tilde{\beta} - 1) \cdot \tilde{\eta}xy - \tilde{\delta}y - \tilde{c}y\ . \tag{B 2}$$

The coexistence fixed points are

$$x^{st} = \frac{\tilde{\delta} + \tilde{c}}{\tilde{\beta}\tilde{\eta}}\,, \tag{B 3}$$

$$\tilde{\eta}y^{st} + \tilde{g}x^{st} = \tilde{g} - \tilde{c}\ . \tag{B.4}$$

A Lyapunov function, $V(x, y)$, exists for int $\mathbb{R}^2_+$. Commonly used trials have the form [60]

$$V(x, y) = H(x^{st}, y^{st}) - H(x, y)\,, \tag{B 5}$$

with

Table 1. The diffusion coefficients used to roughly estimate the travelling time across grid-boxes are $D_n \quad \sqrt{D_{\parallel}^2 + D_{\perp}^2} = 0.17 \times 10^{-12}\,\mathrm{m^2\,s^{-1}}$ [83] for bacteria (*Escherichia coli*) and $D_m = 2.76 \times 10^{-12}\,\mathrm{m^2\,s^{-1}}$ [84] for phages. The decay parameter in the upper layer, $\delta_a \quad 0.01\,\mathrm{min^{-1}}$, is shared among bacteria [63] (*E. coli*) and viruses [33, §2.4]. These parameters have not been picked as an attempt to fully characterize a particular system but to set the typical scales (the order of magnitude of the different rates). For this, we also used $\delta_s \quad 0.005\,\mathrm{h^{-1}}$ [85] (T5-*E. coli* or order of magnitude from table), $\beta \quad 100$ [85] (order of magnitude from table) *E. coli*, $\eta \quad 100 \times 10^{-15}\,\mathrm{m^3\,h^{-1}}$ [85] (order of magnitude from table) *E. coli*. For the growth rate and the carrying capacity, we assume the system to be embedded in an ocean-like context in terms of nutrient availability; with this in mind, we set $K \quad 10^6\,\mathrm{ml^{-1}} = 10^{12}\,\mathrm{m^{-3}}$ and $g \quad 0.5\,\mathrm{d^{-1}}$[86–89].

system-specific parameters					
K ($\mathrm{m^{-3}}$)	β	g ($\mathrm{d^{-1}}$)	η ($\mathrm{m^3\,d}$)	δs ($\mathrm{d^{-1}}$)	δa ($\mathrm{d^{-1}}$)
10^{12} [86–89]	100 [85]	0.5 [86–89]	2.14×10^{-12} [85]	0.12 [85]	864 [33,63]
spatial parameters					
Δx (m)	Δt (s)	N_x	N_y	v ($\mathrm{m\,s^{-1}}$)	τ (s)
50	50	1000	2	1	Δt

$$H(x, y) = x^{st} log(x) - x + y^{st} log(y) - y \ . \tag{B.6}$$

With this choice equation (B 5) is definite positive and $V(\vec{x}^{st}) = 0$. By making the slight modification

$$H(x, y) = x^{st} \log(x) - x + \frac{1}{\tilde{\beta} - 1}(y^{st} \log(y) - y)\,, \tag{B.7}$$

we can see that $\dot{V}(\vec{x}^{st}) < 0 \ \forall \ \vec{x} \in \mathbb{R}_+^2 - \{\vec{x}^{st}\}$. Given that

$$\frac{\partial V}{\partial x} = 1 - \frac{x^{st}}{x}\,, \tag{B.8}$$

$$\frac{\partial V}{\partial y} = \frac{1}{\tilde{\beta} - 1} \cdot \left(1 - \frac{y^{st}}{y}\right), \tag{B 9}$$

we have

$$\begin{aligned} \dot{V} &= (x - x^{st}) \cdot (\tilde{g}(1 - x) - \tilde{\eta} y - \tilde{c}) \\ &+ (y - y^{st}) \cdot ((\tilde{\beta} - 1) \cdot \tilde{\eta} x - \tilde{\eta} - \tilde{c}) \cdot \frac{1}{\tilde{\beta} - 1} \\ &= -\tilde{g} \cdot (x - x^{st})^2 \ . \end{aligned} \tag{B 10}$$

In the last equality, we used (equation B 3) and (equation B 4). The coexistence fixed point is therefore globally asymptotically stable.

Appendix C. LSA of the well-mixed system

System (equation 2.1)–(equation 2.2), which we shall label as 'well-mixed', is known to have a coexistence fixed point:

$$n_s^{st} = \frac{\delta_s}{\eta(\beta - 1)}\,, \tag{C 1}$$

$$m_s^{st} = \frac{g}{\eta}\left(1 - \frac{n^{st}}{K}\right), \tag{C 2}$$

which is globally stable (appendix B) when feasible, that is, $n^{st} < K$.[1] Upon a small perturbation, the transient relaxation to the fixed point can be described as a stable spiral with a decay time scale of

[1]The prey population required to sustain the predator is smaller than the system's carrying capacity.

~ 21.7 years and an oscillation period of ~ 25 days. This can be seen from a linear stability analysis. The Jacobian is

$$\begin{pmatrix} g(1-2n_s/K)-\eta m_s & -\eta n_s \\ (\beta-1)\eta m_s & 0 \end{pmatrix}, \tag{C 3}$$

from which we obtain the eigenvalues, λ_i. Given the system parameters (see appendix A, table 1) the eigenvalues are complex:

$$\lambda_i = \gamma \pm i\omega \ . \tag{C 4}$$

Here $\gamma = -\frac{1}{2}g\alpha$ and $\omega = \frac{1}{2}\sqrt{4\eta\delta_s m_s^{st}}$, with $\alpha = n_s^{st}/K$. This classifies the fixed point as a stable spiral with an oscillation period of

$$T = \frac{2\pi}{\omega} = 0.07 \text{ years} \sim 25 \text{ days}, \tag{C 5}$$

and a time scale for the decay of small perturbations of

$$\tau_{per} = \frac{1}{|\beta|} \sim 21.7 \text{ years}. \tag{C 6}$$

Equations (3.1)–(3.2) can be mapped to system (2.1)–(2.2) with an effective growth rate

$$g^{eff.} = g - pj_0 \ , \tag{C 7}$$

carrying capacity

$$K^{eff.} = \frac{g}{(g-pj_0)\cdot K} \ , \tag{C 8}$$

and phage's decay rate

$$\delta_s^{eff.} = \delta_s + pj_0 \ . \tag{C 9}$$

Consequently, this analysis also applies to system (3.1)–(3.2).

Appendix D. Phage-free survival limit

In the absence of bacteriophages and any sort of spatial structure (and therefore any grid-scale transport scheme), the bacterial density will, in its logistic growth, asymptotically reach the carrying capacity, K. However, when allowed to vertically move across layers a new contribution behaving as a sink might keep the system from reaching a finite density fixed point. This is the first layer of complexity with respect to the 0-dimensional well-mixed case, that is, two 'vertically' aligned grid points where only bacteria are present and vertical transport fluxes are continuous. Analogously to (equation 3.1)–(equation 3.2), the system reads as

$$\frac{\mathrm{d}n_a(t)}{\mathrm{d}t} = -\delta_a n_a + pj_0(n_s - n_a), \tag{D 1}$$

$$\frac{\mathrm{d}n_s(t)}{\mathrm{d}t} = gn_s\left(1-\frac{n_s}{K}\right) - pj_0(n_s - n_a) \ . \tag{D 2}$$

The steady state is

$$n_a^{st} = \frac{g}{\delta_a} n_s^{st}\left(1-\frac{n_s^{st}}{K}\right), \tag{D.3}$$

$$n_s^{st} = \left(1 - \frac{\delta_a \cdot pj_0}{(\delta_a + pj_0)\cdot g}\right)\cdot K \ . \tag{D.4}$$

This yields an extra limit to the feasibility of coexistence:

$$\frac{\delta_a \cdot pj_0}{(\delta_a + pj_0)} < g \ , \tag{D 5}$$

in this case, exclusively related to the capability of bacteria to survive on their own.

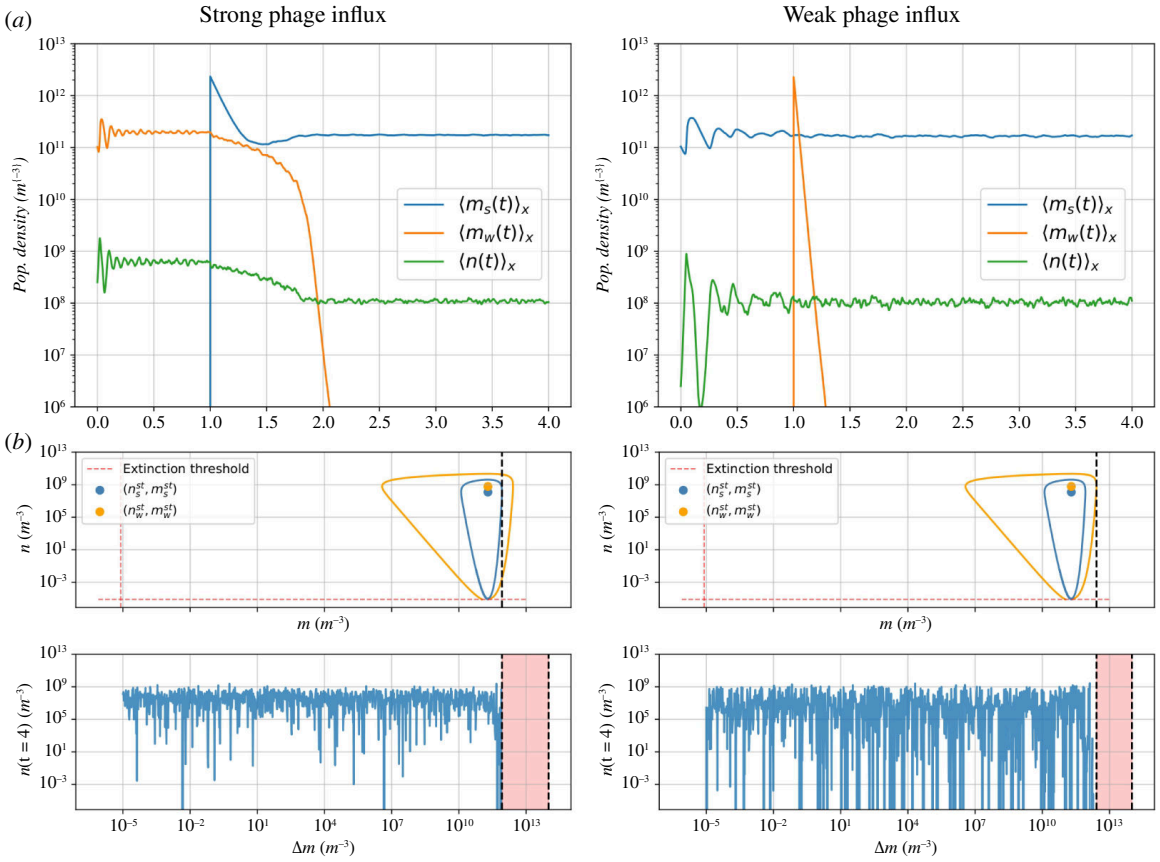

Figure 7. Two phages experiment. (*a*) Ensemble average of independent single habitats. At $t = 1$ year, a different migrated phage quantity, Δm, arrives at each habitat—in all cases, the stronger phage takes over. (*b*) Bacterial population densities at $t = 4$ years as a function of the migrated population, Δm. Each point is an independent habitat. On top, we draw the respective critical trajectories and fixed points for weaker and stronger phages.

Appendix E. Migration experiments

Migration into a downstream habitat: 2 phages case. Here, we study the sytem's response to positive fluxes for the following cases: (i) the stronger phage migrates into a *C* habitat inhabited by the weaker phage; (ii) the weaker phage migrates into a *C* habitat inhabited by the stronger phage. As expected, competitive exclusion applies, that is, the stronger phage dominates on both scenarios, as depicted in figure 7*a*. However, the critical trajectory of the migrating phage determines a value over which the host's population density is doomed to cross the extinction threshold, and thus the whole habitat becomes extinct, as seen in figure 7*b*. This introduces the possibility for the weaker phage to drive its competitor to extinction.

Appendix F. Signal length

Operational definition: To study the effect of local connectivity without interfering with the vertical biomass scheme, one could fine-tune the δ_a parameter. Let us define the signal length, L, as the maximum distance travelled by a biomass emission of magnitude equal to the system's carrying capacity, K, in the $p = 0$ case. From the tendency equation

$$n(t) = Ke^{-\delta\alpha T}, \tag{F 1}$$

$$t^* = L \cdot N \cdot \Delta t = -\frac{1}{\delta_a} \cdot \ln\left(\frac{\rho_{ext}}{K}\right). \tag{F 2}$$

From this, we obtain L. A schematic illustration is depicted in figure 8. This is the definition of signal length that we shall use in the main text (§3.1.2.1). It is of importance to have in mind that only same pair (p, j_0) cases can be compared when studying the ecological effects of the system's connectivity, L.

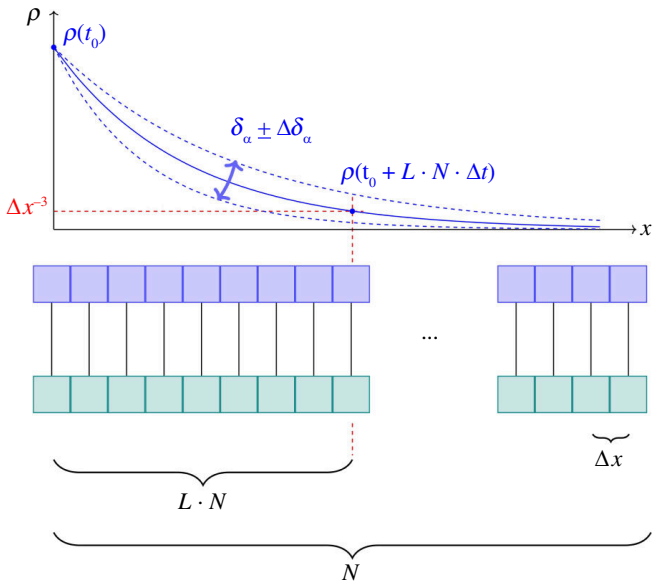

Figure 8. Signal length. Diagram of the system parameters relevant to define a given signal length, L, and the effect of the decay rate, δ_a.

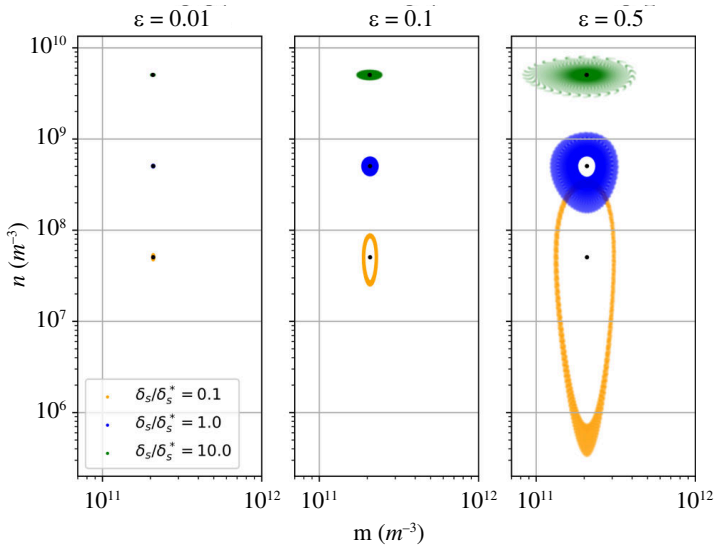

Figure 9. The effect of competitive traits. Response to different biomass influx of three independent single-habitat phage–bacteria systems with distinct parasite intrinsic fitness. This is here measured from the phage's decay rate in the surface, δ_s, which takes the values [0.1, 1, 10] (expressed in units of the experimental value δ_s^* [85]). In each system, either species density, x, is initialized as $x(0) = (1 + \epsilon) \cdot x^{st}$ for $\epsilon = 0.01, 0.1, 0.5$ (panels from left to right, respectively) and integrated for the same time.

Appendix G. Amplitude of oscillations

The amplitude of the transient oscillatory behaviour back to the steady state is a function of the system's deterministic parameters. Here, we explore, in an illustrative manner, how it depends on the values of the phage's decay rate in the surface layer, δ_s. In figure 9, we see that, for lower values of the decay rate, and thus higher competitive ability, the oscillations approach the bacterial population density extinction threshold. This is taken as a sign for the decrease in stability of habitats with stronger viruses figure 9.

References

1. Falkowski PG, Fenchel T, Delong EF. The microbial engines that drive Earth's biogeochemical cycles. See https://www.science.org/.
2. Pomeroy L, Williams PB, Azam F, Hobbie J. 2007 The microbial loop. *Oceanography* **20**, 28–33. (doi:10.5670/oceanog.2007.45)

3. Azam F, Fenchel T, Field JG, Gray JS, Meyer-Reil LA, Thingstad F. 1983 The ecological role of water-column microbes in the sea. *Mar. Ecol. Prog. Ser.* **10**, 257–263. (doi:10.3354/meps010257)
4. Whitman WB, Coleman DC, Wiebe WJ. 1998 Prokaryotes: the unseen majority. *Proc. Natl Acad. Sci. USA* **95**, 6578–6583. (doi:10.1073/pnas.95.12.6578)
5. Suttle CA. 2007 Marine viruses—major players in the global ecosystem. *Nat. Rev. Microbiol.* **5**, 801–812. (doi:10.1038/nrmicro1750)
6. Breitbart M, Rohwer F. 2005 Here a virus, there a virus, everywhere the same virus? *Trends Microbiol.* **13**, 278–284. (doi:10.1016/j.tim.2005.04.003)
7. Breitbart M, Bonnain C, Malki K, Sawaya NA. 2018 Phage puppet masters of the marine microbial realm. *Nat. Microbiol.* **3**, 754–766. (doi:10.1038/s41564-018-0166-y)
8. Munn CB. 2006 Viruses as pathogens of marine organisms—from bacteria to whales. *J. Mar. Biol. Assess.* **86**, 453–467. (doi:10.1017/S002531540601335X)
9. Weinbauer MG, Rassoulzadegan F. 2004 Are viruses driving microbial diversification and diversity? *Environ. Microbiol.* **6**, 1–11. (doi:10.1046/j.1462-2920.2003.00539.x)
10. Hewson I, Winget DM, Williamson KE, Fuhrman JA, Wommack KE. 2006 Viral and bacterial assemblage covariance in oligotrophic waters of the West Florida Shelf (Gulf of Mexico). *J. Mar. Biol. Assess.* **86**, 591–603. (doi:10.1017/S0025315406013506)
11. Thingstad TF. 2000 Elements of a theory for the mechanisms controlling abundance, diversity, and biogeochemical role of lytic bacterial viruses in aquatic systems. *Limnol. Oceanogr.* **45**, 1320–1328. (doi:10.4319/lo.2000.45.6.1320)
12. Haerter JO, Mitarai N, Sneppen K. 2014 Phage and bacteria support mutual diversity in a narrowing staircase of coexistence. *ISME J.* **8**, 2317–2326. (doi:10.1038/ismej.2014.80)
13. Howard-Varona C *et al*. 2020 Phage-specific metabolic reprogramming of virocells. *ISME J.* **14**, 881–895. (doi:10.1038/s41396-019-0580-z)
14. Wommack KE, Colwell RR. 2000 Virioplankton: viruses in aquatic ecosystems. *Microbiol. Mol. Biol. Rev.* **64**, 69–114. (doi:10.1128/MMBR.64.1.69-114.2000)
15. Zimmerman AE, Howard-Varona C, Needham DM, John SG, Worden AZ, Sullivan MB, Waldbauer JR, Coleman ML. 2020 Metabolic and biogeochemical consequences of viral infection in aquatic ecosystems. *Nat. Rev. Microbiol.* **18**, 21–34. (doi:10.1038/s41579-019-0270-x)
16. Rosenwasser S, Ziv C, Creveld S van, Vardi A. 2016 Virocell metabolism: metabolic innovations during host-virus interactions in the ocean. *Trends Microbiol.* **24**, 821–832. (doi:10.1016/j.tim.2016.06.006)
17. Fuhrman JA. 1999 Marine viruses and their biogeochemical and ecological effects. *Nature* **399**, 541–548. (doi:10.1038/21119)
18. Wilhelm SW, Suttle CA. 1999 Viruses and nutrient cycles in the sea. *BioScience* **49**, 781–788. (doi:10.2307/1313569)
19. Middelboe M, Jørgensen NOG. 2006 Viral lysis of bacteria: an important source of dissolved amino acids and cell wall compounds. *J. Mar. Biol. Assess.* **86**, 605–612. (doi:10.1017/S0025315406013518)
20. Lønborg C, Middelboe M, Brussaard CPD. 2013 Viral lysis of Micromonas pusilla: impacts on dissolved organic matter production and composition. *Biogeochemistry* **116**, 231–240. (doi:10.1007/s10533-013-9853-1)
21. Shelford EJ, Middelboe M, Møller EF, Suttle CA. 2012 Virus-driven nitrogen cycling enhances phytoplankton growth. *Aquat. Microb. Ecol.* **66**, 41–46. (doi:10.3354/ame01553)
22. Poorvin L, Rinta-Kanto JM, Hutchins DA, Wilhelm SW. 2004 Viral release of iron and its bioavailability to marine plankton. *Limnol. Oceanogr.* **49**, 1734–1741. (doi:10.4319/lo.2004.49.5.1734)
23. Gobler CJ, Hutchins DA. 1997 Release and bioavailability of C, N, P Se, and Fe following viral lysis of a marine chrysophyte. *Limnol. Oceanogr.* **42**, 1492–1504. (doi:10.4319/lo.1997.42.7.1492)
24. Moebus K, Nattkemper H. 1981 Bacteriophage sensitivity patterns among bacteria isolated from marine waters. *Helgoländer Meeresunters.* **34**, 375–385. (doi:10.1007/BF02074130)
25. Flores CO, Valverde S, Weitz JS. 2013 Multi-scale structure and geographic drivers of cross-infection within marine bacteria and phages. *ISME J.* **7**, 520–532. (doi:10.1038/ismej.2012.135)
26. Kauffman KM, Chang WK, Brown JM, Hussain FA, Yang J, Polz MF, Kelly L. 2022 Resolving the structure of phage-bacteria interactions in the context of natural diversity. *Nat. Commun.* **13**, 372. (doi:10.1038/s41467-021-27583-z)
27. Hardin G. 1960 The competitive exclusion principle. *Science* **131**, 1292–1297. (doi:10.1126/science.131.3409.1292)
28. Tilman D. 1994 Competition and biodiversity in spatially structured habitats. *Ecology* **75**, 2–16. (doi:10.2307/1939377)
29. Bonsall MB, French DR, Hassell MP. 2002 Metapopulation structures affect persistence of predator–prey interactions. *J. Anim. Ecol.* **71**, 1075–1084. (doi:10.1046/j.1365-2656.2002.00670.x)
30. Holyoak M, Lawler SP. 1996 Persistence of an extinction-prone predator-prey interaction through metapopulation dynamics. *Ecology* **77**, 1867–1879. (doi:10.2307/2265790)
31. Kellogg CA, Griffin DW. 2006 Aerobiology and the global transport of desert dust. *Trends Ecol. Evol*. **21**, 638–644. (doi:10.1016/j.tree.2006.07.004)
32. Griffin DW, Kellogg CA, Garrison VH, Lisle JT, Borden TC, Shinn EA. 2003 Atmospheric microbiology in the northern Caribbean during African dust events. *Aerobiologia* **19**, 143–157. (doi:10.1023/B:AERO.0000006530.32845.8d)
33. Després VR *et al*. 2012 Primary biological aerosol particles in the atmosphere: a review. *Tellus B* **64**, 15598. (doi:10.3402/tellusb.v64i0.15598)
34. Burrows SM, Butler T, Jöckel P, Tost H, Kerkweg A, Pöschl U, Lawrence MG. 2009 Bacteria in the global atmosphere—Part 2: modeling of emissions and transport between different ecosystems. *Atmos. Chem. Phys.* **9**, 9281–9297. (doi:10.5194/acp-9-9281-2009)

35. Šantl-Temkiv T, Amato P, Casamayor EO, Lee PKH, Pointing SB. 2022 Microbial ecology of the atmosphere. *FEMS Microbiol. Rev.* **46**, fuac009. (doi:10.1093/femsre/fuac009)
36. Matias MG, Mouquet N, Chase JM. 2013 Dispersal stochasticity mediates species richness in source–sink metacommunities. *Oikos* **122**, 395–402. (doi:10.1111/j.1600-0706.2012.20479.x)
37. Jones SE, Newton RJ, McMahon KD. 2008 Potential for atmospheric deposition of bacteria to influence bacterioplankton communities. *FEMS Microbiol. Ecol.* **64**, 388–394. (doi:10.1111/j.1574-6941.2008.00476.x)
38. Hoose C, Kristjánsson JE, Burrows SM. 2010 How important is biological ice nucleation in clouds on a global scale? *Environ. Res. Lett.* **5**, 024009. (doi:10.1088/1748-9326/5/2/024009)
39. Spracklen DV, Heald CL. 2014 The contribution of fungal spores and bacteria to regional and global aerosol number and ice nucleation immersion freezing rates. *Atmos. Chem. Phys.* **14**, 9051–9059. (doi:10.5194/acp-14-9051-2014)
40. Lowe WH, McPeek MA. 2014 Is dispersal neutral? *Trends Ecol. Evol.* **29**, 444–450. (doi:10.1016/j.tree.2014.05.009)
41. Tong Y, Lighthart B. Effect of simulated solar radiation on mixed outdoor atmospheric bacterial populations. *FEMS Microbiol. Ecol.* **26**, 311–316. (doi:10.1111/j.1574-6941.1998.tb00515.x)
42. Levin BR, Stewart FM, Chao L. 1977 Resource-limited growth, competition, and predation: a model and experimental studies with bacteria and bacteriophage. *Am. Nat.* **111**, 3–24. (doi:10.1086/283134)
43. Hobbs Z, Abedon ST. 2016 Diversity of phage infection types and associated terminology: the problem with 'lytic or lysogenic'. *FEMS Microbiol. Lett.* **363**, fnw047. (doi:10.1093/femsle/fnw047)
44. Seymour JR, Seuront L, Doubell M, Waters RL, Mitchell JG. 2006 Microscale patchiness of virioplankton. *J. Mar. Biol. Assess.* **86**, 551–561. (doi:10.1017/S0025315406013464)
45. Simon M, Grossart HP, Schweitzer B, Ploug H. 2002 Microbial ecology of organic aggregates in aquatic ecosystems. *Aquat. Microb. Ecol.* **28**, 175–211. (doi:10.3354/ame028175)
46. Carreira C, Larsen M, Glud RN, Brussaard CPD, Middelboe M. 2013 Heterogeneous distribution of prokaryotes and viruses at the microscale in a tidal sediment. *Aquat. Microb. Ecol.* **69**, 183–192. (doi:10.3354/ame01639)
47. Dann LM, Paterson JS, Newton K, Oliver R, Mitchell JG. 2016 Distributions of virus-like particles and prokaryotes within microenvironments. *PLoS ONE* **11**, e0146984. (doi:10.1371/journal.pone.0146984)
48. Eriksen RS, Svenningsen SL, Sneppen K, Mitarai N. 2018 A growing microcolony can survive and support persistent propagation of virulent phages. Proc. Natl Acad. Sci. USA **115**, 337–342. (doi:10.1073/pnas.1708954115)
49. Eriksen RS, Mitarai N, Sneppen K. 2020 Sustainability of spatially distributed bacteria-phage systems. *Sci. Rep.* **10**, 3154. (doi:10.1038/s41598-020-59635-7)
50. Sneppen K. 2014 Competition and diversity. In *Models of life*, pp. 242–278. Cambridge, UK: Cambridge University Press. (doi:10.1017/CBO9781107449442)
51. Wilkinson DM, Koumoutsaris S, Mitchell EAD, Bey I. 2012 Modelling the effect of size on the aerial dispersal of microorganisms. *J. Biogeogr.* **39**, 89–97. (doi:10.1111/j.1365-2699.2011.02569.x)
52. Gillette DA, Passi R. 1988 Modeling dust emission caused by wind erosion. *J. Geophys. Res.* **93**, 14233–14242. (doi:10.1029/JD093iD11p14233)
53. Ginoux P, Chin M, Tegen I, Prospero JM, Holben B, Dubovik O, Lin S. 2001 Sources and distributions of dust aerosols simulated with the GOCART model. *J. Geophys. Res. Atmos.* **106**, 20255–20273. (doi:10.1029/2000JD000053)
54. Foken T. 2017 *Micrometeorology*, 2nd edn. Berlin, Germany: Springer-Verlag. See http://link.springer.com/10.1007/978-3-642-25440-6
55. Michaud JM *et al*. 2018 Taxon-specific aerosolization of bacteria and viruses in an experimental ocean-atmosphere mesocosm. *Nat. Commun.* **9**, 2017. (doi:10.1038/s41467-018-04409-z)
56. Rastelli E *et al*. 2017 Transfer of labile organic matter and microbes from the ocean surface to the marine aerosol: an experimental approach. *Sci. Rep.* **7**, 11475. (doi:10.1038/s41598-017-10563-z)
57. Reche I, D'Orta G, Mladenov N, Winget DM, Suttle CA. 2018 Deposition rates of viruses and bacteria above the atmospheric boundary layer. *ISME J.* **12**, 1154–1162. (doi:10.1038/s41396-017-0042-4)
58. Woo C, Yamamoto N. 2020 Falling bacterial communities from the atmosphere. *Environ. Microbiome* **15**, 22. (doi:10.1186/s40793-020-00369-4)
59. Moore RA, Hanlon R, Powers C, Schmale DG, Christner BC. 2020 Scavenging of sub-micron to micron-sized microbial aerosols during simulated rainfall. *Atmosphere* **11**, 80. (doi:10.3390/atmos11010080)
60. Hofbauer J, Sigmund K. 1988 *The theory of evolution and dynamical systems: mathematical aspects of selection*. New York, NY: Cambridge University Press.
61. McKane AJ, Newman TJ. 2005 Predator-prey cycles from resonant amplification of demographic stochasticity. *Phys. Rev. Lett.* **94**, 218102. (doi:10.1103/PhysRevLett.94.218102)
62. Alsved M *et al*. 2018 Effect of aerosolization and drying on the viability of *Pseudomonas syringae* cells. *Front. Microbiol.* **9**, 3086. (doi:10.3389/fmicb.2018.03086)
63. Jiang G, Ma J, Wang C, Wang Y, Laghari AA. 2022 Kinetics and mechanism analysis on self-decay of airborne bacteria:biological and physical decay under different temperature. *Sci. Total Environ.* **832**, 155033. (doi:10.1016/j.scitotenv.2022.155033)
64. Tang JW. 2009 The effect of environmental parameters on the survival of airborne infectious agents. *J. R. Soc. Interface* **6**, S737–S746. (doi:10.1098/rsif.2009.0227.focus)
65. Verreault D, Marcoux-Voiselle M, Turgeon N, Moineau S, Duchaine C. 2015 Resistance of aerosolized bacterial viruses to relative humidity and temperature. *Appl. Environ. Microbiol.* **81**, 7305–7311. (doi:10.1128/AEM.02484-15)

66. Angle KJ *et al*. 2021 Acidity across the interface from the ocean surface to sea spray aerosol. *Proc. Natl Acad. Sci. USA* **118**, e2018397118. (doi:10.1073/pnas.2018397118)
67. Sugawara S, Sato T, Minamiyama T, Neale FE, Cusack NE, Ewing CT. 1982 Factors controlling the acidity of natural rainwater
68. Archer S *et al*. Global biogeography of atmospheric microorganisms reflects diverse recruitment and environmental filtering. *In Review*.
69. Tignat-Perrier R, Dommergue A, Thollot A, Magand O, Amato P, Joly M, Sellegri K, Vogel TM, Larose C. 2020 Seasonal shift in airborne microbial communities. *Sci. Total Environ.* **716**, 137129. (doi:10.1016/j.scitotenv.2020.137129)
70. Cáliz J, Triadó-Margarit X, Camarero L, Casamayor EO. 2018 A long-term survey unveils strong seasonal patterns in the airborne microbiome coupled to general and regional atmospheric circulations. *Proc. Natl Acad. Sci. USA* **115**, 12229–12234. (doi:10.1073/pnas.1812826115)
71. Womack AM, Bohannan BJM, Green JL. 2010 Biodiversity and biogeography of the atmosphere. *Philos. Trans. R. Soc. Lond. B* **365**, 3645–3653. (doi:10.1098/rstb.2010.0283)
72. Sattler B, Puxbaum H, Psenner R. 2001 Bacterial growth in supercooled cloud droplets. *Geophys. Res. Lett.* **28**, 239–242. (doi:10.1029/2000GL011684)
73. Klein AM, Bohannan BJM, Jaffe DA, Levin DA, Green JL. 2016 Molecular evidence for metabolically active bacteria in the atmosphere. *Front. Microbiol.* **7**, 772. (doi:10.3389/fmicb.2016.00772)
74. Amato P, Parazols M, Sancelme M, Laj P, Mailhot G, Delort AM. 2007 Microorganisms isolated from the water phase of tropospheric clouds at the Puy de Dôme: major groups and growth abilities at low temperatures. *FEMS Microbiol. Ecol.* **59**, 242–254. (doi:10.1111/j.1574-6941.2006.00199.x)
75. Maki LR, Galyan EL, Chang-Chien MM, Caldwell DR. 1974 Ice nucleation induced by *Pseudomonas syringae*. *Appl. Microbiol.* **28**, 456–459. (doi:10.1128/am.28.3.456-459.1974)
76. Lazaridis M. 2019 Bacteria as cloud condensation nuclei (CCN) in the atmosphere. *Atmosphere* **10**, 786. (doi:10.3390/atmos10120786)
77. Möhler O, DeMott PJ, Vali G, Levin Z. 2007 Microbiology and atmospheric processes: the role of biological particles in cloud physics. *Biogeosciences* **4**, 1059–1071. (doi:10.5194/bg-4-1059-2007)
78. Khaled A, Zhang M, Amato P, Delort AM, Ervens B. 2021 Biodegradation by bacteria in clouds: an underestimated sink for some organics in the atmospheric multiphase system. *Atmos. Chem. Phys*. **21**, 3123–3141. (doi:10.5194/acp-21-3123-2021)
79. Delort AM, Vaïtilingom M, Amato P, Sancelme M, Parazols M, Mailhot G, Laj P, Deguillaume L. 2010 A short overview of the microbial population in clouds: potential roles in atmospheric chemistry and nucleation processes. *Atmos. Res.* **98**, 249–260. (doi:10.1016/j.atmosres.2010.07.004)
80. Hu W, Niu H, Murata K, Wu Z, Hu M, Kojima T, Zhang D. 2018 Bacteria in atmospheric waters: detection, characteristics and implications. *Atmos. Environ.* **179**, 201–221. (doi:10.1016/j.atmosenv.2018.02.026)
81. Morris CE, Conen F, Alex Huffman J, Phillips V, Pöschl U, Sands DC. 2014 Bioprecipitation: a feedback cycle linking earth history, ecosystem dynamics and land use through biological ice nucleators in the atmosphere. *Glob. Chang. Biol.* **20**, 341–351. (doi:10.1111/gcb.12447)
82. Garrido M. 2023 Mgarrizor/ecology_paper: eco_submit (v1.0.0). Zenodo. https://doi.org/10.5281/zenodo.8344181
83. Tavaddod S, Charsooghi MA, Abdi F, Khalesifard HR, Golestanian R. 2011 Probing passive diffusion of flagellated and deflagellated *Escherichia coli*. *Eur. Phys. J. E* **34**, 16. (doi:10.1140/epje/i2011-11016-9)
84. Moldovan R, Chapman-McQuiston E, Wu XL. 2007 On kinetics of phage adsorption. *Biophys. J.* **93**, 303–315. (doi:10.1529/biophysj.106.102962)
85. De Paepe M, Taddei F. 2006 Viruses' life history: towards a mechanistic basis of a trade-off between survival and reproduction among phages. *PLoS Biol.* **4**, e193. (doi:10.1371/journal.pbio.0040193)
86. Huete-Stauffer TM, Arandia-Gorostidi N, Díaz-Pérez L, Morán XAG. 2015 Temperature dependences of growth rates and carrying capacities of marine bacteria depart from metabolic theoretical predictions. *FEMS Microbiol. Ecol.* **91**, fiv111. (doi:10.1093/femsec/fiv111)
87. Fuhrman JA, Noble RT. 1995 Viruses and protists cause similar bacterial mortality in coastal seawater. *Limnol. Oceanogr.* **40**, 1236–1242. (doi:10.4319/lo.1995.40.7.1236)
88. Silva L, Calleja ML, Huete-Stauffer TM, Ivetic S, Ansari MI, Viegas M, Morán XAG. 2018 Low abundances but high growth rates of coastal heterotrophic bacteria in the red sea. *Front. Microbiol.* **9**, 3244. (doi:10.3389/fmicb.2018.03244)
89. Kirchman DL. 2016 Growth rates of microbes in the oceans. *Ann. Rev. Mar. Sci.* **8**, 285–309. (doi:10.1146/annurev-marine-122414-033938)

3 A regional study on the Asian tiger mosquito, *Aedes Albopictus*

3.1 Synopsis

3.1.1 Introduction

In this chapter we study an **insect** of the **order** *Diptera* (di- "two", pteron "wing", or, in the common language, fly) and **family** *Culicidae*, *i.e.,* a mosquito (small *mosca*, or fly, from Portuguese and Spanish). Mosquitoes have a complex life cycle, comprising 4 distinct stages: egg, larva, pupa and adult. The first three are aquatic stages, whereas the last is mostly "aereal". Eggs are laid by adult mosquitoes in water bodies with specific characteristics, such as odour, taste, flow or shade, either at the surface or the edge of the body, depending on the species [48]. When eggs hatch, motile larvae emerge to feed, being capable of inter- [49] and intra-specific [49, 50] predation, and grow until they become pupae. The future adult develops within and, when fully formed, emerges as the pupa floats in the surface. Some mosquitoes are capable to enter a state of dormancy known as diapause [51], which has been observed at different developmental stages, depending on the species. Diapause is triggered by adverse environmental conditions, such as drought or short photoperiods [51]. Upon re-activation, triggered in return by some advantageous environmental factor, *e.g.*, a long enough photoperiod [52], indicating the end of winter and beginning of spring, development continues, providing the mosquito, in this case, with an overwinter mechanism.

From this description one can realize that environmental variables, such as near-surface air temperature, water temperature, rainfall (marking the potential creation of temporary water bodies) or solar irradiation may be

used as proxies to describe the dynamics of the mosquito in its different life stages. Indeed, many studies use this information to build models that help us understand the current and future geographic distribution as well as the temporal dynamics of diverse mosquitoes [52–55], most of which act as vectors of disease, such as malaria [56], posing a significant risk to public health. Let us now focus on the topic of this study.

The mosquito *Aedes albopictus* (Skuse, 1894) (Genus: *Aedes*, species: *Aedes albopictus*), commonly known as the Asian tiger mosquito, originates in tropical and subtropical forested areas of the Asian southeast [57]. Globalization has, however, enabled this mosquito to successfully colonize all continents except Antarctica [58], including temperate regions of North America [59] and Europe [60]. Given its role as capable vector of diverse arboviruses such as dengue (DENV) [5], Zika (ZIKV) [6] and chikungunya (CHIKV) [7], understanding the geographical distribution and activity of the arthropod constitutes an important challenge, relevant for public health activities such as the design of guided intervention strategies.

Similar to other diptera the tiger mosquito's life cycle, including the larval and the gonotrophic (egg development within the adult) cycles, is affected by local climatic conditions, such as the availability of rain-fed temporary ponds and near-surface air temperature. In this chapter we used a regional climate-aware dynamical model of the ecology of *Ae. albopictus* to tackle climate-related problems. The region of study is Italy during the years 1980-2023, with the possibility to extrapolate the tools developed here to other regions.

3.1.2 Objectives

In particular, the goal of this study was four-fold:

0.- Adapting the model to the Asian tiger mosquito: The dynamical model used in this study was initially formulated for *Anopheles gambiae s.s.* and the associated *P. falciparum* parasite. The model structure is however generic to other mosquito species and we here adapted it to describe temperate *Aedes albopictus* populations. This adaptation exercise has successfully been performed before [54] and encompassed the re-evaluation of model parameters

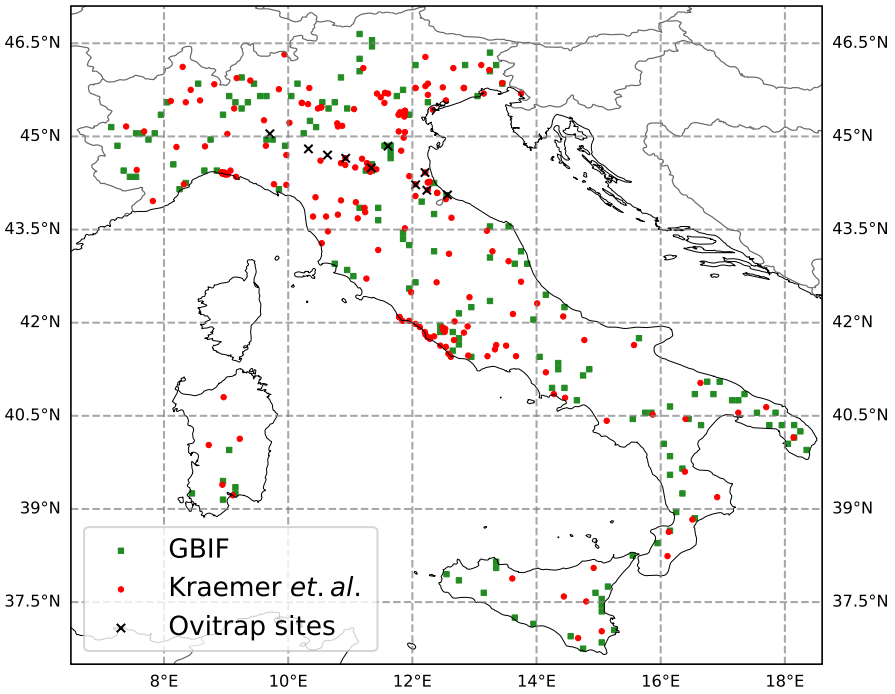

Figure 3.1: (Ovi)trap sites used in the model calibration (black crosses) and occurrence data derived from the data bases [65] (red circles) and [66] (green squares).

and implementation of temperature-driven and vector-specific mortality rates for adult vectors, larvae and eggs.

1.- Calibration and validation: The model contains a set of mosquito-related parameters that can be constrained by field and laboratory observations. These, nevertheless, have a remaining range of uncertainty which can be exploited to perform a constrained optimization employing the genetic algorithm (GA) developed in [61]. During the optimization process parameter values are sampled within their uncertainty range to minimize the difference between a chosen model's output and an observation database, in this case, temporal egg data collected by a network of traps spread across ten Italian cities in the Emilia-Romagna region [62–64]. This is the calibration step. Once calibrated, the model was validated against the same temporal database as well as against spatial information on the presence of the vector in the region of study. The spatial occurrence information was obtained from the two databases [65, 66] (Fig. 3.1). Once validated we addressed climate-related questions.

2.- Average and long-term behaviour: What is the geographical distribution and average density of the vector? What is the activity season duration and is this length changing in time as a consequence of climate change?

3.- Short-term response to heatwaves: What is the impact of extreme heatwave events on the behaviour of the vector? Are these warm events beneficial or detrimental for the population of the mosquito?

3.1.3 Methods

The dynamical model used in this study is the VECtor-borne disease community model of ICTP, TRIeste (VECTRI) [53]. The model was initially developed for *Anopheles gambiae* and *P. falciparum* malaria [67–69] and has been, in this study, adapted for *Ae. albopictus*. At any particular location, the dynamics of the mosquito in its adult (V), egg (E) and larval (L) stages is modelled as the set of coupled differential equations

$$\frac{dE(t)}{dt} = N_{egg} \cdot R_{gono}(T_{2m}) \cdot V(t) - \delta_E(T_{wat}) \cdot E(t) - g_E \cdot E(t) \ , \tag{3.1}$$

$$\frac{\partial L(f,t)}{\partial t} = [f = 0] \cdot g_E \cdot E(t) - \delta_L(T_{wat}) \cdot L(f,t) - \delta_{crowd}(R_d, L) \cdot L(f,t) - R_L(T_{wat}) \cdot \frac{\partial L(f,t)}{\partial f} \ , \tag{3.2}$$

$$\frac{dV(t)}{dt} = R_L(T_{wat}) \cdot \left.\frac{\partial L(f,t)}{\partial f}\right|_{f=1} - \delta_V(T_{2m}) \cdot V(t) \ . \tag{3.3}$$

Here, N_{egg} is the average number of laid eggs per batch that result in female vectors, R_{gono} the rate of the gonotrophic cycle, δ_i decay rates associated to temperature (E, V and L) and crowding effects ($crowd$), g_E the egg hatching rate, $[*]$ the Iverson bracket with f describing the fractional developmental stage of larvae, whose evolution is modelled as an advection equation along f, bounded to $[0, 1]$, and R_L the advection velocity of larvae development. The dependencies T_{2m}, T_{wat} and R_d are the two-metre air temperature ($^\circ C$), the pond water temperature ($^\circ C$) and the daily rainfall (mm/day), respectively. The model is summarized in the schematics of Fig. (3.2). For numerical treatment, the fractional development stage interval, $[0, 1]$, is discretized into

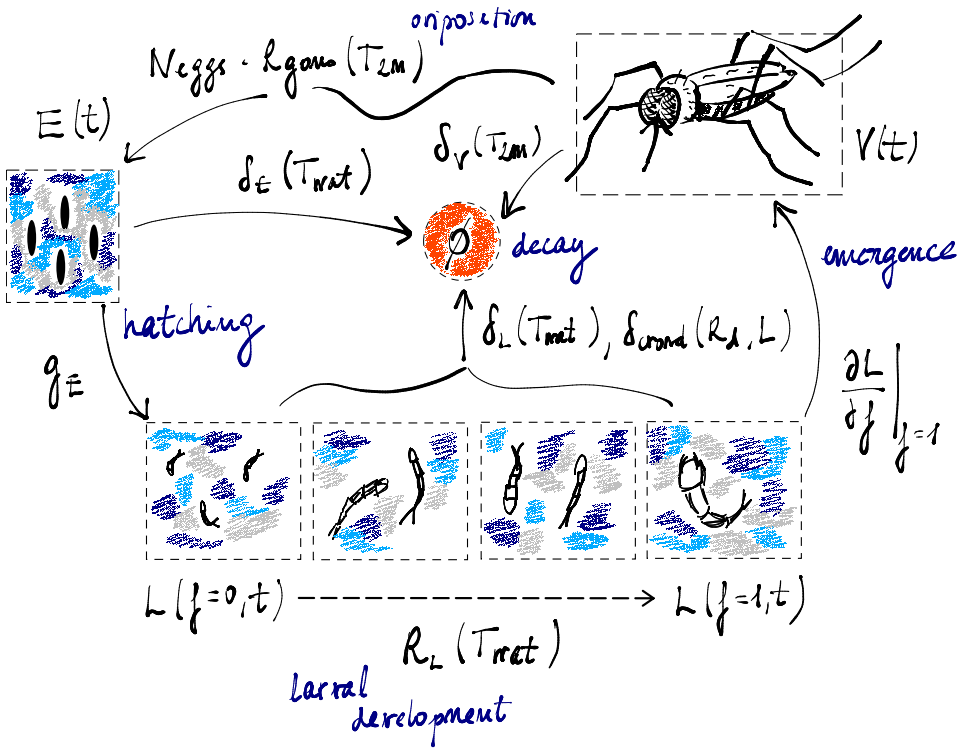

Figure 3.2: Schematics of VECTRI's climate-aware dynamical model of the ecology of mosquitoes.

N_L boxes and we will refer to f in terms of the associated integer-valued index $i \in \{1, 2, ..., N_L\}$.

The model does not account for vector movement across grid points and assumes the mosquito has been introduced everywhere, giving its density solely as a function of the local climatic features. VECTRI needs two-metre air temperature, rainfall and human population density values as input data to drive its dynamics. The human population density, ρ_h, is used to estimate part of the larval carrying capacity, discussed further in the text. In this study temperature and rainfall are functions of time, *i.e.*, $T_{2m} = T_{2m}(t)$ and $R_d = R_d(t)$, while human population values are kept constant. These can either be idealized or realistic, depending on the goal of the study. In this thesis we used realistic values for temperature and rainfall obtained from the E-OBS data set version $28.0e$ [70] with a $0.1^\circ \times 0.1^\circ$ spatial resolution. Human population density values were obtained from the *Gridded Population of the World GPwv4 project* [71] and interpolated to the grid defined by the climate variables using the CDO software [72].

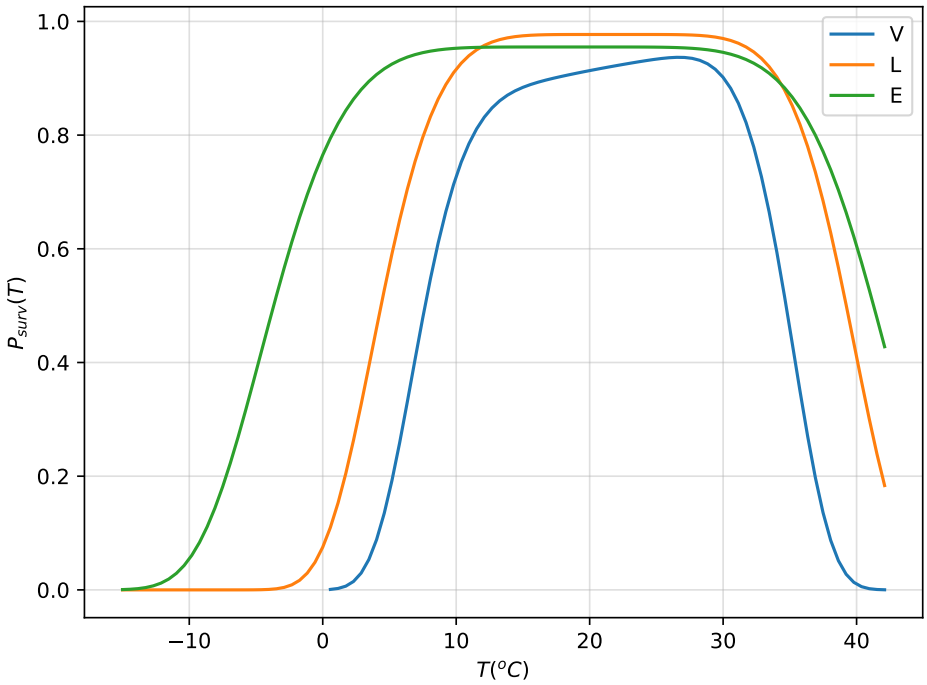

Figure 3.3: Vector (V), larval (L) and egg (E) survival probabilities fitted in [52] and implemented for this study in VECTRI for the parameterization of *Ae. albopictus*.

Mortality scheme

- **Temperature:** temperature drives mortality among eggs, larvae and mosquitoes (*e.g.,* [73]). In the model this is factored in as a set of decay rates, $\{\delta_E, \delta_L, \delta_V\}$, whose values are taken from empirical functions fitted from field and laboratory studies. These functions vary greatly among vectors and are typically reported as daily survival probabilities [52] (Fig 3.3).

- **Predation and overcrowding:** the parameter δ_{crowd} encompasses larval predation and crowding effects. The first is modelled as a constant survival probability, $P_{L,surv0} = 0.9$, and the second takes the form of a logistic term, whose carrying capacity is determined by a maximum larval biomass surface density, M_{max} ($mg\ m^{-2}$), and the fractional area of potential breeding sites in a particular location, $w(R_d)$, *i.e.,*

$$P_{crowd}(L, R_d) = \left(1 - \frac{\sum_{i=1}^{N_L} M_{L_i}}{w(R_d) \cdot M_{max}}\right) . \tag{3.4}$$

Here, M_{L_i} is the total surface biomass of larvae in the $i\text{-}th$ fractional developmental stage, with

$$M_{L_i} = \frac{i}{N_L} \cdot L_4 \ . \tag{3.5}$$

L_4 is the biomass of a single larva in its fully-grown stage, typically referred to as stage 4. From now on, the notation "L" stands for $L = \sum_i L_i$.

- **Flushing:** heavy rainfall flushes out larvae and contributes to their mortality [74]. This is represented in VECTRI as a survival probability function of the local daily rainfall, R_d. The final expression accounting for predation, overcrowding and flushing effects reads as

$$P_{L,surv} = P_{crowd}(L, R_d) \cdot P_{L,surv0} \cdot P_{flush}(R_d) \ , \tag{3.6}$$

with $\delta_{crowd} = 1 - P_{L,surv}$. For more information on the flushing function the reader is referred to [53].

Pond fraction estimation

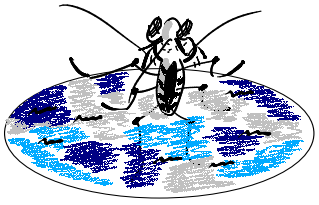

A proper estimation of the fraction of potential breeding sites in each grid point is of major importance, since it affects larval development via the carrying capacity. Distinct vectors have different breeding preferences. For example, *Anopheles gambiae* is known to prefer rural areas [75], whereas the Asian tiger mosquito, *Ae. albopictus*, is a urban-adapted species [76] and benefits from the presence of human-made objects. Based on this variety, VECTRI builds the fraction as a contribution of three sources:

- **Permanent:** breeding sites related to features such as rivers or natural lakes.

- **Temporary:** precipitation-fed temporary ponds.

- **Urban:** human-related features that can cause water storage, like used tires, plant pots or gutters.

Each source, i, is weighted by a vector-specific "usage" coefficient, $r_i \in [0, 1]$, representing the breeding habitat preference of a particular vector in that source. The total availability of breeding sites reads as

$$w(R_d) = r_{urbn} \underbrace{\cdot w_{urbn}(\rho_h)}_{\text{stationary}} + r_{perm} \cdot \underbrace{w_{perm}}_{\text{stationary}} + r_{pond} \cdot \underbrace{w_{pond}(R_d)}_{\text{dynamic}} \ . \tag{3.7}$$

In braces are pointed the stationary and dynamic terms. w_{perm} is by default set to a very low value (10^{-6}) and one has to manually feed the model a file containing these features. The logarithm of human population density is used as a proxy for the availability of human-related breeding sites,

$$w_{urbn}(\rho_h) = s \cdot ln\left(\frac{\rho_h}{\tau} + 1\right) \ , \tag{3.8}$$

with s and τ being free and tunable parameters. Since the human population density in this study is constant, the only fraction that changes over time is that determined by rainfall. To see an explicit development of the dynamic term the reader is now referred to [77, 78]. Usage coefficients are highly uncertain and must be calibrated for each vector against empirical data.

Numerics

In VECTRI, equations (3.1-3.3) are not integrated simultaneously, instead, the different terms are integrated sequentially and fed into the next. This technique is called *operator splitting* and is frequently used in, *e.g.,* atmospheric sciences. Symbolically, the integration algorithm for, *e.g.,* equation (3.1) can be written as

$$E(t + \Delta t) = E(t) + \left(\frac{\partial E}{\partial t}\right)_{gono} \cdot \Delta t + \left(\frac{\partial E}{\partial t}\right)_{decay} \cdot \Delta t + \left(\frac{\partial E}{\partial t}\right)_{hatch} \cdot \Delta t \ . \tag{3.9}$$

In practice, as mentioned before, these are solved one by one, and each result is fed into the next term. The model has a fixed time step of one day, *i.e.,* $\Delta t = 1\ day$, and time-stepping is performed with an explicit Euler scheme. One time-step integration of equation (3.1) would be

$$E^{gono} = E(t) + \left(\frac{\partial E(t)}{\partial t}\right)_{gono} \cdot \Delta t \tag{3.10}$$

$$E^{decay} = E^{gono} + \left(\frac{\partial E^{gono}}{\partial t}\right)_{decay} \cdot \Delta t \tag{3.11}$$

$$E(t+\Delta t) = E^{decay} + \left(\frac{\partial E^{decay}}{\partial t}\right)_{hatch} \cdot \Delta t\ . \tag{3.12}$$

Mortality rates associated to temperature and overcrowding, δ_i, are written as daily survival probabilities, p_i, and the corresponding densities, ϕ, are integrated as

$$\phi^a = \phi^b - (1-p_i)\cdot\phi^b\cdot\underbrace{\Delta t}_{=1} = p_i\cdot\phi^b\ . \tag{3.13}$$

For example,

$$E^{decay} = E^{gono} - \delta_E(T_{2m})\cdot E^{gono}\cdot\Delta t = E^{gono} - (1-p_E(T_{2m}))\cdot E^{gono} \tag{3.14}$$

$$= p_E(T_{2m})\cdot E^{gono}\ , \tag{3.15}$$

with $p_E(T_{2m})$ being the survival probability shown in Fig. 3.3. The integration order, in model version 1.11.3, is the following:

1. Gonotrophic cycle
2. Temperature-driven mortality for the vector
3. Vector oviposition
4. Pond model
5. Crowding mortality for larvae

6. Larval progression/development
7. Larval and egg mortality (predation, overcrowding and water temperature)
8. Larval hatching/ vector emergence

Aquatic stages

In VECTRI, two-metre air temperature is used as a proxy to estimate pond water temperature, assumed to have a permanent shift of $+2K$ with respect to the first. This relation is however highly dependent on the features of the water body and can be improved with external hydrology models, not included in VECTRI's core code. In turn, water temperature is used as a proxy to estimate egg and larval developments.

For larvae, the advection velocity, R_L, follows the degree-day concept from Detinova [79, 80], a measure of accumulated heat above a given developmental threshold. Particularly, it follows the linear function of water temperature

$$R_L = \frac{T_{wat} - T_{L,min}}{K_L} \in [0, 1] \, . \tag{3.16}$$

Here $T_{L,min}$ is the minimal water temperature for larval development, below which growth ceases, and K_L ($K\ day$) the necessary number of degree-days for a complete progression into the pupal stage. The advection velocity can thus be interpreted as a fractional growth rate.

The default advection algorithm for larval development is a simple "integer box-shifting" algorithm, namely, if $T_{wat} > T_{L,min}$, all larvae are advected a number of boxes

$$\lfloor N_L \cdot \Delta_L \rfloor \, , \tag{3.17}$$

with $\lfloor * \rfloor$ being the floor function and Δ_L the fractional shift, set by the advection velocity, *i.e.,*

$$\Delta_L = \texttt{min}(\texttt{max}(0.0, R_L \cdot \Delta t), 1) \; . \tag{3.18}$$

The duration of both egg hatching and pupal development stages are of the order of one day [81, 82] and thus not well resolved by VECTRI. In order to avoid truncation issues these are set to be constant and equal to the time step. As we can see from the model equations (3.1-3.3), pupae are not explicitly modelled, instead all larvae advected into the final fractional growth stage, $f = 1$, become adults (first term in the right hand side of equation (3.3)).

Adult stage

Adult mosquitoes are those coupled to the "disease side" of the model. We will, however, not dive into it and will stay focused on the ecology side. We do have to know that, in the model, the vector density, V, is split into a number of stages, N_{infc}, reflecting the development of the parasite within. An explicit description of the gonotrophic cycle would then require V to have a matrix structure (meaning to be a 2-dimensional vector), one dimension for parasite development and the other for egg development. From $v1.8$ VECTRI stopped having the former and V is just 1-dimensional. Equation (3.3) thus reffers to the sum of this vector, and the advected larval influx (typically known as emergence rate) feeds into its first element. Even though the gonotrophic cycle is not explicitly resolved, egg development within the mosquito and the subsequent oviposition has kept the numerical treatment of having a discretized structure and is treated in the same manner as larval advection. The egg laying rate, which follows as well a degree-day concept, reads as

$$R_{gono}(T_{2m}) = \frac{T_{2m} - T_{gono,min}}{K_{gono}} \in [0, 1] \; . \tag{3.19}$$

Here, $T_{gono,min}$ is the minimal air temperature for the gonotrophic cycle and K_{gono} the necessary number of degree-days for a full egg development. Conceptually, the advection velocity, R_{gono}, may be interpreted as the fraction of vectors ready to lay eggs. Consequently, the update rule reads as

$$\left(\frac{\partial E}{\partial t}\right)_{gono} \cdot \Delta t = N_{egg} \cdot \left(\Delta_{gono} \cdot \sum_{i=1}^{N_{infc}} V(i)\right) \cdot \Delta t \ , \tag{3.20}$$

with

$$\Delta_{gono} = \texttt{min}(\texttt{max}(0.0, R_{gono} \cdot \Delta t), 1) \ . \tag{3.21}$$

Calibration process

As mentioned above, some parameters are subject to a high degree of uncertainty, such as the usage coefficients. Others, on the other hand, are constrained by field and/or laboratory measurements, but remain nevertheless undetermined, within a narrower degree of uncertainty. Optimization tools can here be used to adjust the value of these parameters to improve the model's performance against empirical data. The performance can generally be thought as the degree of discrepancy between an observed signal and that of the model's output. This signal can take many forms, from the number of egg counts in an ovitrap to the number of recorded malaria cases in a village. In this study ovitrap data (data of trapped mosquito eggs) was used to calibrate model parameters using the genetic algorithm (GA) from [61]. The algorithm allows for a set of specified model parameters to be adjusted within the bounds of their assessed uncertainty and, in this sense, differs from a free parameter search, *i.e.,* it is a **constrained** optimization tool.

3.1.4 Results

0.- Adapting the model to the Asian tiger mosquito: The temperature-driven mortality was obtained from the study [52] (Fig. 3.3) and vector-specific life cycle parameters were obtained from literature (see Electronic Supplementary Material in the manuscript). These parameters, among others, were then calibrated.

1.- Calibration and validation: Once calibrated, the model could successfully reproduce the seasonal activity of the vector for all Italian sites where

ovitrap data was available and, to a lesser extend, the inter-annual variability in population density. Spatially, the model also reproduced the geographical distribution of the vector, inferred from the occurrence data bases and, importantly, scored higher with the one that is most complete and up-to-date.

2.- Average and long-term behaviour: Populated areas such as Rome, Naples and Milan are modelled to be the main vector hotspots (Fig. 3.4a). The Po Valley as well as regions in Firenze and Apulia show moderate values whereas highland areas such as the Central Apenine mountains and the Alps remain low. The model describes a pronounced north-south gradient in the mosquito's seasonal activity length, with especially high values in southern coastal areas of $\sim$ 30-40 weeks (Fig. 3.4b). A risk map integrating average mosquito density and activity length is provided in Fig. 3.4c. Overlaid, we show densely populated areas, which coincide with risk hospots such as Rome, Naples, Foggia, Catania, Palermo, Lecce and Cagliari, among others. The mosquito's seasonal activity duration is modelled to experience a linear increase in time (Fig. 3.4d), with a higher rate of increase, of around $\sim$ 2-3 weeks per decade, in the south. Some southern coastal regions are modelled to be homodynamic, namely the vector is active all year-round.

3.- Short-term response to heatwaves: Warm events considered as heatwaves have three distinct effects on the modelled population dynamics of *Ae. albopictus*. They can be *Consistently beneficial*, namely remain in a temperature range where growth terms overcome temperature-dependent mortality rates and thus experiment higher population densities than a counterfactual equivalent, where the heatwaves have been suppressed ; *Consistently detrimental*, the opposite of the previous ; *Temporarily detrimental*, where vector populations experience an initial decrease followed by a rebound, partly driven by the age-structured description of larval development in the dynamical model.

3.1.5 Discussion

In this study the climate-sensitive dynamics of the mosquito *Ae. albopictus* were modelled. The arthropod, vector of diverse arboviruses, poses a significant threat to public health. Consequently, the development of calibrated tools with

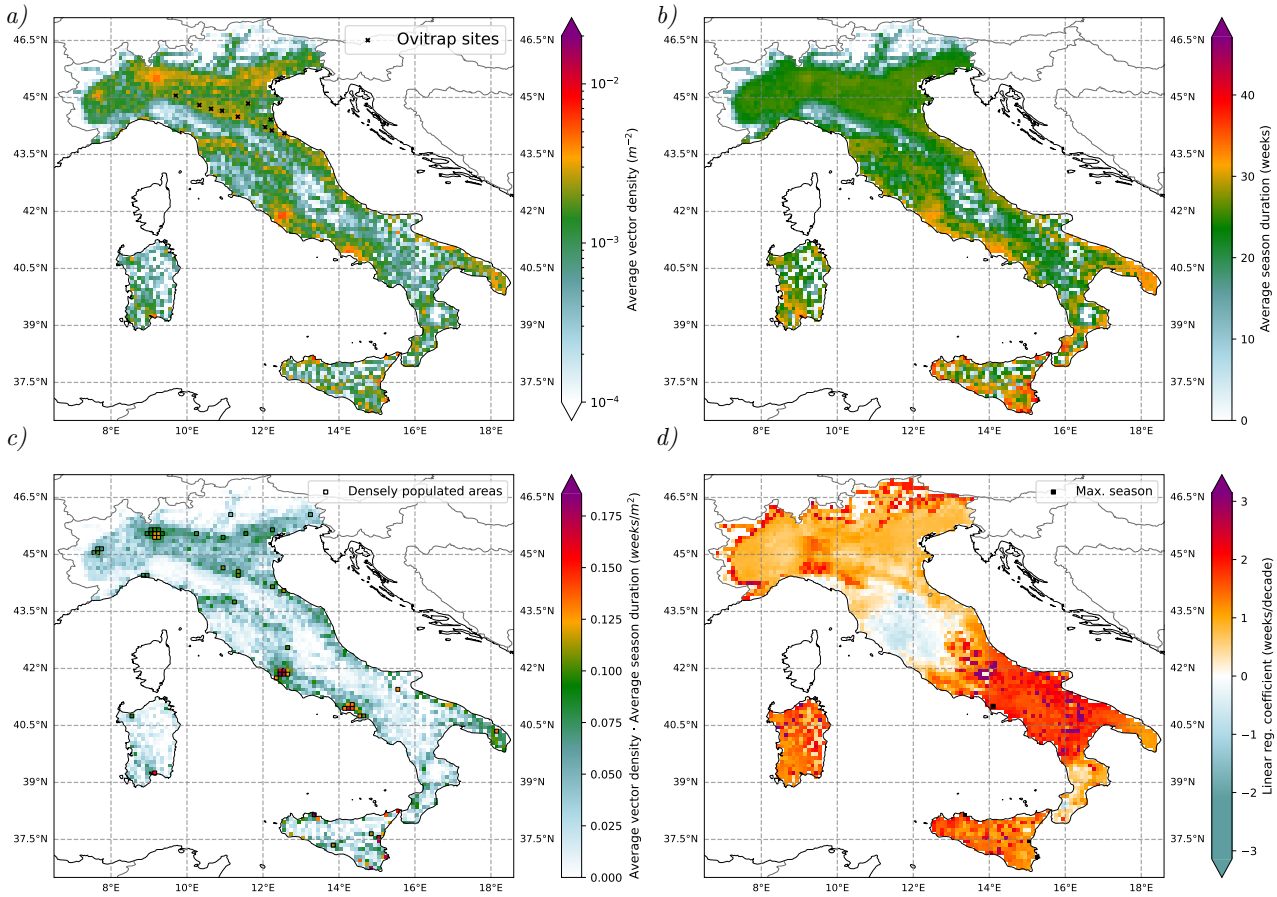

Figure 3.4: a) Mean vector density for the 1980-2023 period. The Italian sites used for the model calibration are depicted with black crosses. b) Average season duration (weeks), defined as the number of days in the year were the vector density is above $1.5 \cdot 10^{-4} m^{-2}$ (see manuscript for threshold selection discussion). c) As a plausible metric to describe the average level of risk we here show the product of a) and b). d) Linear regression coefficients of simulated activity season duration (weeks/decade) across Italy. In black we have masked regions where the season has already reached 365 days at least for one year throughout the simulated period.

the ability to describe its geographic distribution and temporal dynamics have the potential to be used as useful guide for surveillance activities, to generate risk estimates and forecast sort and long-term future trends in mosquito activity. Future model developments could include the implementation of egg diapause, since, contrary to those found in tropical places, temperate *Ae. albopictus* strains are capable of entering such state [83]. For further details, in-depth development and discussion the reader is now referred to the manuscript included in the next section.

3.2 Manuscript

Title: "The effect of climate change and temperature extremes on *Aedes albopictus* populations: a regional case study for Italy"
Authors: Miguel Garrido Zornoza[1], Cyril Caminade[2], Adrian M. Tompkins[2]

[1] The Niels Bohr Institute, University of Copenhagen, 2100 Copenhagen, Denmark

[2] Earth System Physics, Abdus Salam International Centre for Theoretical Physics (ICTP), Strada Costiera 11, Trieste, Italy

My contribution: conceptualization, project administration, methodology, validation, investigation, data curation, visualization, formal analysis, writing – original draft, writing – review & editing
Publication status: under second review round in *The Royal Society Interface*
Hyperlink: None

The effect of climate change and temperature extremes on *Aedes albopictus* populations: a regional case study for Italy

Miguel Garrido Zornoza *[1], Cyril Caminade[2], and Adrian M. Tompkins[2]

[1]The Niels Bohr Institute, University of Copenhagen, Blegdamsvej 17, Copenhagen, 2100 Ø, Denmark
[2]Earth System Physics, Abdus Salam International Centre for Theoretical Physics (ICTP), Strada Costiera 11, Trieste, Italy

August 24, 2024

Abstract

The Asian tiger mosquito, *Aedes albopictus*, has spread widely throughout Italy since its introduction, with significant public health implications. We examine how decadal temperature trends and sub-monthly heatwave events affect its climate-driven geographical distribution and temporal dynamics using a new regional-scale dynamical *Aedes* model. The model is calibrated using 12 years of ovitrap data for Emilia-Romagna, reproduces the vector seasonality and, to a lesser extent, its inter-annual variability. Simulated vector density hotspots overlap with densely populated areas in Rome, Milan, Naples, Foggia, Catania, Palermo, Lecce, Cagliari, Genoa, Turin and large urban centres in Emilia-Romagna. Lower risk is simulated over the Central Apennine mountains and the Alps. At decadal time-scale, we simulate a lengthening of the active mosquito season by 0.5-3 weeks per decade, with the vector becoming homodynamic in southern Italy. Depending on the climatic setting, heatwaves can increase or reduce vector populations and, in some locations, can temporarily decrease mosquito populations. Such decreases can be followed by a population rebound and overshoot. Given the model skill in reproducing key spatio-temporal *Ae. albopictus* features, there is potential to develop an early warning system to inform control efforts at national scale.

Keywords: *Aedes albopictus*; climate change ; temperature extremes ; regional modelling ; vector-borne diseases ; dynamical modelling

1 Introduction

Aedes albopictus (Skuse, 1894)(Diptera: Culicidae), most commonly known as the Asian tiger mosquito, is indigenous to tropical and subtropical regions of southeast Asia [1]. Even though it originates from forested areas, it is extremely well adapted to the urban environment [2], being able to use man-made artificial objects, such as tires and gutters as breeding sites [3]. By increasing movement of goods, globalization has enabled this mosquito species to successfully invade many parts of the world [1], including temperate areas of Europe [4] and North America [5]. The colonization of Europe by the Asian tiger mosquito involved three independent introductions, very likely from used tyres in containers shipped from China. The first one occurred in Albania during the late 1970s, followed by introductions in northern and central Italy during the 1990s [6]. *Ae. albopictus* then rapidly spread from Albania and Italy to neighbouring European countries using motored vehicles and ships [7].

The establishment of the Asian tiger mosquito is of special public health concern due to its role as a competent vector of arboviruses such as dengue (DENV) [8], chikungunya (CHIKV) [9] and Zika virus (ZIKV) [10]. Autochthonous cases of dengue and chikungunya have been reported in southern France, Italy, Croatia and Spain over the past decade [11]. The first outbreak of chikungunya was reported in the province of Ravenna in Italy in 2007, with about 200 cases [12]. In 2023, about 80 dengue cases were reported in Lombardia and in the Lazio region of Italy [13].

Similar to other ectothermic arthropods, *Ae. albopictus* proliferates at a set range of temperatures determined by the sensitivity of the gonotrophic cycle as well as survival rates during aquatic and aerial life stages. Thus,

*mgarrizoraca@gmail.com

climate change in terms of the increase in both global surface temperature and changes in the occurrence of weather extremes, *e.g.,* the frequency and intensity of heatwaves [14], not only has a significant direct impact on human health [15] but may also have it indirectly by affecting *Ae. albopictus* populations [16, 17].

Past modelling studies, published in the early 2010s and based on environmental data, anticipated the spread of the Asian tiger mosquito in Europe [16, 18, 19], and have primarily focused on long-term impact of climate on mosquito population dynamics. These studies underlined that recent climate change caused more favourable overwintering conditions, longer activity seasons, as well as a potential spread of this species to central-northern European countries. More recently, modelling studies have shown that *Ae. albopictus* could become homodynamic, namely able to breed all year round, over southern Europe in the future [20]. Another recent global ecological niche study confirmed that *Ae. albopictus* could contribute to the emergence of chikungunya outbreaks and clusters of dengue autochthonous cases in southern France, Spain and Italy [21]. The Lazio region, that includes the metropolitan city of Rome and its international airport, with established *Ae. albopictus* populations, has already experienced autochthonous cases of dengue and chikungunya, and could potentially be at risk of Yellow Fever infections [22].

In contrast to longer-term climate change, relatively few studies have investigated the impact of short-term weather extremes, such as heatwaves, on *Ae. albopictus* population dynamics on a long time period. In previous work a mechanistic mathematical model was used to show that heatwaves might be beneficial for mosquito development in the short-term while having an overall detrimental impact [23]. Results are however strongly dependent on heatwave timing and intensity. Another study highlights that winter heatwaves favoured off-season survival of diapausing eggs [24].

In this study, we aim to further understand the impact of heatwaves in the context of a warming climate, investigating the effect of daily temperature on *Ae. albopictus* populations. We use a climate-sensitive mathematical vector model to simulate population dynamics at different mosquito life stages in Italy, a major hotspot for this invasive species [25]. Spatio-temporal ovitrap monitoring data is available over a 12y time period for the Emilia-Romagna region, thus allowing a stringent validation and calibration of the model. The objectives of this study are two-fold. First, following a thorough validation of the model, we aim to determine trends in seasonal activity and mosquito abundance hotspots in the vicinity of densely populated regions of Italy. Second, we conduct sensitivity experiments to tease out detrimental from beneficial effects of heatwaves on mosquito dynamics, providing a mechanistic interpretation based on the mosquito life cycle as well as the aggregated overall effect of these extreme events at decadal time scale. Finally, we provide recommendations for public health stakeholders and discuss future perspectives of this work.

2 Methods

2.1 Model

We use the VECtor borne disease community model of ICTP, TRIeste (VECTRI) model, which was originally developed for modelling the life cycle of *An. gambiae s.s.* and associated *P. falciparum* malaria transmission [26–29]. The model explicitly resolves the mosquito life cycle, including the gonotrophic and larval cycles and has been progressively expanded to model additional mosquito species. From v1.11, it includes a parameterization suite for the Asian tiger mosquito, *Ae. albopictus*, including a new temperature-dependent survival scheme [30]. The model version used here is v1.11.3.

The key model inputs are two-metre air temperature, which impacts the gonotrophic and larval growth rates, as well as larvae and vector mortality, and precipitation, which provides breeding sites. An important parameter in the model is the water coverage of each model grid cell which can serve as potential breeding sites, given as a fraction $w(\lambda, \phi, t) \in [0, 1]$, since it controls the instantaneous carrying capacity of larvae biomass. The parameter represents a subset of all water coverage since large bodies of water are unsuitable for mosquito breeding. This potential breeding site coverage, or fraction of potential breeding sites, is built using a variety of climatic, hydrological and human-related features as proxies for the presence of potential breeding sites, constituting their aggregated value. Concretely, from v1.10 of VECTRI, this fraction is composed of 3 categories: the presence of sites that can occur along the borders of permanent features such as rivers or natural lakes (w_{perm}), urban reservoirs such as water storage containers and plant pot drip trays (w_{urbn}) and precipitation-fed temporary ponds (w_{pond}). The w_{pond} category is the only one that evolves dynamically in time in response to rainfall [31, 32]. In rural environments this category refers to ephemeral pools while in urban environments it also includes rain-fed sites such as road side ditches and poorly draining gutters. In contrast, w_{urbn} and w_{perm} are time-invariant. The first simply relates the availability of urban breeding sites proportionally to the logarithm of human population density [33, 34], similar

to other models that use human presence to estimate part of the local carrying capacity [35, 36] . The permanent fraction, w_{perm}, is derived from aggregating water-land border pixels using metre-scale resolution Sentinel-derived land-cover maps aggregated to 5km tiles, but is not used in this study. The model does not account for land surface cover, nor it represents the transport of vectors over long distances, for example by motored vehicles, currently assuming a small seed vector population in each location when initialising from an artificial initial state. We note that the carrying capacity related to breeding site availability is one of the greatest sources of uncertainty in the model, as it is very difficult to evaluate from observations.

For a given mosquito vector parameterized in VECTRI, the total availability of breeding sites, w, is the sum of each water body class i, weighted by a species-specific usage coefficient, r_i, which represents the relative breeding habitat preferences of this vector:

$$w = r_{pond} \cdot w_{pond} + r_{urbn} \cdot w_{urbn} + r_{perm} \cdot w_{perm} \ . \tag{1}$$

Thus, *An. gambiae s. s.* that is primarily found in rural settings [37], would have a high coefficient of r_{pond}, close to unity, while r_{urbn} is close to zero. *An. funestus* would instead have a larger value for r_{perm} [38–40], while urban-adapted species such as *An. stephensi* [41, 42] or *Ae. albopictus* [43, 44] should have larger r_{urbn} values but also a non-zero pond usage fraction, while r_{perm} is set to zero. The r_i usage coefficients are highly uncertain and subject to the calibration process outlined in section 2.3.

2.2 Input data

The model is driven by daily rainfall (mm) and two-metre air temperature, T_{2m} (°C). As climate data input, we used the daily E-OBS data set version 28.0e [45] for the period 1980-2023, with a $\sim 0.1° \times 0.1°$ spatial resolution. We used population density estimates from the Gridded Population of the World GPwv4 project [46] to calculate w_{urbn}. Population data (per km^2) was interpolated to the climate data grid resolution using a conservative interpolation method with the CDO software v2.30 [47].

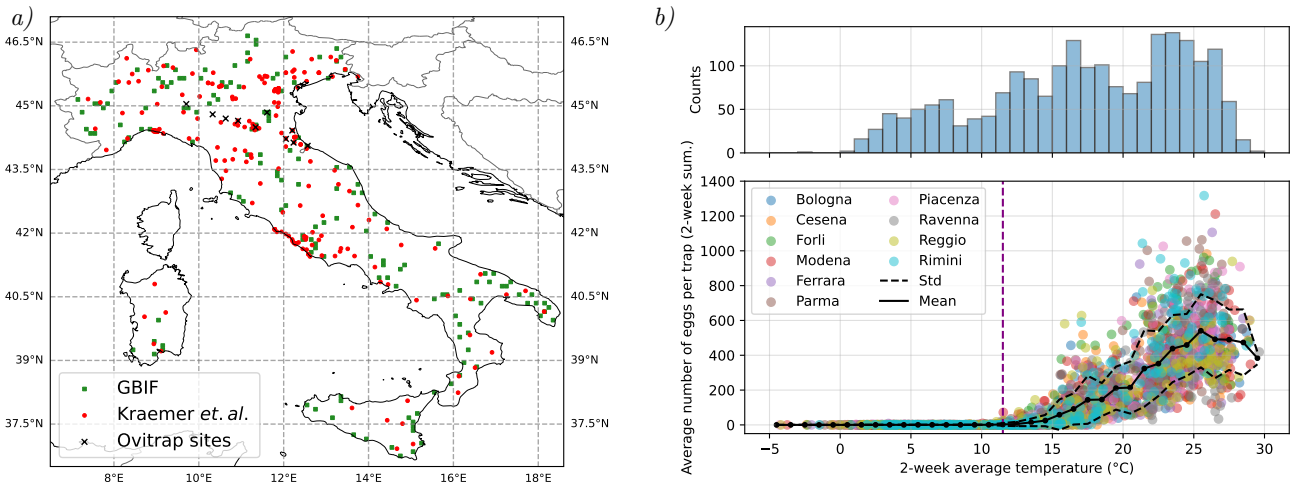

Figure 1: *a*) The Italian sites used for the model calibration (black crosses) and map of reported observations of *Ae. albopictus* based on data from [48] (red circles) and [49] (green squares). *b*) Egg abundance (2 weekly totals per trap) as a function of the bi-weekly average T_{2m} for the ten Italian cities. The mean (dotted-solid) and mean ± one standard deviation (dashed) are shown using 1°C bins. On top we show the associated temperature histogram.

2.3 Model calibration and ovitrap surveillance data

VECTRI has a set of mosquito-related constant parameters which can be constrained by field and laboratory observations but are nevertheless uncertain. Employing a particle filter genetic algorithm (GA) methodology [50–52], we performed a constrained optimization and calibrated these parameters against temporal egg data, which are monitored by a network of ovitraps deployed in ten Italian cities of the Emilia-Romagna region [53–55] (black

crosses in Fig. 1a). This extensive surveillance network was setup shortly after the 2007 Chikungunya outbreak caused by *Ae. albopictus* [56–58]. We used median ovitrap data for the cities of Bologna, Cesena, Forli, Modena, Ferrara, Parma, Piacenza, Ravenna, Reggio and Rimini, from which the first half were used in the calibration and the rest were left as independent data for a posterior validation of the model. This data is recorded bi-weekly and we used the period 2010-2022 for calibration. In this study we adjust r_{urbn}, given the preferential affinity of *Ae. albopictus* for urban sites [2] and r_{pond}. The remaining adjusted parameters and further details on the calibration process are provided in Supp. S1.

Once calibrated against ovitrap data, VECTRI was validated against this temporal data, including all cities, as well as against spatial information on the presence of *Ae. albopictus* in the Italian peninsula and Sardinia (see 2.4). Spatial occurrence data was derived from two sources: the study by [48] and the Global Biodiversity Information Facility (GBIF) [49] (Fig. 1a).

2.4 Validation metrics

To validate our model temporally, we calculated Pearson correlation coefficients between simulated and observed egg abundances, $e(t)$, for the ten Italian sites, as follows.

2.4.1 Seasonality

The first correlation coefficient, $r^2_{site,all}$, calculates the correlation for all bi-weekly time points over the study period (2010-2022) where data is present and sufficiently continuous, *i.e.,* there are no large missing data gaps throughout June-July-August (JJA). This metric is frequently employed in model validation to quantify the model's ability to accurately reproduce observed trends [30, 59, 60]. Since the vector population density signal is strongly seasonal these coefficients assess how well the model captures the mosquito seasonality.

2.4.2 Inter-annual variability

Complementary to the seasonality metric, we also calculate Pearson correlation coefficients using standardized annual mean egg abundances in order to remove seasonality and focus on the ability of the model to represent inter-annual variability. Given that data was missing for Parma, Piacenza, Reggio and Rimini, the calculation is made for the multi-year time domain 2014-2021 for individual sites and referred to as $r^2_{site,y}$.

Assessing inter-annual variability is extremely challenging, however, as non-climatic factors such as vector control measures, micro-climatic features as well as large uncertainties associated with ovitrap data, will cause site-to-site differences that may considerably exceed those driven by climate data, available at coarser spatial scales [55, 61]. One way to try to account for such differences is to consider the spatial scales of climate temperature anomalies, since inter-annual variability and decadal trends of temperature will be relatively uniform across the scale of the ovitraps sites, that is, the inter-trap distances are relatively small compared to the spatial scale of temperature anomalies. This assumption holds for precipitation, but to a lesser degree, since precipitation can be more spatially heterogeneous with respect to temperature on inter-annual timescales (see Supp. S2.1). Thus, by constructing the correlation between each model site and the ensemble mean across all Italian observation sites, $r^2_{ens,y}$, we aim to isolate the climate-driven signal from other factors and data errors that operate on the sub-regional scale. These statistics are calculated as well over the period 2014-2021.

A perfect match between the observed and simulated vector density would mean $r^2 \sim 1$. A lower value of either indicates flaws in different aspects of the simulated signal, as described above.

2.4.3 Spatial validation

To measure the ability of our model to discriminate regions where *Ae. albopictus* is present against regions where it is absent we constructed Receiver Operating Characteristics (ROC) curves [62] using the aforementioned spatial occurrence data. This spatial validation metric, used extensively in species' distribution modelling [63], required the conversion of our model outputs into a binary format, *i.e.,* into presence-absence data. This synthetic presence-absence data was then compared against actual occurrence data to quantify their overlap (see Supp. S2.2). Specifically, to map our continuous data into $0s$ and $1s$ (stating the absence or presence of the mosquito in a particular site, respectively) we used the vector density variable, averaged over the simulated period, as a classifier. If a given threshold value in the vector's density (which was changed para-metrically to construct the curve) was (not) exceeded by the modelled vector density, then the mosquito was considered to be present (absent) in that site. Finally, if this agreed with the observations we then marked it as a true positive (negative), otherwise we considered the model had failed to properly predict the absence (presence) of the mosquito in that site, *i.e.*, the test was

considered a false positive (negative). From this, we report the Area Under the Curve (AUC), *i.e.,* the integral of the ROC curve. As an integrated quantity, the AUC is a threshold-free indicator of the general ability of the model to weight areas particularly suited for a given species. A random predictor model has an AUC of 0.5, a good model lies between $\sim$ 0.6-0.8 and an excellent predictive model is above 0.9.

2.5 Experimental setup

Once calibrated and validated, we analysed two simulations. First, a control simulation, termed *cntl* hereafter, with unmodified observed daily values for temperature and rainfall. Second, a counterfactual simulation, where the temperature series has been modified to remove warm events, and thus does not contain their contribution to simulated mosquito's population density. Heatwaves are events with extreme temperature values. There are, however, many ways to define an extreme [64, 65], most revolving on the choice of threshold. Some studies work with fixed thresholds, such as 25 $^{\circ}C$ [66, 67] , trending thresholds, to correct for the non-stationary baseline provoked by global warming, or thresholds based on the local distribution of the variable [65, 68], such as percentile-based thresholds. In this study we used the boreal summer JJA $90th$ percentile for the period 1980-2023 as a simple heatwave threshold in each grid cell. Threshold values are therefore local and, by construction, 10% of all events are considered to be extreme. In practice, temperature values exceeding the $90th$ percentile were clipped to this value, *i.e.,* if $T_{2m} > T_{90th}$ then we set $T_{2m} = T_{90th}$. We shall denote this second simulation as *clipped*. Our choice of threshold is based on the interest to capture the effect of heatwaves relative to local conditions in a changing climate while keeping the physiological characteristics of the mosquito constant.

3 Results

3.1 Ovitrap data

The relationship between observed bi-weekly egg abundance and two-week average temperature for cities monitored in the Emilia-Romagna region is depicted in Fig 1b. Even though some eggs were found below $10°C$, most eggs were trapped at temperatures exceeding $\sim 11°C$. The average across all sites surpasses 1 egg per trap in the $11 - 12$°C bin, denoted by a vertical dashed line. These temperature thresholds are consistent with early risk modelling assumptions for this species in the UK [69] and Japan [70]. The peak egg densities appear to occur between $25 - 26$°C after which the egg density starts to decline. In the period and location where eggs were sampled, average bi-weekly temperature never exceeded $\sim 30°C$. Egg abundance values for the ten Italian cities are relatively homogeneous, with the largest abundance values being recorded in Rimini.

3.2 Model validation

3.2.1 Seasonality

The seasonality of the observed egg population is well-captured at the ovitrap sites (Bologna in Fig. 2a and Supp. S3). Importantly, our model captures the start and end of the observed egg activity season for all studied sites with a small delay in the onset phase relative to the data. In table 1 (left, first column) we report the seasonal performance of the model for the ten different Italian sites. Most correlation coefficients exceed 0.8 (except Ravenna) and all are significant at the 99% confidence interval. We emphasize that the calibration technique only allows the specified constants of the mathematical dynamical model to be adjusted within the bounds of their assessed uncertainty [50], the prior, and in this respect contrasts with a free parameter search or the free fitting of a statistical model such as commonly-used generalized linear models. In this sense, the constrained optimization approach resembles a Bayesian inference method, such as the one used in a similar study [35], from the use of prior and bounded information in the search for an optimal, yet realistic, solution. The fact that the model is able to simulate the seasonal evolution is only possible if the underlying equations that describe the larvae-adult life cycles are reasonable approximations of the biological system under scope.

3.2.2 Inter-annual variability

$r^2_{ens,y}$ correlation coefficients at inter-annual time scale are moderate, and mostly significant except for Forli and Modena, where the model clearly disagrees with the observed variability (table 1 left, second column). Most points of the simulated ensemble mean, however, lie within 1σ of the observed ensemble mean (Fig. 2b), indicating that part of the climate-driven variability signal is captured by the model. $r^2_{site,y}$ correlation coefficients for Cesena

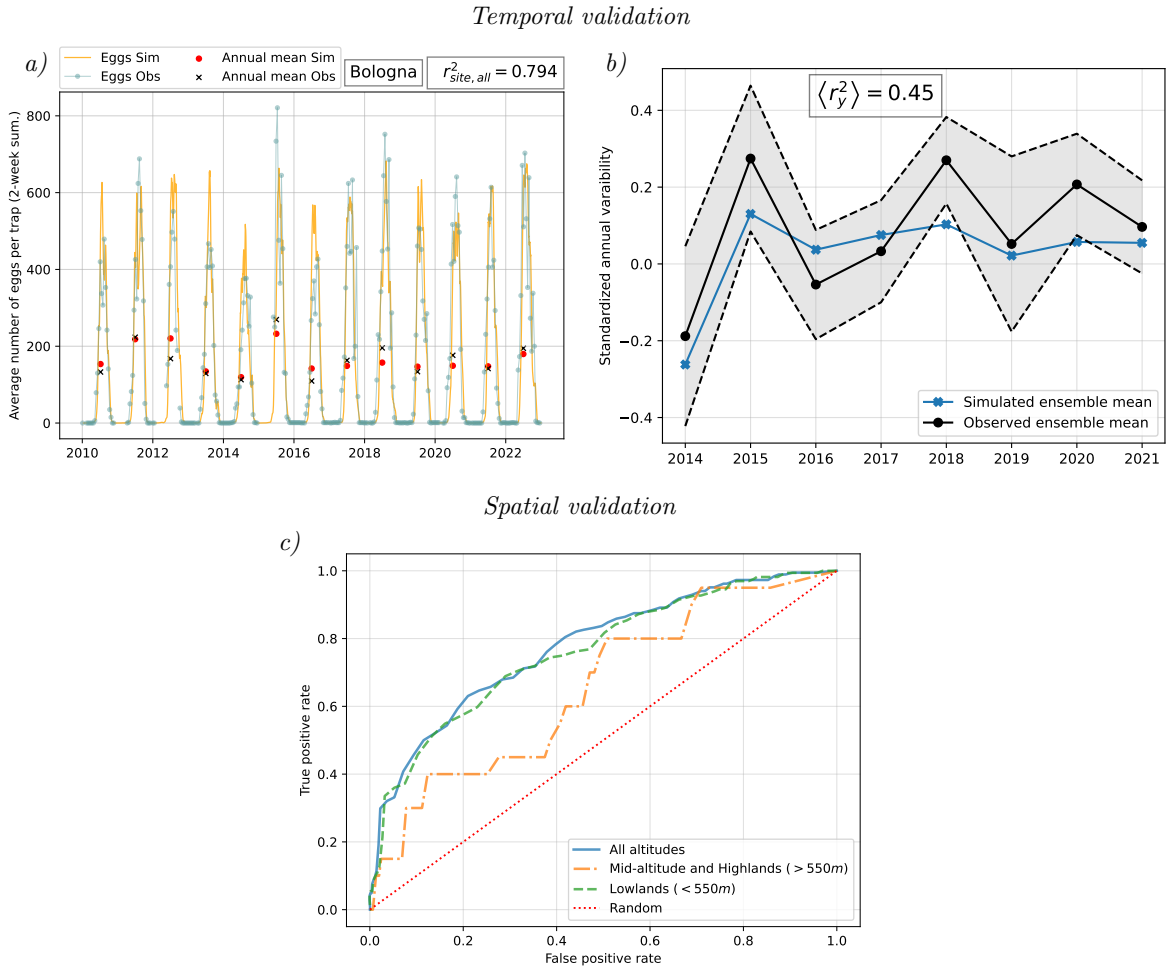

Figure 2: *a*) Example of the temporal calibration in the Bologna site using the GA. Observed egg data is shown against re-scaled model output (see Supp. S1) as well as their respective annual means. *b*) Standardized ensemble annual means of the observed and simulated (*cntl*) egg densities in the ten Italian sites. *c*) Example Receiver Operating Characteristics (ROC) curves for the whole Italian domain, the mid-altitude and highland regions ($550m >$) and the lowland areas ($550m <$) using baseline data from [48].

and Ferrara are lower than their ensemble equivalent, due to some years having opposite trends between on site simulated and observed signals (2017, 2020 for Cesena and 2017 for Ferrara). Ravenna, Reggio, Piacenza, Forli and Parma show an improvement that misrepresents the quality of the simulated signal, given that sporadic missing data in these locations during the peak vector activity weights the metric towards a seasonality estimate (see Fig. S3 in Supp. S3). Six out of ten site-to-site correlation coefficients ($r^2_{site,y}$) are significant at the 95% confidence level, denoting the model's capability in reproducing low-high egg abundance years per city. However, these correlation values but should be considered carefully, given the small sample size ($8y$) and the amount of missing data.

3.2.3 Spatial validation

The spatial validation is performed using different subdomains, each defined for different altitude ranges (Fig. 2c). In table 1 (right) we report the area under the (ROC) curve, AUC, for the different altitude strata and data sets. Most AUC exceed 0.7, and there are differences depending on the observed occurrence data that was used as baseline. Notably, AUC exceed 0.75 when using the latest, most up to date, occurrence database from the Global Biodiversity Information Facility as baseline. Consequently, the model is able to reproduce the geographical extent of the vector to a good degree, especially accounting for the limitations of such databases and the fact that the vector is still in a phase of expansion and may still not have invaded all possible climatically suitable niches within the country, as reflected by its recent spread to higher altitude regions of Italy [71].

	Temporal		
Location	$r^2_{site,all}$	$r^2_{ens,y}$	$r^2_{site,y}$
Bologna	0.79^{***}	0.50^{**}	0.84^{***}
Cesena	0.69^{***}	0.61^{**}	0.12
Ferrara	0.72^{***}	0.70^{***}	0.48^{*}
Forli	0.71^{***}	0.06	0.53^{**}
Modena	0.68^{***}	0.22	0.14
Parma	0.78^{***}	0.49^{*}	0.63^{**}
Piacenza	0.81^{***}	0.50^{*}	0.77^{***}
Ravenna	0.63^{***}	0.47^{*}	0.67^{**}
Reggio	0.72^{***}	0.43^{*}	0.51^{**}
Rimini	0.80^{***}	0.50^{**}	0.11

Spatial	
AUC	Height
[48]	
0.77	All
0.76	$550m <$
0.66	$550m >$
[49]	
0.77	All
0.75	$550m <$
0.84	$550m >$
[48] & [49]	
0.69	All
0.66	$550m <$
0.72	$550m >$

Table 1: **Left.** Temporal validation of the VECTRI model against egg data from the Italian sites. We report $r^2_{site,all}$, $r^2_{ens,y}$ and $r^2_{site,y}$ for each city. We mark significant results at the 90% (*), 95% (**) and 99% (***) confidence intervals. **Right.** Spatial validation of the model against two occurrence databases of observed *Ae. albopictus*.

3.3 Average risk: 1980-2023

We examine the averaged vector density for the *cntl* simulation (Fig. 3a.), recalling that the model assumes that *Ae. albopictus* has been introduced at all locations and thus simulates population dynamics solely based on the local climatic conditions.

Densely populated urban areas such as Milan, Rome and Naples are simulated to be the main *Ae. albopictus* hotspots. The Po valley, the Firenze area and the Apulia region (SE) also show large simulated density values whereas highland areas such as the Central Apennine mountains, show low density values. There is a pronounced north-south gradient in the simulated length of the vector activity season (Fig. 3b). Longest activity seasons ($\sim$ 30-40 weeks) are simulated over southern coastal areas (Puglia, Basilicata and Calabria), the Lazio region, most of Sicily and parts of Sardinia. Northern regions including the Po valley are simulated to experience shorter activity seasons ($\sim$ 20-30 weeks). Since the average vector density in the Po Valley is however high this indicates a shorter but therefore more pronounced activity, as compared to southern regions that might have a longer season with lower vector population density values.

We provide a metric assessing integrated risk of mosquito density and the length of its activity season in Fig 3c, where we overlaid regions with human population densities above $1500 km^{-2}$, following the EU criterion for urban centers [72]. This map highlights regions where high simulated risk values coincide with densely populated areas. Largest simulated risk values coincide with population hotspots in Rome, Naples, Foggia, Catania, Palermo, Lecce and Cagliari. To a lesser extent, Milan, Genoa, Turin and large urban centres in the Emilia-Romagna region (Bologna, Modena and Ravenna) are also concomitant with high risk values.

3.4 Decadal trends

We observe a linear trend in the mosquito season length, defined as the period where the vector density is higher than a small threshold value ($1.5 \cdot 10^{-4}\ m^2$, see Fig. S4 in Supp. S4 for further details about threshold selection). In Fig. 3d we show the heatmap of linear regression coefficients (slopes) across Italy. Most of the Italian peninsula and Sardinia experience an increase in the season length, with the exception of lower Tuscany and upper Lazio regions. The largest increasing trend is shown over the southernmost regions, with a lengthening of the activity season that ranges between 2 and 3 weeks per decade over the study period. According to the model, climatic factors can be suitable for the vector to remain active all-year round (homodynamic activity) over a few southern coastal areas (depicted by black squares in Fig. 3d).

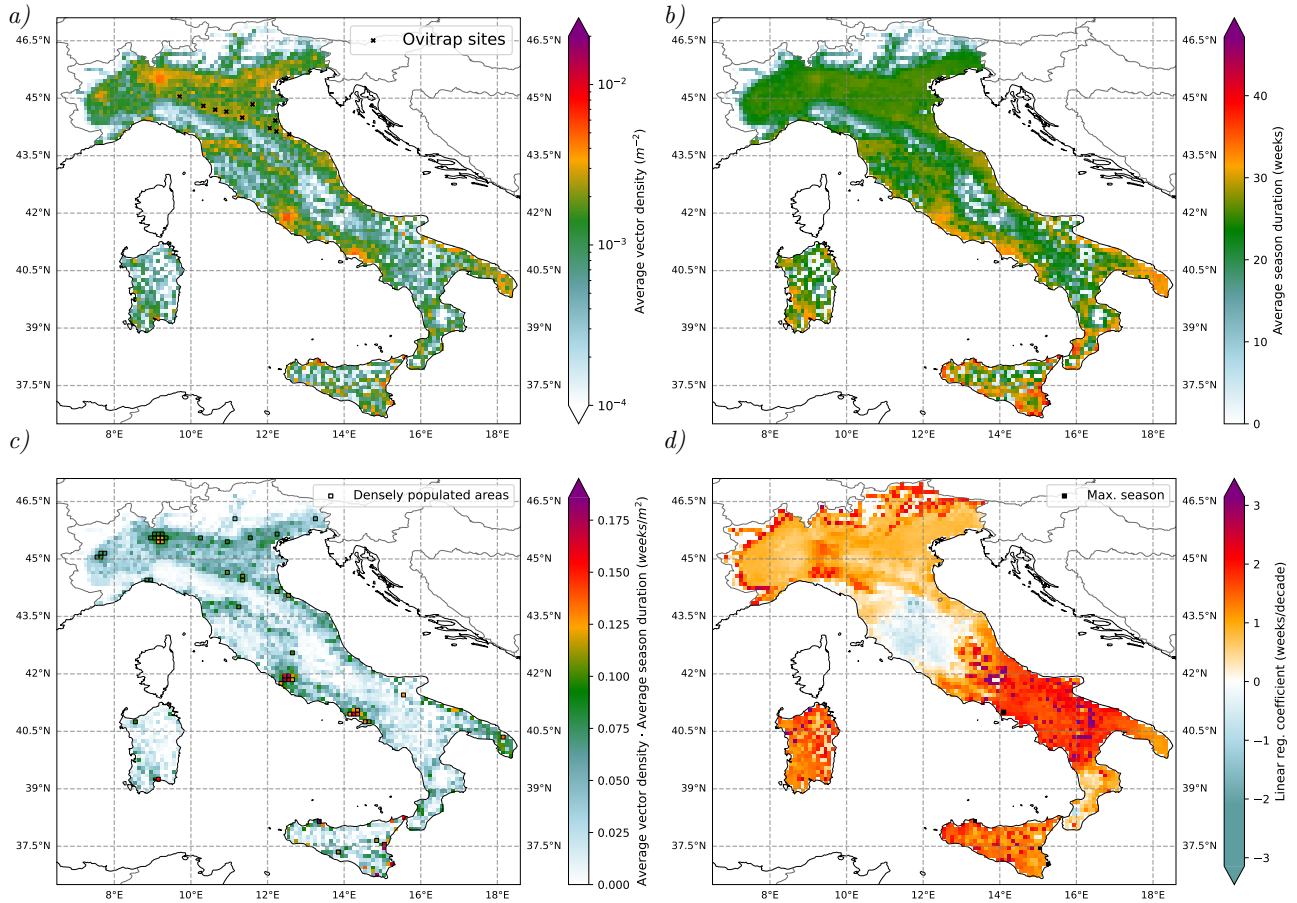

Figure 3: *a*) Mean vector density for the $1980 - 2023$ period. The Italian sites used for the model calibration are depicted again with black crosses. *b*) Average season duration (weeks), defined as the number of days in the year were the vector density is above $1.5 \cdot 10^{-4} m^{-2}$. *c*) As a plausible metric to describe the average level of risk we here show the product of *a*) and *b*). *d*) Linear regression coefficients of simulated activity season duration (weeks/decade) across Italy. In black we have masked regions where the season has already reached 365 days at least for one year throughout the simulated period.

3.5 Impact of short-term heatwave events

3.5.1 Mean seasonal effect

By comparing *cntl* and *clipped* simulations, we can measure the integrated effect of warm temperature events across Italy. We see that, on average, heatwaves are beneficial to the vector and result in a net increase of the mosquito population (see Fig. S5 in Supp. S4). The increase is non-linear in time with the mean impact of heatwaves being larger in the 2010s with respect to the earlier period. This is the result of having a fixed 90th percentile threshold over the studied period, which is thus exceeded more frequently and by further in later years due to global warming. The spatial distribution of temperature-driven effects on vector density populations can be quantified by calculating the temporal covariance of the temperature difference and the rate of change of the egg density difference, between *cntl* and *clipped*, *i.e.*,

$$c(\lambda, \phi) = cov \left[\Delta T_{2m}(\lambda, \phi, t) \cdot \frac{d(\Delta e(\lambda, \phi, t))}{dt} \right] . \quad (2)$$

Here $\Delta T_{2m}(\lambda, \phi, t) \equiv T_{2m}(\lambda, \phi, t) - T_{2m}^{90th}(\lambda, \phi, t)$ and $\Delta e(\lambda, \phi, t) \equiv e(\lambda, \phi, t) - e^{90th}(\lambda, \phi, t)$, with $90th$ denoting the *clipped* experiment. We chose to use the egg density in the covariance calculation since this variable shows a faster

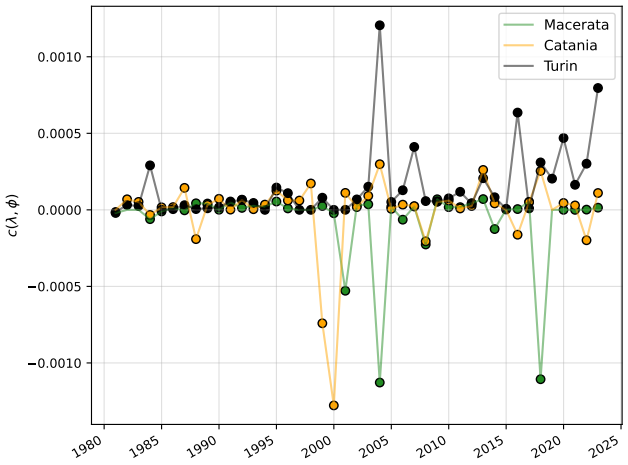

Figure 4: Temporal distribution of temperature-driven effects on mosquito populations in three Italian cities: Macerata (E), Turin (NW) and Catania (SE).

response to temperature changes than the vector density, which presents a small delay with temperatures due to inherent biological lags. Importantly, if the rate of change was calculated on the temperature difference instead of on the egg difference our metric would miss-represent the effect of increased temperatures, namely the first term could then be negative (positive) while the actual temperature difference, and thus the perturbation, was positive (negative) and the second term could be positive (negative) even though the last increased temperature had a detrimental (beneficial) effect on the egg population. An example case for three cities in distinct regions shows how temperature-driven effects are temporally distributed and its effect can vary widely across the Italian peninsula (Fig. 4). For Turin, covariance values are mostly positive over the study period, while they are mostly negative for Macerata (Fig. 4). For Catania, these can either be positive or negative depending on the year. Since we have already observed a long-term trend in the length of the mosquito activity season, we split the covariance calculation into decades 1980*s*, 1990*s*, 2000*s* and 2010*s* (Fig. 5). There are discernible spatial heterogeneities, which are accentuated in time. Despite representing a suitable habitat for *Ae. albopictus*, southern coastal regions, especially in Sicily, include areas where warm events increase the net mortality and thereby have a net detrimental effect on mosquito population. There is, however, a clear tendency of these events to be beneficial elsewhere. Particularly, parts of the Po valley and northern lowland regions, central valley areas in Trentino and the Rome-Naples coastal urban areas have experienced a clear beneficial effect of warm events on mosquito population at decadal time scales.

3.5.2 Sub-monthly dynamics

The long-term mean responses mask short-term impacts that can be positive or negative for the mosquito, as suggested by Fig. 4. In order to demonstrate this, we have identified three types of short-term responses that we illustrate with three case studies.

Case 1: Consistently beneficial events

In this example, the warm events remain within a "beneficial" temperature suitability range. Namely, the temperature-induced vector mortality is secondary compared to temperature-induced increases in the larval and adult growth rates and thus mosquito populations tend to increase incrementally throughout the whole duration of the heatwave. In Fig. 6a we show an example for Genoa where the aforementioned criterion is true for the whole activity season. At the start of the season, vector density values for both *cntl* and *clipped* experiments remain identical. However, in late June 2019, temperatures start rising above the 90th JJA percentile, as depicted by the cumulative number of degree days (black line), and population densities start to diverge between *cntl* and *clipped* simulations. This beneficial effect, namely that the vector density in the *cntl* simulation is systematically larger than the *clipped* analogue, remains the same until September 2019. In other words, temperatures did not reach values large enough to have a net detrimental effect on the simulated vector density in Genoa in 2019.

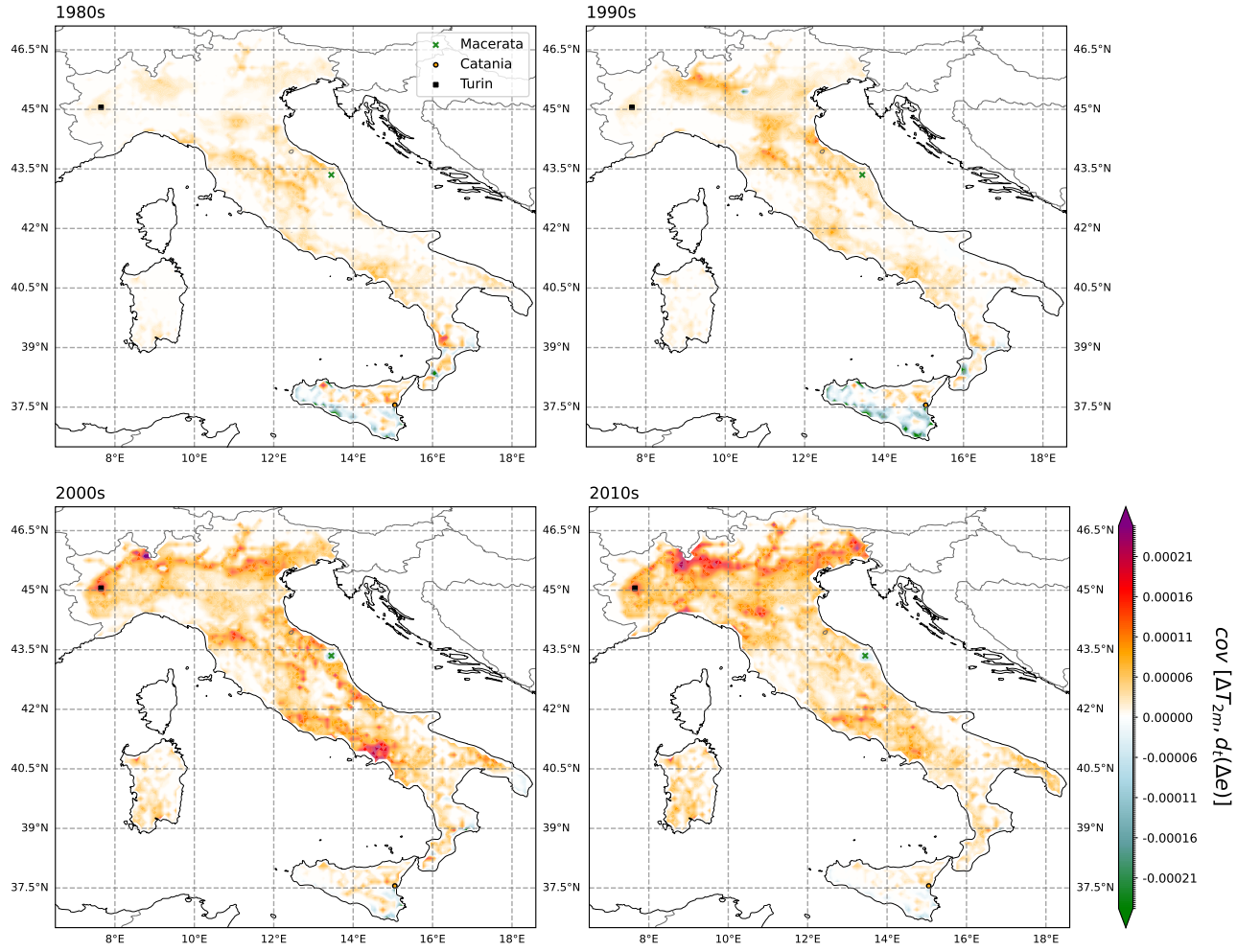

Figure 5: Covariance of the temperature difference and the rate of change in the egg density difference between the *cntl* and the *clipped* simulations for the $1980s, 1990s, 2000s$ and $2010s$. Positive values mean that the increased temperature conditions, that we define as heatwaves, translate into an increase in simulated egg density, whereas negative values indicate a detrimental effect of higher temperatures. Here we show the integrated effect per decade. We mark the location of the cities shown in the previous figure.

Case 2: Consistently detrimental events

Analogously to the previous case we find situations where extreme temperatures have a detrimental effect to vector populations. Such is the case in Macerata in 2000 (Fig. 6b), where temperatures exceeded the 90th percentile twice, in early July and late August, both resulting in a simulated decrease in mosquito populations. This example case study of Macerata, where the two major heat events are separated by a long period, enables us to ascertain a lag between the climate and *Ae. albopictus* population, observed in a different *Ae. albopictus* modelling study focused on sub-tropical regions of China (Guangzhou) [23]. The extreme heat starts to have an immediate impact on vector populations due to the increase in mortality, but the effect of the heatwave continues to be felt for the first eight days after the event termination due to the recovery associated with the vector life cycle (Fig. 6b). The recovery timescale will itself be dependent on temperature, being higher at cooler temperatures given the decreased larval and gonotrophic development rates.

Case 3: Temporarily detrimental

In this category, warm events occasionally lead to periods of lower vector density due to the detrimental impact

of extreme temperatures on mosquito survival. These periods are however followed by a population density rebound in *cntl* which, in some cases, exceeds the *clipped* equivalent. In Fig. 6c-i we show an example for Lecce, in the region of Apulia. During the heatwave that occurred in August 1999, vector and larval densities are initially reduced in *cntl* with respect to *clipped* (Fig. 6c-ii,iii). This is especially true for larvae in their early development stage (Fig. 6c-iii), where increased temperatures act to decrease young larval density while increasing the older larval density and the emergence rate (the rate at which larvae transition to adult vectors). Such increases are concomitant with a higher survival probability due to lower overcrowding effects and indicate a shift of the distribution towards further developed larvae. A couple of days later, this effect leads to the simulated overshoot in vector and larval populations. The cause of these transient dynamics might therefore be related to the bin-resolved age structure of larval development in the VECTRI model which is investigated further below.

Overall, such differences occur during periods when the *cntl* two-metre air temperature, T_{2m}, is above the *clipped* analogue. When both temperatures are again identical, simulated vector population densities of *cntl* and *clipped* tend towards the same value, with some transient relaxation caused by the finite memory of the model. Further examples of detrimental/beneficial cases are shown in Supp. S5.

3.6 Conceptual models

In order to better understand the underlying mechanisms driving the observed system response to warm events (case 3), we study the dynamics of two simplified models of the ecology of the vector, eggs and larvae. The aim is to identify the key features that provoke the transient behaviour observed in the VECTRI model. The most basic representation that explicitly resolves vector (V) egg (E) and larval (L) densities, is a three-state model of the type

$$\frac{dV}{dt} = \alpha_L \cdot L(t) - \delta_V(t) \cdot V(t) \tag{3}$$

$$\frac{dE}{dt} = N_{eggs} \cdot \alpha_V \cdot V(t) - \alpha_E \cdot E(t) - \delta_E(t) \cdot E(t) \tag{4}$$

$$\frac{dL}{dt} = \alpha_E \cdot E(t) \cdot \left(1 - \frac{L(t)}{K}\right) - \alpha_L \cdot L(t) - \delta_L(t) \cdot L(t) \ , \tag{5}$$

with α_i being the transition (larval and gonotrophical cycle development) rates, N_{eggs} the average number of laid eggs per batch, K the system's carrying capacity and $\delta_i(t)$ a time-dependent mortality rate. The time dependence in the former is incorporated with the aim to model a transient increase, mimicking the effect of a detrimental warm event, on vector, larvae and egg mortality. As in VECTRI, larvae are here modelled to grow logistically up to a certain carrying capacity, K, specific to the environmental context. In VECTRI, the transition/growth and mortality rates are a function of temperature, given by relationships derived in laboratory experiments, while here are modelled to be constant. Furthermore, since the observed system response in the climate-aware model is not specific to a particular location or year we can safely assume transition rates are not fundamental and thus set them to unity, *i.e.,* $\alpha_i = 1 \ \forall i \in [V, E, L]$. Time is therefore expressed in normalized generational units.

We study the dynamics of our conceptual model against a transient increase in the decay rate, modelled as

$$\delta_i(t) = \delta_0 \cdot \left(1 + w \cdot e^{\frac{-(t-t_0)^2}{\tau}}\right) + \delta_i \ , \tag{6}$$

i.e., as a Gaussian-like transient pulse centred at t_0 and with a spread of $\sim \tau$. The second term in the right hand side of the decay rate is let to be specific to the state ($i = V$, E or L). The magnitude of the pulse is controlled by the parameter w. The response of the conceptual model against this pulse is shown in Fig. 7a. Logistic growth does not suffice to qualitatively describe the observed behaviour. We thus expand the model to describe the age structure in larval populations, introducing two larval (L) stages: L_1 and L_2, that can be considered as an idealized analogue of 1st/2nd and 3rd/4th instar populations, respectively:

$$\frac{dV}{dt} = L_2(t) - \delta_V(t) \cdot V(t) \tag{7}$$

$$\frac{dE}{dt} = N_{eggs} \cdot V(t) - E(t) - \delta_E(t) \cdot E(t) \tag{8}$$

$$\frac{dL_1}{dt} = E(t) \cdot \left(1 - \frac{L_1(t) + \alpha \cdot L_2(t)}{K}\right) - L_1(t) - \delta_L(t) \cdot L_1(t) \tag{9}$$

$$\frac{dL_2}{dt} = L_1(t) \cdot \left(1 - \frac{L_1(t) + \alpha \cdot L_2(t)}{K}\right) - L_2(t) - \delta_L(t) \cdot L_2(t) \ . \tag{10}$$

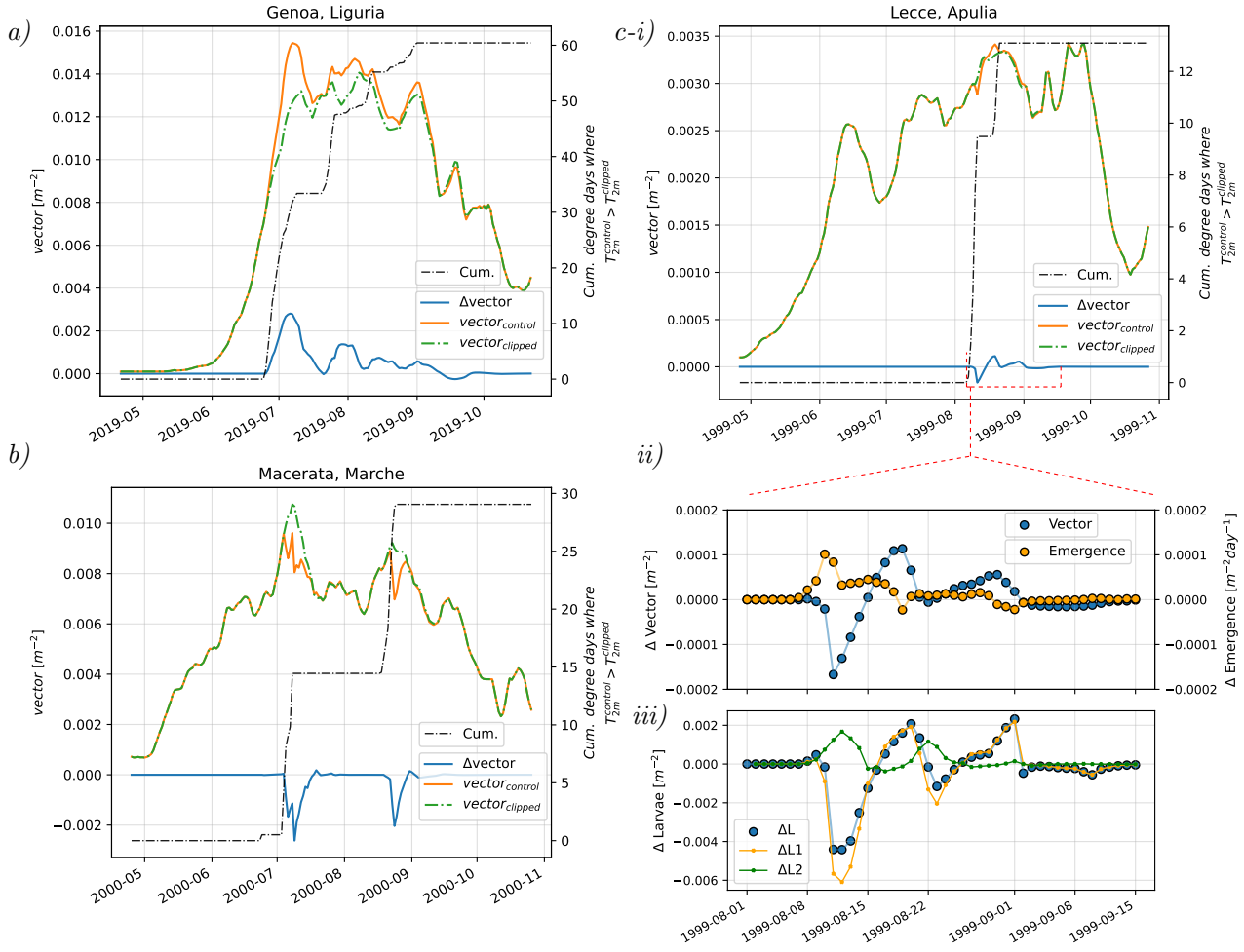

Figure 6: *a*) Consistently beneficial warm events. We here show the *cntl* and *clipped* vector densities in Genoa during the summer of 2019, their difference, Δvector, and the cumulative number of degree days when the *cntl* temperature has exceeded the *clipped* one. The former indicates the time, magnitude and duration of warm events. *b*) Consistently detrimental warm events. *c*) Temporarily detrimental warm event. *i*) Example case in Lecce in 2007. *ii*) Zoomed-in vector density throughout the heatwave accompanied by the emergence rate, *i.e.,* the rate at which larvae transition to the vector state. As before, population densities are the difference between *cntl* and *clipped*. *iii*) Larvae dynamics for the total population, ΔL, young larvae ΔL_1 (aggregate of the first 12 bins of VECTRI's bin-resolved larval age structure) and old larvae ΔL_2 (aggregate of the remaining bins).

A key element of this model is the two larval stages sharing the available resources. Since older larvae tend to have a higher biomass and energy requirements, their contribution to the total carrying capacity should in principle be weighted by a factor $\sim \alpha \cdot L_2$. However, without altering the model behaviour, for simplicity we take $\alpha = 1$.

The dynamics of this age-structured model are shown in Fig. 7b-i. The bin-resolved age structure is a fundamental driver for the observed rebound, overshoot and relaxation dynamics. In Fig. 7b-ii we show the larval density split in L_1 and L_2: upon the passing of the "heatwave" pulse, younger larvae, whose steady-state population densities are higher, undergo a steep decrease, driven by the larger decay rate, d_1 (negative contribution in equation (9)), as compared to the growth term, g_1 (positive contribution in the same equation). This is not the case for older larvae, L_2, whose decay and growth rates (analogously determined from equation (10)) remain of the same magnitude, with the growth rate initially being slightly higher. This is caused by the respective decay and growth rates being proportional to distinct population densities, *i.e.,* to L_1 and L_2 in equation (10). The shared carrying capacity acts now as a boost for older larvae, which find an empty niche to grow, increasing above their steady-state

point and leading to the subsequent overshoot in vector population. The system parameters can be found in table 2.

This simplified model thus highlights a weakness in the dynamical VECTRI model. In reality, environmental resource limitations are mitigated for late stage larvae through cannibalism of early stages [73] which can have a net benefit for larvae numbers reaching emergence [74, 75]. This would act to smooth the impact of heatwaves on larvae numbers, and could indicate that the rebound effect produced in some settings is exaggerated in the VECTRI model simulations.

K	δ_0	N_{eggs}	τ	t_0	δ_V	δ_E	δ_L
10^2	0.01	100	1	50	1	0	0

Table 2: System parameters used in the logistic and age-structured models. The remaining parameters shown in the equations are provided in the main text.

4 Discussion

We have modelled the population dynamics of the Asian tiger mosquito, *Ae. albopictus*, an invasive species which is currently a threat to public health in Europe given its competence to transmit arboviruses. The climate-sensitive VECTRI model has been calibrated and validated against ovitrap field data, successfully reproduces the seasonal cycle and, to a lesser extent, the year-to-year variability in observed vector population. Importantly, our model accurately simulates the start and end of the mosquito activity season for the ten Italian cities located in the Emilia-Romagna region. Spatially, the model captures the observed distribution of *Ae. albopictus* in Italy, with AUC values above 0.7. Our findings underline that simulated mosquito abundance hotspots coincide with densely populated centres in Rome, Naples, Foggia, Catania, Palermo, Cagliari, Lecce, Milan, Genoa, Turin and in most large cities of the Emilia-Romagna region.

Regarding global warming trends, we show a lengthening in the seasonal activity of *Ae. albopictus* in Italy which is more pronounced over southern regions, and can reach about 3 extra weeks per decade. Furthermore, we demonstrate that heatwave summer conditions can have both beneficial and detrimental impacts on simulated mosquito densities depending on the location and year under focus. Beneficial impacts tend to occur when temperatures increase larvae growth rates and decrease the gonotrophic cycle time, which dominate decreases in vector survival. On the other hand, detrimental effects occur when temperatures tend to increase larval mortality in the model to such an extent that they overcome the increased growth rates. In some cases, such effects can be followed by a subsequent rebound related to a decrease in the system's carrying capacity and biological delays intrinsic to the bin-resolved larval scheme, although our model does not consider larval cannibalism, and thus could exaggerate the magnitude of this rebound effect.

Our model still does not consider other environmental factors such as photoperiods. Photoperiod is an important factor that triggers a diapause in *Ae. albopictus* in temperate regions [30]. The non-inclusion of photoperiods could explain simulated year-round activity of this mosquito in southern Italian cities, such as Palermo, where recent field observations tend to suggest a 10-months activity season [76]. However, modelling studies have highlighted that *Ae. albopictus* could become homodynamic in southern Mediterranean countries in the near-future [20], a claim supported by the recently reported activity of *Ae. albopictus* during the 2022-2023 winter season in Attica (Greece), where it was found in large numbers [77]. Even though most winter observations in Italy, Albania and Spain are sporadic and in low numbers, *Ae. albopictus* has shown a remarkable degree of ecological plasticity in the past [78], with diapause adaptation to local climatic conditions [79, 80]. There is thus a need to extend surveillance periods outside the usual expected activity range of *Ae. albopictus*.

We have modelled mosquito dynamics but we did not consider pathogen transmission in our modelling framework. However, simulated hotspots coinciding with densely populated areas match reported autochthonous cases of chikungunya in Ravenna in 2007, and recently observed transmission of dengue virus in the Lazio region and in Lombardia in 2023. Future modelling efforts could focus on developing early warning tools based on numerical weather prediction systems as well as producing higher resolution risk estimates to guide control and surveillance activities.

Funding. MGZ acknowledges funding from the Novo Nordisk Foundation Interdisciplinary Synergy Program (grant number: NNF19OC0057374). The authors acknowledge ICTP-IAEA funding from the project "*Using the VECTRI mosquito model with machine learning to derive optimal strategies for the Sterile Insect Technique (SIT)*". We gratefully acknowledge the E-OBS dataset from the EU-FP6 project UERRA (http://www.uerra.eu), the Copernicus Climate Change Service and the data providers in the ECA&D project (https://www.ecad.eu).

a) Logistic

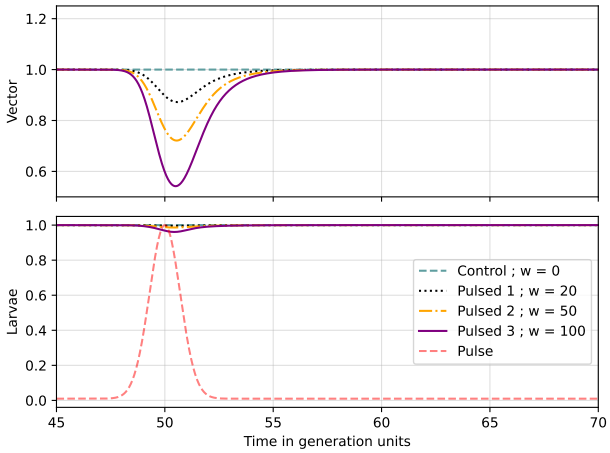

b-i) Age-structured

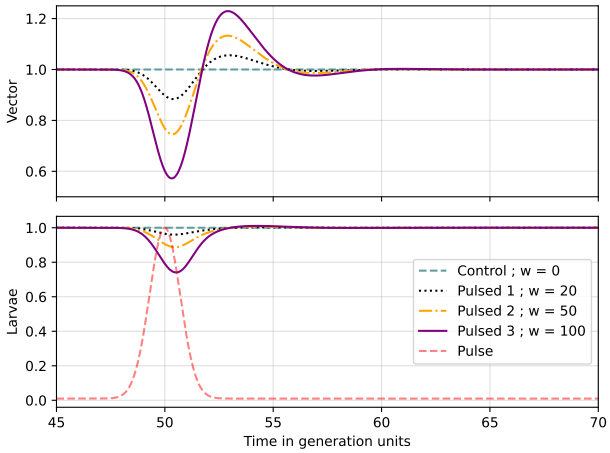

b-ii) Larvae dynamics

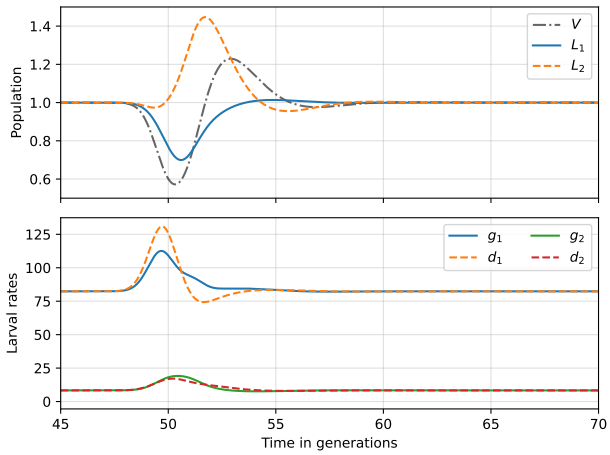

Figure 7: *a*) Population dynamics of the "logistic" model normalized by the respective steady-state values. In red/dashed we show the normalized pulse. $b-i$) Population dynamics of the "age-structured" model and $b-ii$) the corresponding larvae dynamics along with their growth, g_i, and decay, d_i, rates for both young, L_1, and older, L_2, larvae for the case $w = 100$.

Data accessibility. All data used in this study are open source and freely accessible from their respective citations. The model is open source and can be found, installed and used at AMT's webpage https://users.ictp.it/~tompkins/vectri/. Instructions on how to reproduce our results, including the model inputs and post-processing files can be found at https://osf.io/3gcfb/. The ovitrap surveillance data used in this study was last accessed on the 2nd of February, 2023, and is publicly available at https://zanzaratigreonline.it/it/monitoraggio/dati-di-monitoraggio.

References

[1] L. Philip Lounibos. "Invasions by Insect Vectors of Human Disease". en. In: *Annual Review of Entomology* 47.1 (Jan. 2002), pp. 233–266. ISSN: 0066-4170, 1545-4487. DOI: 10.1146/annurev.ento.47.091201.145206. URL: https://www.annualreviews.org/doi/10.1146/annurev.ento.47.091201.145206 (visited on 12/03/2023).

[2] C. Paupy et al. "Aedes albopictus, an arbovirus vector: From the darkness to the light". en. In: *Microbes and Infection* 11.14-15 (Dec. 2009), pp. 1177–1185. ISSN: 12864579. DOI: 10.1016/j.micinf.2009.05.005. URL: https://linkinghub.elsevier.com/retrieve/pii/S1286457909001051 (visited on 11/15/2023).

[3] WA Hawley. "The biology of Aedes albopictus". In: *Journal of the American Mosquito Control Association. Supplement* 1 (Dec. 1988), pp. 1–39. ISSN: 1046-3607. URL: http://europepmc.org/abstract/MED/3068349.

[4] *European Centre for Disease Prevention and Control and European Food Safety Authority. Mosquito maps.* Stockholm, 2023. URL: https://ecdc.europa.eu/en/disease-vectors/surveillance-and-disease-data/mosquito-maps.

[5] P Reiter and D Sprenger. "The used tire trade: a mechanism for the worldwide dispersal of container breeding mosquitoes". In: *J. Am. Mosq. Control. Assoc* 3 (1987), pp. 494–501.

[6] Stéphanie Sherpa et al. "Unravelling the invasion history of the Asian tiger mosquito in Europe". en. In: *Molecular Ecology* 28.9 (May 2019), pp. 2360–2377. ISSN: 0962-1083, 1365-294X. DOI: 10.1111/mec.15071. URL: https://onlinelibrary.wiley.com/doi/10.1111/mec.15071 (visited on 03/20/2024).

[7] Ross N. Cuthbert et al. "Invasive hematophagous arthropods and associated diseases in a changing world". en. In: *Parasites & Vectors* 16.1 (Aug. 2023), p. 291. ISSN: 1756-3305. DOI: 10.1186/s13071-023-05887-x. URL: https://parasitesandvectors.biomedcentral.com/articles/10.1186/s13071-023-05887-x (visited on 03/20/2024).

[8] Giovanni Rezza. "Aedes albopictus and the reemergence of Dengue". en. In: *BMC Public Health* 12.1 (Dec. 2012), p. 72. ISSN: 1471-2458. DOI: 10.1186/1471-2458-12-72. URL: http://bmcpublichealth.biomedcentral.com/articles/10.1186/1471-2458-12-72 (visited on 12/03/2023).

[9] Leon Philip Lounibos and Laura D. Kramer. "Invasiveness of *Aedes aegypti* and *Aedes albopictus* and Vectorial Capacity for Chikungunya Virus". en. In: *Journal of Infectious Diseases* 214.suppl 5 (Dec. 2016), S453–S458. ISSN: 0022-1899, 1537-6613. DOI: 10.1093/infdis/jiw285. URL: https://academic.oup.com/jid/article-lookup/doi/10.1093/infdis/jiw285 (visited on 12/03/2023).

[10] Benjamin A. McKenzie, Alan E. Wilson, and Sarah Zohdy. "Aedes albopictus is a competent vector of Zika virus: A meta-analysis". en. In: *PLOS ONE* 14.5 (May 2019). Ed. by Luciano Andrade Moreira, e0216794. ISSN: 1932-6203. DOI: 10.1371/journal.pone.0216794. URL: https://dx.plos.org/10.1371/journal.pone.0216794 (visited on 03/20/2024).

[11] *European Centre for Disease Prevention and Control and European Food Safety Authority. Autochthonous vectorial transmission of dengue virus in mainland EU/EEA, 2010-present.* Stockholm, 2024. URL: https://www.ecdc.europa.eu/en/all-topics-z/dengue/surveillance-and-disease-data/autochthonous-transmission-dengue-virus-eueea.

[12] R. Angelini et al. "An outbreak of chikungunya fever in the province of Ravenna, Italy". In: *Weekly releases (1997–2007)* 12.36 (2007). Type: doi:https://doi.org/10.2807/esw.12.36.03260-en, p. 3260. URL: https://www.eurosurveillance.org/content/10.2807/esw.12.36.03260-en.

[13] Gabriella De Carli et al. "Outbreaks of autochthonous Dengue in Lazio region, Italy, August to September 2023: preliminary investigation". In: *Eurosurveillance* 28.44 (2023). Type: doi:https://doi.org/10.2807/1560-7917.ES.2023.28.44.2300552, p. 2300552. URL: https://www.eurosurveillance.org/content/10.2807/1560-7917.ES.2023.28.44.2300552.

[14] Gerald A. Meehl and Claudia Tebaldi. "More Intense, More Frequent, and Longer Lasting Heat Waves in the 21st Century". en. In: *Science* 305.5686 (Aug. 2004), pp. 994–997. ISSN: 0036-8075, 1095-9203. DOI: 10.1126/science.1098704. URL: https://www.science.org/doi/10.1126/science.1098704 (visited on 12/01/2023).

[15] Kim R Van Daalen et al. "The 2024 Europe report of the Lancet Countdown on health and climate change: unprecedented warming demands unprecedented action". en. In: *The Lancet Public Health* 9.7 (July 2024), e495–e522. ISSN: 24682667. DOI: 10.1016/S2468-2667(24)00055-0. URL: https://linkinghub.elsevier.com/retrieve/pii/S2468266724000550 (visited on 08/14/2024).

[16] Cyril Caminade et al. "Suitability of European climate for the Asian tiger mosquito *Aedes albopictus* : recent trends and future scenarios". en. In: *Journal of The Royal Society Interface* 9.75 (Oct. 2012), pp. 2708–2717. ISSN: 1742-5689, 1742-5662. DOI: 10.1098/rsif.2012.0138. URL: https://royalsocietypublishing.org/doi/10.1098/rsif.2012.0138 (visited on 12/03/2023).

[17] David Roiz et al. "Climatic Factors Driving Invasion of the Tiger Mosquito (Aedes albopictus) into New Areas of Trentino, Northern Italy". en. In: *PLoS ONE* 6.4 (Apr. 2011). Ed. by Matthew Baylis, e14800. ISSN: 1932-6203. DOI: 10.1371/journal.pone.0014800. URL: https://dx.plos.org/10.1371/journal.pone.0014800 (visited on 11/30/2023).

[18] *Development of Aedes albopictus Risk Maps, Technical Report 0905*. 2009. URL: http://ecdc.europa.eu/en/publications/Publications/0905_TER_Development_of_Aedes_Albopictus_Risk_Maps.pdf.

[19] Dominik Fischer et al. "Projection of climatic suitability for Aedes albopictus Skuse (Culicidae) in Europe under climate change conditions". en. In: *Global and Planetary Change* 78.1-2 (July 2011), pp. 54–64. ISSN: 09218181. DOI: 10.1016/j.gloplacha.2011.05.008. URL: https://linkinghub.elsevier.com/retrieve/pii/S0921818111000798 (visited on 03/20/2024).

[20] Irene Del Lesto et al. "Is Asian tiger mosquito (*Aedes albopictus*) going to become homodynamic in Southern Europe in the next decades due to climate change?" en. In: *Royal Society Open Science* 9.12 (Dec. 2022), p. 220967. ISSN: 2054-5703. DOI: 10.1098/rsos.220967. URL: https://royalsocietypublishing.org/doi/10.1098/rsos.220967 (visited on 03/20/2024).

[21] Agnese Zardini et al. "Estimating the potential risk of transmission of arboviruses in the Americas and Europe: a modelling study". en. In: *The Lancet Planetary Health* 8.1 (Jan. 2024), e30–e40. ISSN: 25425196. DOI: 10.1016/S2542-5196(23)00252-8. URL: https://linkinghub.elsevier.com/retrieve/pii/S2542519623002528 (visited on 01/09/2024).

[22] Mattia Manica et al. "Assessing the risk of autochthonous yellow fever transmission in Lazio, central Italy". en. In: *PLOS Neglected Tropical Diseases* 13.1 (Jan. 2019). Ed. by Christopher M. Barker, e0006970. ISSN: 1935-2735. DOI: 10.1371/journal.pntd.0006970. URL: https://dx.plos.org/10.1371/journal.pntd.0006970 (visited on 03/20/2024).

[23] Pengfei Jia et al. "Potential effects of heat waves on the population dynamics of the dengue mosquito Aedes albopictus". en. In: *PLOS Neglected Tropical Diseases* 13.7 (July 2019). Ed. by Laith Yakob, e0007528. ISSN: 1935-2735. DOI: 10.1371/journal.pntd.0007528. URL: https://dx.plos.org/10.1371/journal.pntd.0007528 (visited on 03/29/2024).

[24] Samantha L. Sturiale and Peter A. Armbruster. "Contrasting effects of an extended fall period and winter heatwaves on the overwintering fitness of diapausing disease vector, Aedes albopictus". en. In: *Current Research in Insect Science* 4 (2023), p. 100067. ISSN: 26665158. DOI: 10.1016/j.cris.2023.100067. URL: https://linkinghub.elsevier.com/retrieve/pii/S2666515823000161 (visited on 03/29/2024).

[25] Jolyon M. Medlock et al. "A Review of the Invasive Mosquitoes in Europe: Ecology, Public Health Risks, and Control Options". en. In: *Vector-Borne and Zoonotic Diseases* 12.6 (June 2012), pp. 435–447. ISSN: 1530-3667, 1557-7759. DOI: 10.1089/vbz.2011.0814. URL: https://www.liebertpub.com/doi/10.1089/vbz.2011.0814 (visited on 03/08/2024).

[26] Adrian M Tompkins and Volker Ermert. "A regional-scale, high resolution dynamical malaria model that accounts for population density, climate and surface hydrology". en. In: *Malaria Journal* 12.1 (Dec. 2013), p. 65. ISSN: 1475-2875. DOI: 10.1186/1475-2875-12-65. URL: https://malariajournal.biomedcentral.com/articles/10.1186/1475-2875-12-65 (visited on 11/30/2023).

[27] Adrian M. Tompkins and Francesca Di Giuseppe. "Potential Predictability of Malaria in Africa Using ECMWF Monthly and Seasonal Climate Forecasts". en. In: *Journal of Applied Meteorology and Climatology* 54.3 (Mar. 2015), pp. 521–540. ISSN: 1558-8424, 1558-8432. DOI: 10.1175/JAMC-D-14-0156.1. URL: https://journals.ametsoc.org/view/journals/apme/54/3/jamc-d-14-0156.1.xml (visited on 06/26/2023).

[28] Alizée Chemison et al. "Impact of an accelerated melting of Greenland on malaria distribution over Africa". en. In: *Nature Communications* 12.1 (June 2021), p. 3971. ISSN: 2041-1723. DOI: 10.1038/s41467-021-24134-4. URL: https://www.nature.com/articles/s41467-021-24134-4 (visited on 06/26/2023).

[29] Cyril Caminade et al. "Impact of climate change on global malaria distribution". en. In: *Proceedings of the National Academy of Sciences* 111.9 (Mar. 2014), pp. 3286–3291. ISSN: 0027-8424, 1091-6490. DOI: 10.1073/pnas.1302089111. URL: https://pnas.org/doi/full/10.1073/pnas.1302089111 (visited on 06/26/2023).

[30] S. Metelmann et al. "The UK's suitability for *Aedes albopictus* in current and future climates". en. In: *Journal of The Royal Society Interface* 16.152 (Mar. 2019), p. 20180761. ISSN: 1742-5689, 1742-5662. DOI: 10.1098/rsif.2018.0761. URL: https://royalsocietypublishing.org/doi/10.1098/rsif.2018.0761 (visited on 11/28/2023).

[31] Ernest Ohene Asare, Adrian Mark Tompkins, and Arne Bomblies. "A Regional Model for Malaria Vector Developmental Habitats Evaluated Using Explicit, Pond-Resolving Surface Hydrology Simulations". en. In: *PLOS ONE* 11.3 (Mar. 2016). Ed. by Francesco Pappalardo, e0150626. ISSN: 1932-6203. DOI: 10.1371/journal.pone.0150626. URL: https://dx.plos.org/10.1371/journal.pone.0150626 (visited on 12/31/2023).

[32] Ernest O. Asare et al. "A breeding site model for regional, dynamical malaria simulations evaluated using in situ temporary ponds observations". en. In: *Geospatial Health* 11.1s (Mar. 2016). ISSN: 1970-7096, 1827-1987. DOI: 10.4081/gh.2016.390. URL: http://www.geospatialhealth.net/index.php/gh/article/view/390 (visited on 08/23/2024).

[33] Muhammad Shahzad Sarfraz et al. "Mapping urban and peri-urban breeding habitats of Aedes mosquitoes using a fuzzy analytical hierarchical process based on climatic and physical parameters". en. In: *Geospatial Health* 8.3 (Dec. 2014), p. 685. ISSN: 1970-7096, 1827-1987. DOI: 10.4081/gh.2014.297. URL: http://www.geospatialhealth.net/index.php/gh/article/view/297 (visited on 04/11/2024).

[34] Antonios Kolimenakis et al. "The role of urbanisation in the spread of Aedes mosquitoes and the diseases they transmit—A systematic review". en. In: *PLOS Neglected Tropical Diseases* 15.9 (Sept. 2021). Ed. by Pattamaporn Kittayapong, e0009631. ISSN: 1935-2735. DOI: 10.1371/journal.pntd.0009631. URL: https://dx.plos.org/10.1371/journal.pntd.0009631 (visited on 04/11/2024).

[35] Kamil Erguler et al. "Large-Scale Modelling of the Environmentally-Driven Population Dynamics of Temperate Aedes albopictus (Skuse)". en. In: *PLOS ONE* 11.2 (Feb. 2016). Ed. by Pedro L. Oliveira, e0149282. ISSN: 1932-6203. DOI: 10.1371/journal.pone.0149282. URL: https://dx.plos.org/10.1371/journal.pone.0149282 (visited on 08/07/2024).

[36] Victoria Romeo-Aznar et al. "Mosquito-borne transmission in urban landscapes: the missing link between vector abundance and human density". en. In: *Proceedings of the Royal Society B: Biological Sciences* 285.1884 (Aug. 2018), p. 20180826. ISSN: 0962-8452, 1471-2954. DOI: 10.1098/rspb.2018.0826. URL: https://royalsocietypublishing.org/doi/10.1098/rspb.2018.0826 (visited on 08/20/2024).

[37] M. Kristan et al. "Pyrethroid resistance/susceptibility and differential urban/rural distribution of *Anopheles arabiensis* and *An. gambiae s.s.* malaria vectors in Nigeria and Ghana". en. In: *Medical and Veterinary Entomology* 17.3 (Sept. 2003), pp. 326–332. ISSN: 0269-283X, 1365-2915. DOI: 10.1046/j.1365-2915.2003.00449.x. URL: https://resjournals.onlinelibrary.wiley.com/doi/10.1046/j.1365-2915.2003.00449.x (visited on 08/15/2024).

[38] Isaac A. Hinne et al. "Larval habitat diversity and Anopheles mosquito species distribution in different ecological zones in Ghana". en. In: *Parasites & Vectors* 14.1 (Apr. 2021), p. 193. ISSN: 1756-3305. DOI: 10.1186/s13071-021-04701-w. URL: https://parasitesandvectors.biomedcentral.com/articles/10.1186/s13071-021-04701-w (visited on 08/15/2024).

[39] Najat F. Kahamba et al. "Using ecological observations to improve malaria control in areas where Anopheles funestus is the dominant vector". en. In: *Malaria Journal* 21.1 (Dec. 2022), p. 158. ISSN: 1475-2875. DOI: 10.1186/s12936-022-04198-3. URL: https://malariajournal.biomedcentral.com/articles/10.1186/s12936-022-04198-3 (visited on 08/15/2024).

[40] Ismail H. Nambunga et al. "Aquatic habitats of the malaria vector Anopheles funestus in rural south-eastern Tanzania". en. In: *Malaria Journal* 19.1 (Dec. 2020), p. 219. ISSN: 1475-2875. DOI: 10.1186/s12936-020-03295-5. URL: https://malariajournal.biomedcentral.com/articles/10.1186/s12936-020-03295-5 (visited on 08/15/2024).

[41] Marianne E Sinka et al. "The dominant Anopheles vectors of human malaria in the Asia-Pacific region: occurrence data, distribution maps and bionomic précis". en. In: *Parasites & Vectors* 4.1 (Dec. 2011), p. 89. ISSN: 1756-3305. DOI: 10.1186/1756-3305-4-89. URL: https://parasitesandvectors.biomedcentral.com/articles/10.1186/1756-3305-4-89 (visited on 08/15/2024).

[42] M. E. Sinka et al. "A new malaria vector in Africa: Predicting the expansion range of *Anopheles stephensi* and identifying the urban populations at risk". en. In: *Proceedings of the National Academy of Sciences* 117.40 (Oct. 2020), pp. 24900–24908. ISSN: 0027-8424, 1091-6490. DOI: 10.1073/pnas.2003976117. URL: https://pnas.org/doi/full/10.1073/pnas.2003976117 (visited on 08/15/2024).

[43] Yiji Li et al. "Urbanization Increases Aedes albopictus Larval Habitats and Accelerates Mosquito Development and Survivorship". en. In: *PLoS Neglected Tropical Diseases* 8.11 (Nov. 2014). Ed. by Pattamaporn Kittayapong, e3301. ISSN: 1935-2735. DOI: 10.1371/journal.pntd.0003301. URL: https://dx.plos.org/10.1371/journal.pntd.0003301 (visited on 08/14/2024).

[44] Julien B. Z. Zahouli et al. "Urbanization is a main driver for the larval ecology of Aedes mosquitoes in arbovirus-endemic settings in south-eastern Côte d'Ivoire". en. In: *PLOS Neglected Tropical Diseases* 11.7 (July 2017). Ed. by Cheng-Chen Chen, e0005751. ISSN: 1935-2735. DOI: 10.1371/journal.pntd.0005751. URL: https://dx.plos.org/10.1371/journal.pntd.0005751 (visited on 08/14/2024).

[45] Richard C. Cornes et al. "An Ensemble Version of the E-OBS Temperature and Precipitation Data Sets". en. In: *Journal of Geophysical Research: Atmospheres* 123.17 (Sept. 2018), pp. 9391–9409. ISSN: 2169-897X, 2169-8996. DOI: 10.1029/2017JD028200. URL: https://agupubs.onlinelibrary.wiley.com/doi/10.1029/2017JD028200 (visited on 02/25/2024).

[46] Center for International Earth Science Information Network - CIESIN - Columbia University. *Gridded Population of the World, Version 4 (GPWv4): Population Density, Revision 11*. Palisades, New York, 2018. URL: https://doi.org/10.7927/H49C6VHW.

[47] Uwe Schulzweida. *CDO User Guide*. Version Number: 2.3.0. Oct. 2023. DOI: 10.5281/zenodo.10020800. URL: https://doi.org/10.5281/zenodo.10020800.

[48] Moritz Ug Kraemer et al. "The global distribution of the arbovirus vectors Aedes aegypti and Ae. albopictus". en. In: *eLife* 4 (June 2015), e08347. ISSN: 2050-084X. DOI: 10.7554/eLife.08347. URL: https://elifesciences.org/articles/08347 (visited on 07/06/2024).

[49] *Aedes albopictus (Skuse, 1894) in GBIF Secretariat (2023). GBIF Backbone Taxonomy. Checklist dataset https://doi.org/10.15468/39omei accessed via GBIF.org on 2024-03-04.*

[50] Adrian M. Tompkins and Madeleine C. Thomson. "Uncertainty in malaria simulations in the highlands of Kenya: Relative contributions of model parameter setting, driving climate and initial condition errors". en. In: *PLOS ONE* 13.9 (Sept. 2018). Ed. by Ana Paula Arez, e0200638. ISSN: 1932-6203. DOI: 10.1371/journal.pone.0200638. URL: https://dx.plos.org/10.1371/journal.pone.0200638 (visited on 11/30/2023).

[51] M Shafii and F De Smedt. "Multi-objective calibration of a distributed hydrological model (WetSpa) using a genetic algorithm". en. In: *Hydrol. Earth Syst. Sci.* (2009).

[52] Q.J. Wang. "Using genetic algorithms to optimise model parameters". en. In: *Environmental Modelling & Software* 12.1 (Jan. 1997), pp. 27–34. ISSN: 13648152. DOI: 10.1016/S1364-8152(96)00030-8. URL: https://linkinghub.elsevier.com/retrieve/pii/S1364815296000308 (visited on 08/23/2024).

[53] Marco Carrieri et al. "Surveillance of the chikungunya vector Aedes albopictus (Skuse) in Emilia-Romagna (northern Italy): organizational and technical aspects of a large scale monitoring system". en. In: *Journal of Vector Ecology* 36.1 (June 2011), pp. 108–116. ISSN: 10811710. DOI: 10.1111/j.1948-7134.2011.00147.x. URL: http://doi.wiley.com/10.1111/j.1948-7134.2011.00147.x (visited on 02/26/2024).

[54] Marco Carrieri et al. "Quality control and data validation procedure in large-scale quantitative monitoring of mosquito density: the case of *Aedes albopictus* in Emilia-Romagna region, Italy". en. In: *Pathogens and Global Health* 111.2 (Feb. 2017), pp. 83–90. ISSN: 2047-7724, 2047-7732. DOI: 10.1080/20477724.2017.1292992. URL: https://www.tandfonline.com/doi/full/10.1080/20477724.2017.1292992 (visited on 02/26/2024).

[55] Marco Carrieri et al. "Egg data validation in quantitative monitoring of *Aedes albopictus* in Emilia-Romagna region, Italy". en. In: *Pathogens and Global Health* 115.2 (Feb. 2021), pp. 125–131. ISSN: 2047-7724, 2047-7732. DOI: 10.1080/20477724.2020.1866375. URL: https://www.tandfonline.com/doi/full/10.1080/20477724.2020.1866375 (visited on 02/26/2024).

[56] P Angelini et al. "Chikungunya epidemic outbreak in Emilia-Romagna (Italy) during summer 2007". en. In: *Parassitologia* 50.1-2 (June 2008), pp. 97–98.

[57] Paolo Bonilauri et al. "Chikungunya virus in Aedes albopictus, Italy." eng. In: *Emerging infectious diseases* 14.5 (May 2008). Place: United States, pp. 852–854. ISSN: 1080-6059 1080-6040. DOI: 10.3201/eid1405.071144.

[58] Martin Enserink. "Tropical Disease Follows Mosquitoes to Europe". en. In: *Science* 317.5844 (2007), p. 1485. ISSN: 0036-8075, 1095-9203. DOI: 10.1126/science.317.5844.1485a. URL: https://www.science.org/doi/10.1126/science.317.5844.1485a (visited on 01/30/2024).

[59] Annelise Tran et al. "Complementarity of empirical and process-based approaches to modelling mosquito population dynamics with Aedes albopictus as an example—Application to the development of an operational mapping tool of vector populations". en. In: *PLOS ONE* 15.1 (Jan. 2020). Ed. by Suzanne Touzeau, e0227407. ISSN: 1932-6203. DOI: 10.1371/journal.pone.0227407. URL: https://dx.plos.org/10.1371/journal.pone.0227407 (visited on 08/19/2024).

[60] Adrian M. Tompkins et al. "Dynamical Malaria Forecasts Are Skillful at Regional and Local Scales in Uganda up to 4 Months Ahead". en. In: *GeoHealth* 3.3 (Mar. 2019), pp. 58–66. ISSN: 2471-1403, 2471-1403. DOI: 10.1029/2018GH000157. URL: https://agupubs.onlinelibrary.wiley.com/doi/10.1029/2018GH000157 (visited on 08/23/2024).

[61] Yiji Li et al. "Spatial heterogeneity and temporal dynamics of mosquito population density and community structure in Hainan Island, China". en. In: *Parasites & Vectors* 13.1 (Dec. 2020), p. 444. ISSN: 1756-3305. DOI: 10.1186/s13071-020-04326-5. URL: https://parasitesandvectors.biomedcentral.com/articles/10.1186/s13071-020-04326-5 (visited on 08/14/2024).

[62] J A Hanley and B J McNeil. "The meaning and use of the area under a receiver operating characteristic (ROC) curve." en. In: *Radiology* 143.1 (Apr. 1982), pp. 29–36. ISSN: 0033-8419, 1527-1315. DOI: 10.1148/radiology.143.1.7063747. URL: http://pubs.rsna.org/doi/10.1148/radiology.143.1.7063747 (visited on 08/07/2024).

[63] Jane Elith* et al. "Novel methods improve prediction of species' distributions from occurrence data". en. In: *Ecography* 29.2 (Apr. 2006), pp. 129–151. ISSN: 0906-7590, 1600-0587. DOI: 10.1111/j.2006.0906-7590.04596.x. URL: https://onlinelibrary.wiley.com/doi/10.1111/j.2006.0906-7590.04596.x (visited on 02/05/2024).

[64] David B. Stephenson. "Definition, diagnosis, and origin of extreme weather and climate events". en. In: *Climate Extremes and Society*. Ed. by Henry F. Diaz and Richard J. Murnane. 1st ed. Cambridge University Press, May 2008, pp. 11–23. ISBN: 978-0-521-87028-3 978-0-511-53584-0 978-0-521-29848-3. DOI: 10.1017/CBO9780511535840.004. URL: https://www.cambridge.org/core/product/identifier/CBO9780511535840A011/type/book_part (visited on 03/30/2024).

[65] Xuebin Zhang et al. "Indices for monitoring changes in extremes based on daily temperature and precipitation data". en. In: *WIREs Climate Change* 2.6 (Nov. 2011), pp. 851–870. ISSN: 1757-7780, 1757-7799. DOI: 10.1002/wcc.147. URL: https://wires.onlinelibrary.wiley.com/doi/10.1002/wcc.147 (visited on 08/09/2024).

[66] Mark New et al. "Evidence of trends in daily climate extremes over southern and west Africa". en. In: *Journal of Geophysical Research: Atmospheres* 111.D14 (July 2006), 2005JD006289. ISSN: 0148-0227. DOI: 10.1029/2005JD006289. URL: https://agupubs.onlinelibrary.wiley.com/doi/10.1029/2005JD006289 (visited on 08/08/2024).

[67] L. V. Alexander et al. "Global observed changes in daily climate extremes of temperature and precipitation". en. In: *Journal of Geophysical Research: Atmospheres* 111.D5 (Mar. 2006), 2005JD006290. ISSN: 0148-0227. DOI: 10.1029/2005JD006290. URL: https://agupubs.onlinelibrary.wiley.com/doi/10.1029/2005JD006290 (visited on 08/08/2024).

[68] Robert J H Dunn and Colin P Morice. "On the effect of reference periods on trends in percentile-based extreme temperature indices". en. In: *Environmental Research Letters* 17.3 (Mar. 2022), p. 034026. ISSN: 1748-9326. DOI: 10.1088/1748-9326/ac52c8. URL: https://iopscience.iop.org/article/10.1088/1748-9326/ac52c8 (visited on 08/08/2024).

[69] Jolyon M. Medlock et al. "Analysis of the potential for survival and seasonal activity of Aedes albopictus (Diptera: Culicidae) in the United Kingdom". en. In: *Journal of Vector Ecology* 31.2 (Dec. 2006), pp. 292–304. ISSN: 1081-1710, 1081-1710. DOI: 10.3376/1081-1710(2006)31[292:AOTPFS]2.0.CO;2. URL: http://www.bioone.org/doi/abs/10.3376/1081-1710(2006)31[292:AOTPFS]2.0.CO;2 (visited on 03/20/2024).

[70] M. Kobayashi, N. Nihei, and T. Kurihara. "Analysis of Northern Distribution of ¡I¿Aedes albopictus¡/I¿ (Diptera: Culicidae) in Japan by Geographical Information System". en. In: *Journal of Medical Entomology* 39.1 (Jan. 2002), pp. 4–11. ISSN: 00222585, 00222585. DOI: 10.1603/0022-2585-39.1.4. URL: https://academic.oup.com/jme/article-lookup/doi/10.1603/0022-2585-39.1.4 (visited on 03/20/2024).

[71] Giulia Battistin et al. "Colonization by tiger mosquito (Aedes albopictus Skuse, 1894) of mountain areas over 600 m above sea level in the surroundings of Trento city, Northeast Italy". en. In: *Journal of Entomological and Acarological Research* 56.1 (Apr. 2024). ISSN: 2279-7084, 2038-324X. DOI: 10.4081/jear.2024.12185. URL: https://www.pagepressjournals.org/jear/article/view/12185 (visited on 04/13/2024).

[72] *Global Human Settlement Layer. The classes of the Degree of urbanisation.* URL: https://ghsl.jrc.ec.europa.eu/degurbaDefinitions.php.

[73] Valentina Mastrantonio et al. "Cannibalism in temporary waters: Simulations and laboratory experiments revealed the role of spatial shape in the mosquito Aedes albopictus". en. In: *PLOS ONE* 13.5 (May 2018). Ed. by Guido Favia, e0198194. ISSN: 1932-6203. DOI: 10.1371/journal.pone.0198194. URL: https://dx.plos.org/10.1371/journal.pone.0198194 (visited on 03/26/2024).

[74] Stuart C. Church and T. N. Sherratt. "The selective advantages of cannibalism in a Neotropical mosquito". en. In: *Behavioral Ecology and Sociobiology* 39.2 (Aug. 1996), pp. 117–123. ISSN: 0340-5443, 1432-0762. DOI: 10.1007/s002650050273. URL: http://link.springer.com/10.1007/s002650050273 (visited on 05/08/2024).

[75] Valentina Mastrantonio et al. "Cannibalism and Necrophagy Promote a Resource Loop and Benefit Larval Development in Insects of Temporary Waters". en. In: *Insects* 12.7 (July 2021), p. 657. ISSN: 2075-4450. DOI: 10.3390/insects12070657. URL: https://www.mdpi.com/2075-4450/12/7/657 (visited on 04/02/2024).

[76] Alessandra Torina et al. "Modelling time-series Aedes albopictus abundance as a forecasting tool in urban environments". en. In: *Ecological Indicators* 150 (June 2023), p. 110232. ISSN: 1470160X. DOI: 10.1016/j.ecolind.2023.110232. URL: https://linkinghub.elsevier.com/retrieve/pii/S1470160X23003746 (visited on 03/20/2024).

[77] Daniela Sofie Lührsen et al. "Adult Aedes albopictus in winter: implications for mosquito surveillance in southern Europe". en. In: *The Lancet Planetary Health* 7.9 (Sept. 2023), e729–e731. ISSN: 25425196. DOI: 10.1016/S2542-5196(23)00170-5. URL: https://linkinghub.elsevier.com/retrieve/pii/S2542519623001705 (visited on 03/20/2024).

[78] Verena Pichler et al. "Complex interplay of evolutionary forces shaping population genomic structure of invasive Aedes albopictus in southern Europe". en. In: *PLOS Neglected Tropical Diseases* 13.8 (Aug. 2019). Ed. by Philip M. Armstrong, e0007554. ISSN: 1935-2735. DOI: 10.1371/journal.pntd.0007554. URL: https://dx.plos.org/10.1371/journal.pntd.0007554 (visited on 04/10/2024).

[79] Peter A. Armbruster. "Photoperiodic Diapause and the Establishment of *Aedes albopictus* (Diptera: Culicidae) in North America". en. In: *Journal of Medical Entomology* 53.5 (Sept. 2016), pp. 1013–1023. ISSN: 0022-2585, 1938-2928. DOI: 10.1093/jme/tjw037. URL: https://academic.oup.com/jme/article-lookup/doi/10.1093/jme/tjw037 (visited on 04/11/2024).

[80] L. P. Lounibos, R. L. Escher, and R. Lourenço-De-Oliveira. "Asymmetric Evolution of Photoperiodic Diapause in Temperate and Tropical Invasive Populations of ¡I¿Aedes albopictus¡/I¿ (Diptera: Culicidae)". en. In: *Annals of the Entomological Society of America* 96.4 (July 2003), pp. 512–518. ISSN: 00138746, 00138746. DOI: 10.1603/0013-8746(2003)096[0512:AEOPDI]2.0.CO;2. URL: https://academic.oup.com/aesa/article/96/4/512-518/97508 (visited on 04/11/2024).

Journal of the Royal Society Interface

Supplemantary Information

The effect of climate change and temperature extremes on *Aedes albopictus* populations: a regional case study for Italy

Miguel Garrido Zornoza[1,*] Cyril Caminade[2] Adrian M. Tompkins[2]

[1] The Niels Bohr Institute, University of Copenhagen, Blegdamsvej 17, Copenhagen, 2100 Ø, Denmark
[2] Earth System Physics, Abdus Salam International Centre for Theoretical Physics (ICTP), Strada Costiera 11, Trieste, Italy

[*] Corresponding author: mgarrizoraca@gmail.com

S1 Comparison with observations and genetic algorithm calibration

In this study we use ovitrap data from [1–3] to calibrate the temporal dynamics of the vector, as simulated by the model. The ongoing field campaigns behind this dataset have distributed ovitraps in the vicinity of a number of cities in the Emilia-Romagna region (Italy). Ovitrapped eggs are counted and emptied every two weeks. Consequently, for each ovitrap, the available information is the two-week sum of newly laid eggs, *i.e.,* the integrated flux. We here use the median of this flux among all ovitraps in a given city, which we shall denote as $O(\vec{x},t)$. Here, $\vec{x}=(\lambda,\phi)$ points to the geographical location of the cities where the campaign takes place. The median number of observed eggs per unit area of potential breeding sites is thus given by

$$\frac{O(\vec{x},t_k)}{A_{ovitrap}}\ , \tag{S1}$$

with $A_{ovitrap}$ being the area covered by one ovitrap. The assumption here is that the quantity provided by $O(\vec{x},t_k)$ is a perfect proxy for the usage of breeding sites in any other *Ae. albopictus* breeding habitat. This is not necessarily true and is accounted for in the calibration process, as discussed below. Eqn (S1) is then compared against the simulated equivalent, *i.e.,*

$$\sum_{\text{two-week sum}}\left(\frac{\left[\begin{array}{c}\text{Simulated number of newly}\\ \text{laid eggs in the grid cell}\end{array}\right]}{\left[\begin{array}{c}\text{Estimated area of potential}\\ \text{breeding sites in the grid cell}\end{array}\right]}\right)=\sum_{i=0}^{13}\frac{e(\vec{x},t_{k-i})\cdot \cancel{A_{cell}}}{w(\vec{x},t_{k-i})\cdot \cancel{A_{cell}}}\equiv S(\vec{x},t_k)\ , \tag{S2}$$

where $e(\vec{x},t)$ and $w(\vec{x},t)$ are the newly laid egg density and the fraction of potential breeding sites, respectively. The role of the parameter calibration is to make the difference between (S1) and (S2) as small as possible while keeping model parameters, $\vec{K}$, within realistic values, *i.e.,*

$$\vec{K}\qquad s.t.\qquad \frac{O(\vec{x},t_k)}{A_{ovitrap}}-S(\vec{x},t_k;\vec{K})\to 0\ , \tag{S3}$$

$$\vec{K}_{min.}\le\vec{K}\le\vec{K}_{max.}\ . \tag{S4}$$

Even though the ovitrap area, $A_{ovitrap}$, is a known value ($\sim 0.0095m^{-2}$, see referenced sources), ovitraps might not be representative enough for the average "quality" or usage of potential breeding sites found by *Ae. albopictus* mosquitoes in urban and sub-urban environments. In the language of the model, if all urban breeding sites, w_{urbn}, were ovitraps, then $r_{urbn}\to 1$. For this, we allow this parameter ($A_{ovitrap}$) to be calibrated as well, with a maximum allowed value of $0.15m^{-2}$. In this study we maximize the Pearson correlation coefficient, $r^2_{site,all}$, the student's T-Test p-value of the difference in annual means (null hypothesis being the difference is zero), p_T, and the Pearson correlation coefficient of the standardized annual means, $r^2_{ens,y}$ for the observed and simulated egg density signals.

With this, we aim to both, capture the seasonality in the vector activity as well as the inter-annual variability in population densities. In table (S1) we report the ensemble mean and standard deviation resulting from the best 6 out of 60 models of the aforementioned constrained optimization. From these we use the best member's model parameters throughout the study. In Figure (S1) we can see an example convergence of the genetic algorithm to the final values.

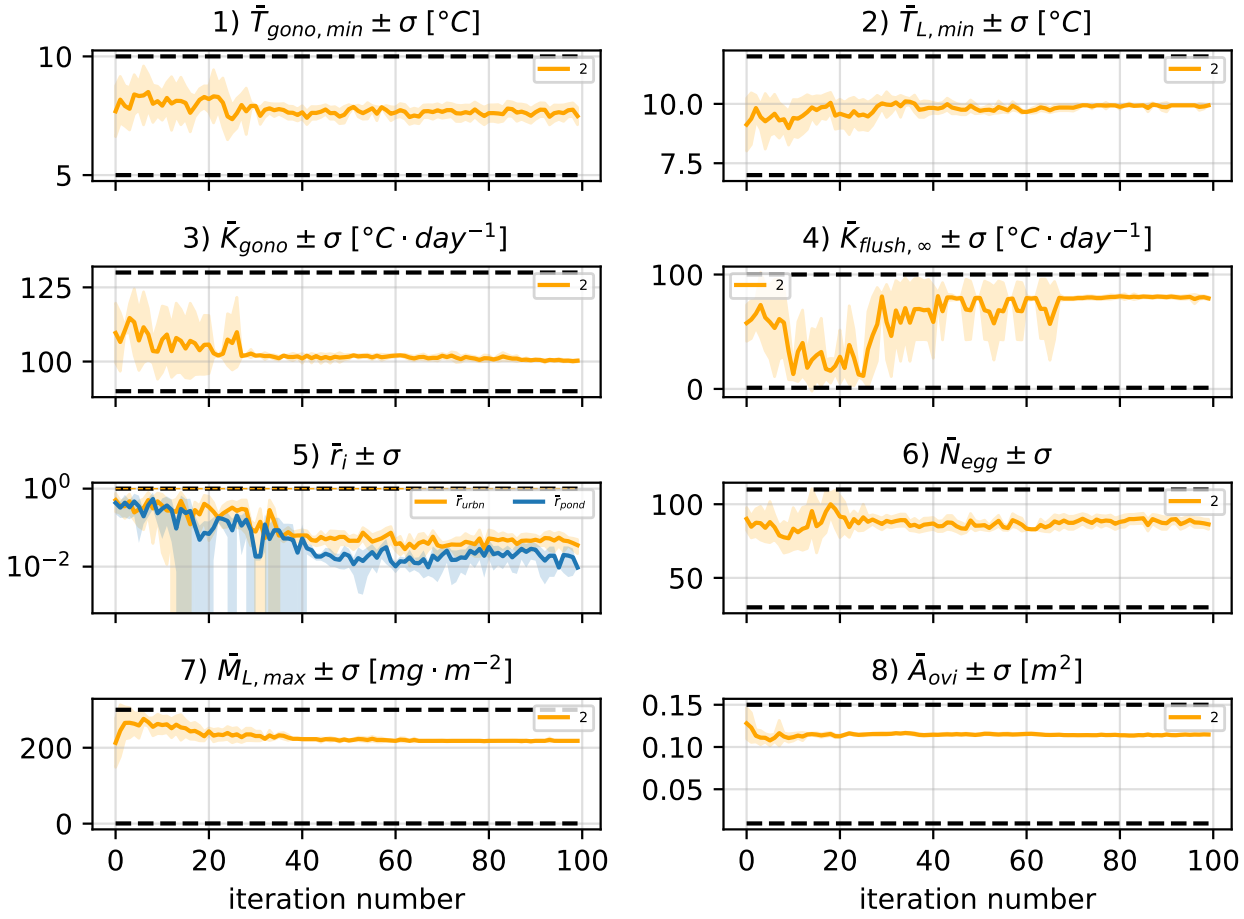

Figure S1: Example convergence of the genetic algorithm calibration. Numbers correspond to those from table S1. Dashed lines indicate upper (*Max.*) and lower (*Min.*) parameter constrains in the optimization process.

Calibrated parameters						
Parameter K	K_μ	K_σ	Best	Default	Min.	Max.
1− Minimum air temperature for gonotrophic cycle $[°C]$	7.48	0.36	7.12	7.5	5 [1]	10 [4, 5] [6, 7][1]
2− Minimum water temperature for larval development $[°C]$	9.93	0	9.93	9.5	7 [2]	12 [2]
3− Degree-days necessary for egg development $[°C \cdot day^{-1}]$	100.28	0.37	100.54	110 [4][3]	100 [none]	120 [none]
4− Flushing factor by precipitation	79.16	1.24	78.50	50	1 [none]	100 [none]
5a− Vector-specific usage of urban sites	0.035	0.014	0.021	0.5	0	1.0
5b− Vector-specific usage of rainfall-related ponds	0.009	0	0.009	0.5	0	1.0
6− Number of laid eggs per batch	86	3	82.97	45	30 [5]	110 [8]
7− Maximum larvae biomass per unit area $[mg \cdot m^{-2}]$	218.18	0.12	218.09	100	0.5 [4, 9] [4]	300 [9]
8− Effective ovitrap area $[m^{-2}]$	0.1147	0.0006	0.1143	0.1	0.0095 [1]	0.15 [none]

Table S1: Ensemble mean, K_μ and standard deviation, K_σ, of the calibrated model parameters using the genetic algorithm from [10]. We also report the *Best* model parameters, the initial value for the search, *Default*, and the upper and lower bounds of the constrained optimization, *Max.* and *Min.*, respectively. Since most parameters are found in the literature to have diverse values, parameter mutation in the GA is performed here with a uniform distribution bounded by the *Min.* and *Max.* values and without the originally implemented penalty caused by deviating from the *Default*. The latter is thus not relevant except in one case (3). We however provide it for reproducibility. [1] Studies report significant differences in the mean threshold temperature for egg development among geographically separated *Ae. albopictus* strains. While most revolve around 10°C the field study [7] shows temperatures as low as $\sim$ 8°C from a $3y$ survey in the Lazio region and [11] reported threshold temperatures as high as 13°C in North Italy. Air temperature can even be a misleading proxy for the start of egg development, since urban environments contain microhabitats, such as catch basins (considered the most productive breeding sites for the tiger mosquito in Italy) that have proven to have significantly higher temperatures that could induce an earlier appearance of the first generation of mosquitoes in spring [12]. We therefore set a low temperature threshold, oriented by the observed counts in the ovitrap data we use in this work. [2] Since, in VECTRI, the water temperature of potential breeding sites is set to have an off-set of +2°C with respect to T_{2m} and we assume the larval and gonotrophic cycles can start at the same time, we simply set the bound for the start of the larval cycle to be +2°C higher than that of the gonotrophic. [3] This value is reported in the modelling study [4], where is sourced however to unpublished work. We thus allow the GA to search around it. [4] Studies of *Ae. Albopictus* abundance have used diverse larval carrying capacities, ranging from $250,000$ [4] to $800,000$ [13] individuals per hectare. VECTRI, however, currently bases its carrying capacity in terms of larval biomass (mg/m^2) rather than individuals. Since the larval age-distribution (and therefore mass distribution) is highly non-trivial this parameter is subject to a high degree of uncertainty. We can establish a lower bound by setting the average weight of each individual to $\sim 0.02\ mg$. This comes from assuming most larvae will be in early development stages (L2 $\sim$ L3 $\sim$ L4 $\sim$ 0) and using the L1 mass value from [9]. With this, if we use the density value from [4] we obtain $0.5\ mg/m^2$.

S2 Validation metrics

S2.1 Correlation matrices for temperature and rainfall

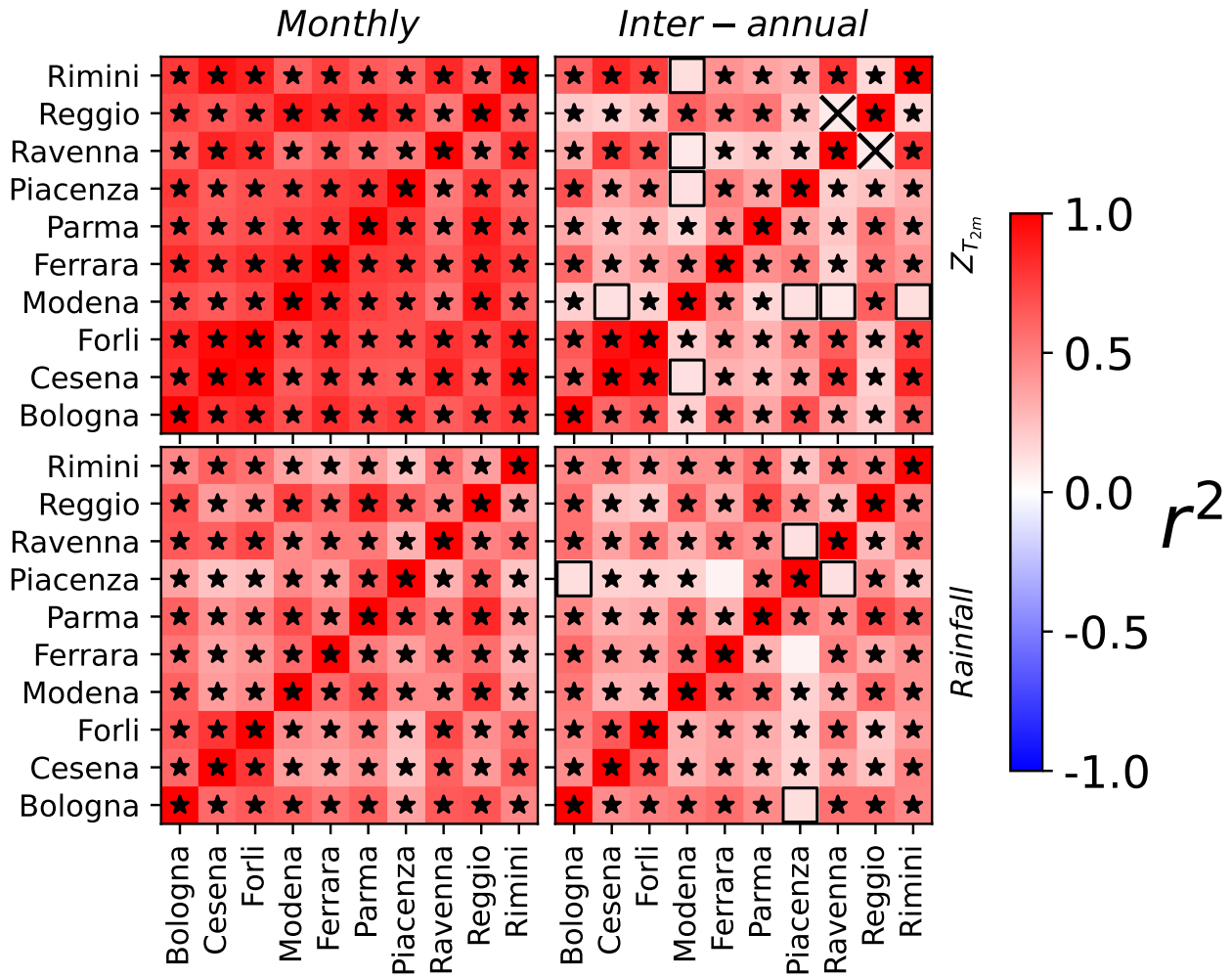

Figure S2: Correlation matrices for two-metre air temperature (upper row) and rainfall (bottom row) among all Italian sites where ovitraps are deployed. Monthly and yearly averages are used (left and right, respectively) to compute the correlations for rainfall and for the detrended and deseasonalized temperature z-score. We indicate significance at the 90% (X), 95% (□) and 99% (*) confidence intervals. Most values for all matrices are significant at the 99% confidence interval, indicating a high degree of spatial homogeneity in monthly and yearly averaged rainfall and in monthly and inter-annual temperature variability among cities in the Emilia-Romagna region.

S2.2 Constructing the ROC curve

The observation datasets [14, 15] contain the longitude and latitude of reported *Ae. albopictus* observations, $\{(\lambda, \phi)\}_o$. In this study we assume *Ae. albopictus* to be absent in locations without a reported observation, being aware of the potential bias introduced by imperfect detection [16]. Each observation point is mapped to the closest box in the model (m) grid $\{(\lambda, \phi)\}_m$. This box is then considered as "positive" (1), whereas the remaining are considered to be "negative" (0). Several observation points can be mapped into the same model grid box.

Model output is somewhat continuous (species are reported as densities) and needs to be transformed into the binary representation of the observation dataset in order to make a comparison. Since occurrence reports are based on mosquito observations we chose the vector population density as the model output to be compared against. In particular, the time average over the study period (1980-2023), $\overline{V}(\lambda, \phi)$. For this, a threshold value of population density, V_{th}, is selected and all model values above (below) it are transformed into 1s (0s). In this way one gets two binary maps, one for the observations and the other for the modelled vector densities. The overlap of both maps is used to compute the true (TPR) and false (FPR) positive rates, as explained in the main text. By iteratively changing the threshold value one can get a set of $\{(TPR,\ FPR)\}$ pairs to build the ROC curve. The interval of sampled threshold values depends on the problem at hand. The lower bound, V^l_{th}, must be such that $V^l_{th} < \overline{V}(\lambda, \phi)\ \forall (\lambda, \phi) \in \{(\lambda, \phi)\}_m$, which means the model predicts *Ae. albopictus* to be present everywhere. In this limit the TPR is equal to one, since each occurrence spot is matched with a positive prediction by the model. The downside is that the FPR is also one, since true negatives will be missed (this scenario is the upper right corner in the ROC curve of Fig. 2c). The opposite argument applies when defining an upper threshold value, V^u_{th}. Typically, one has to compromise with a threshold value $V^l_{th} < V_{th} < V^u_{th}$ when calibrating a diagnostic tool.

In Alg. (1) we present the pseudocode used to build the ROC curve.

Algorithm 1: Pseudocode to build the ROC curve

input : $\{\overline{V}(\lambda, \phi)\}_m$, $\{(\lambda, \phi)\}_o$
output: $TPR(V_{th}), FPR(V_{th})$

Map observation locations to closest point in the model grid;
$M(\lambda, \phi) = 0\ \forall (\lambda, \phi) \in \{(\lambda, \phi)\}_m$; /* Initialize observed map (M) */
for $(\lambda_i, \phi_i) \in \{(\lambda, \phi)\}_o$ **do** /* For all observed points */
  $(\lambda_m, \phi_m) \leftarrow (\lambda_i, \phi_i)$; /* get closest coordinates of model grid */
  if $M(\lambda_m, \phi_m)\ != 1$ **then**
    $M(\lambda_m, \phi_m) = 1$; /* Update if no previous iteration has mapped an observation here */
  else
    Pass ; /* Otherwise, pass */
  end
end
Compute True and False Positive Rates for all thresholds, V_{th}, in the list $V_{list} = [V^l_{th}, V^1_{th}, V^2_{th}, ..., V^u_{th}]$;
for V_{th} *in* V_{list} **do** /* For all sampled thresholds */
  $N_p = \sum_{(\overline{V} > V_{th})} 1$; /* Sum over all places where density is bigger than threshold */
  $N_n = \sum_{(\overline{V} < V_{th})} 1$; /* Equivalently: number of predicted negatives */
  $N_{tp} = \sum_{(\overline{V} > V_{th}\ \&\ M=1)} 1$; /* Number of true positives */
  $N_{fn} = \sum_{(\overline{V} < V_{th}\ \&\ M=1)} 1$; /* Number of false negatives */
  $N_{fp} = N_p - N_{tp}$; /* Number of false positives */
  $N_{tn} = N_n - N_{fn}$; /* Number of true negatives */
  $TPR = \frac{N_{tp}}{N_{tp}+N_{fn}}$; /* True Positive Rate */
  $FPR = \frac{N_{fp}}{N_{fp}+N_{tn}}$; /* False Positive Rate */
end

S3 Temporal validation of the model against egg data in Italian sites

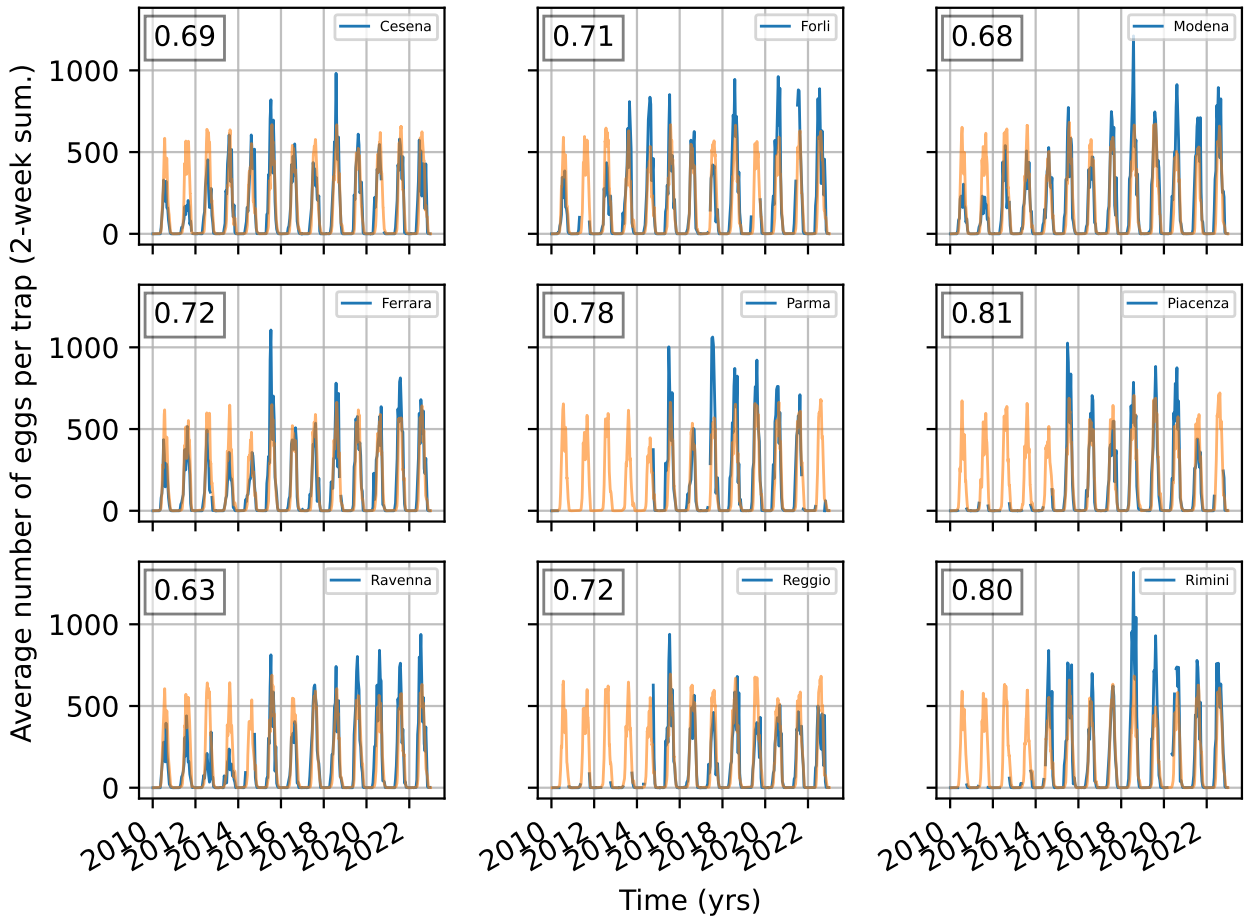

Figure S3: Temporal validation of the Italian sites (excluding Bologna). We show the 2-week total simulated (orange) and observed (blue) average egg density. The $r^2_{site,all}$ coefficent is reported for each site.

S4 Season duration threshold and bulk net effect of warm events

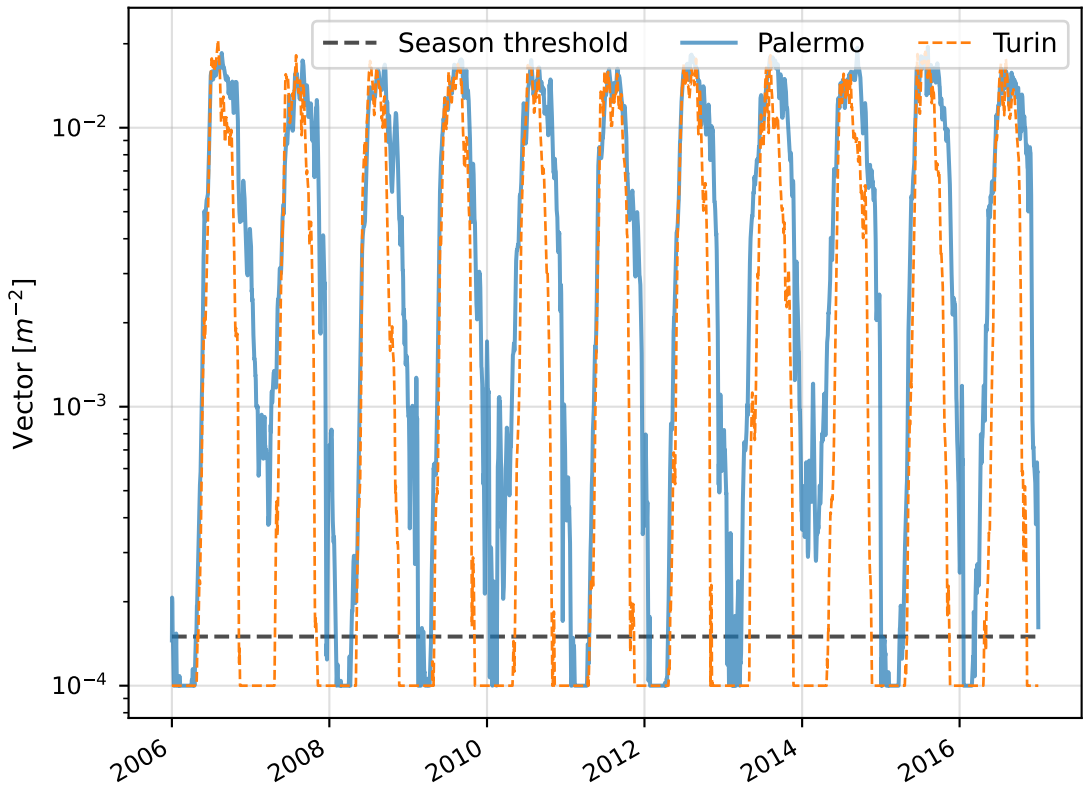

Figure S4: Time series of the vector density in Palermo and Turin throughout 10y of the *cntl* simulation. In VECTRI, the lowest population densities are around $\sim 10^{-4}\ m^{-2}$, marking the inactive state of the mosquito. We here define the density threshold of $1.5 \cdot 10^{-4}\ m^{-2}$ as the start of the mosquito season. With this metric, locations such as Palermo can be homodynamic.

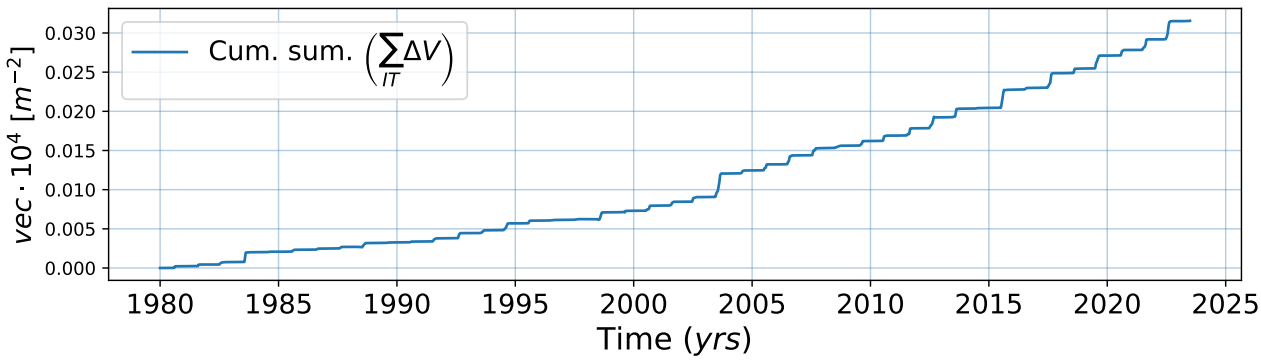

Figure S5: Cumulative summation over the whole spatial grid of the difference in vector densities between the *cntl* and *clipped* experiments.

S5 Further examples of short-term heatwave dynamics

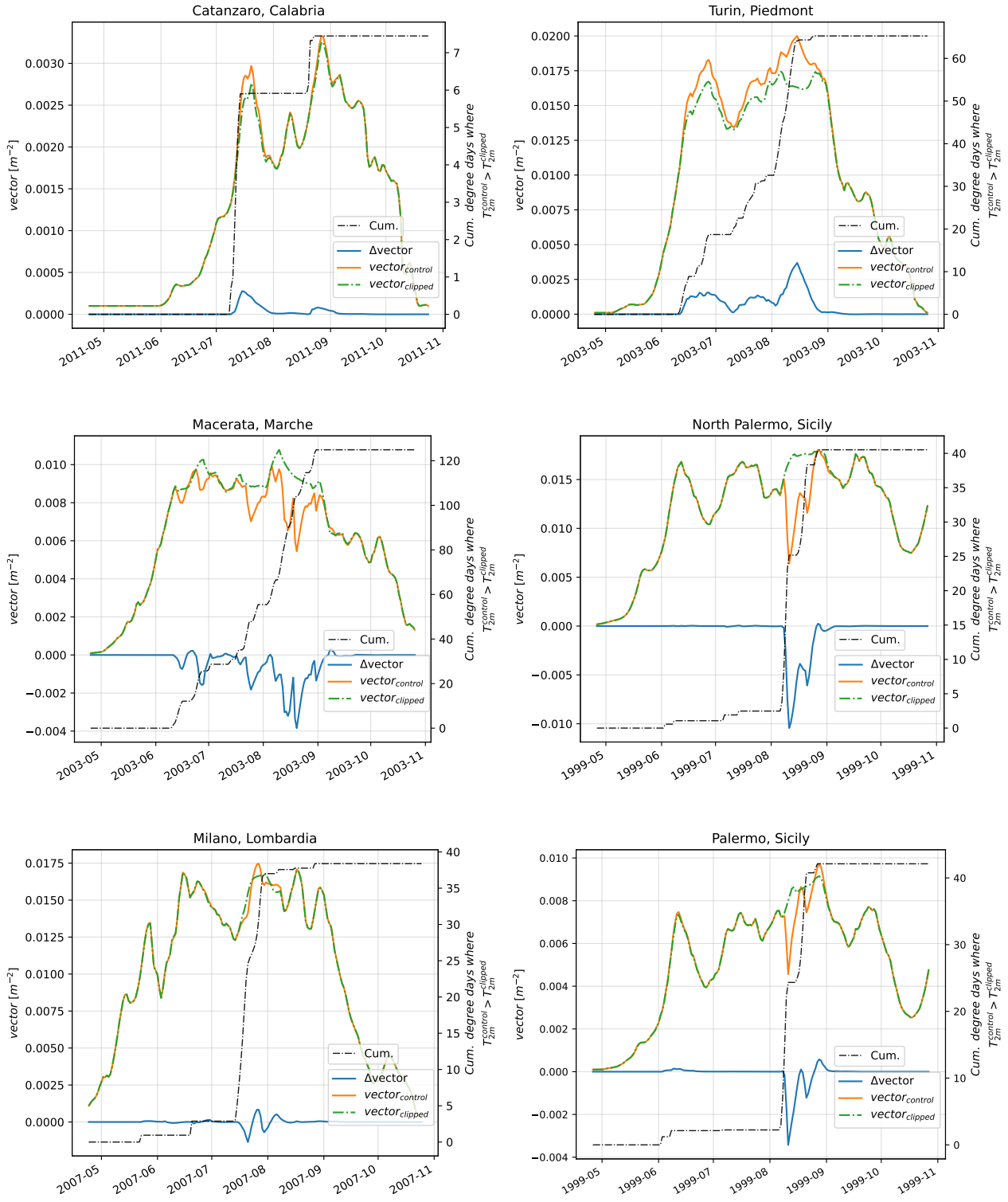

Figure S6: Example dynamics from cases 1 (top), 2 (middle) and 3 (bottom) resulting from short-term warm events.

References

[1] Marco Carrieri et al. "Surveillance of the chikungunya vector Aedes albopictus (Skuse) in Emilia-Romagna (northern Italy): organizational and technical aspects of a large scale monitoring system". en. In: *Journal of Vector Ecology* 36.1 (June 2011), pp. 108–116. ISSN: 10811710. DOI: 10.1111/j.1948-7134.2011.00147.x. URL: http://doi.wiley.com/10.1111/j.1948-7134.2011.00147.x (visited on 02/26/2024).

[2] Marco Carrieri et al. "Quality control and data validation procedure in large-scale quantitative monitoring of mosquito density: the case of *Aedes albopictus* in Emilia-Romagna region, Italy". en. In: *Pathogens and Global Health* 111.2 (Feb. 2017), pp. 83–90. ISSN: 2047-7724, 2047-7732. DOI: 10.1080/20477724.2017.1292992. URL: https://www.tandfonline.com/doi/full/10.1080/20477724.2017.1292992 (visited on 02/26/2024).

[3] Marco Carrieri et al. "Egg data validation in quantitative monitoring of *Aedes albopictus* in Emilia-Romagna region, Italy". en. In: *Pathogens and Global Health* 115.2 (Feb. 2021), pp. 125–131. ISSN: 2047-7724, 2047-7732. DOI: 10.1080/20477724.2020.1866375. URL: https://www.tandfonline.com/doi/full/10.1080/20477724.2020.1866375 (visited on 02/26/2024).

[4] Annelise Tran et al. "A Rainfall- and Temperature-Driven Abundance Model for Aedes albopictus Populations". en. In: *International Journal of Environmental Research and Public Health* 10.5 (Apr. 2013), pp. 1698–1719. ISSN: 1660-4601. DOI: 10.3390/ijerph10051698. URL: http://www.mdpi.com/1660-4601/10/5/1698 (visited on 04/04/2024).

[5] Giovanni Marini et al. "Influence of Temperature on the Life-Cycle Dynamics of Aedes albopictus Population Established at Temperate Latitudes: A Laboratory Experiment". en. In: *Insects* 11.11 (Nov. 2020), p. 808. ISSN: 2075-4450. DOI: 10.3390/insects11110808. URL: https://www.mdpi.com/2075-4450/11/11/808 (visited on 04/04/2024).

[6] H. Delatte et al. "Influence of Temperature on Immature Development, Survival, Longevity, Fecundity, and Gonotrophic Cycles of *Aedes albopictus* , Vector of Chikungunya and Dengue in the Indian Ocean". en. In: *Journal of Medical Entomology* 46.1 (Jan. 2009), pp. 33–41. ISSN: 0022-2585, 1938-2928. DOI: 10.1603/033.046.0105. URL: https://academic.oup.com/jme/article-lookup/doi/10.1603/033.046.0105 (visited on 02/01/2024).

[7] Federico Romiti et al. "Aedes albopictus (Diptera: Culicidae) Monitoring in the Lazio Region (Central Italy)". en. In: *Journal of Medical Entomology* 58.2 (Mar. 2021). Ed. by Dina Fonseca, pp. 847–856. ISSN: 0022-2585, 1938-2928. DOI: 10.1093/jme/tjaa222. URL: https://academic.oup.com/jme/article/58/2/847/5940898 (visited on 04/05/2024).

[8] Nor Atikah Farhah Muhammad et al. "Biting rhythm and demographic attributes of Aedes albopictus (Skuse) females from different urbanized settings in Penang Island, Malaysia under uncontrolled laboratory conditions". en. In: *PLOS ONE* 15.11 (Nov. 2020). Ed. by Jiang-Shiou Hwang, e0241688. ISSN: 1932-6203. DOI: 10.1371/journal.pone.0241688. URL: https://dx.plos.org/10.1371/journal.pone.0241688 (visited on 04/05/2024).

[9] Arne Bomblies, Jean-Bernard Duchemin, and Elfatih Ab Eltahir. "A mechanistic approach for accurate simulation of village scale malaria transmission". en. In: *Malaria Journal* 8.1 (Dec. 2009), p. 223. ISSN: 1475-2875. DOI: 10.1186/1475-2875-8-223. URL: https://malariajournal.biomedcentral.com/articles/10.1186/1475-2875-8-223 (visited on 04/04/2024).

[10] Adrian M. Tompkins and Madeleine C. Thomson. "Uncertainty in malaria simulations in the highlands of Kenya: Relative contributions of model parameter setting, driving climate and initial condition errors". en. In: *PLOS ONE* 13.9 (Sept. 2018). Ed. by Ana Paula Arez, e0200638. ISSN: 1932-6203. DOI: 10.1371/journal.pone.0200638. URL: https://dx.plos.org/10.1371/journal.pone.0200638 (visited on 11/30/2023).

[11] David Roiz et al. "Effects of Temperature and Rainfall on the Activity and Dynamics of Host-Seeking *Aedes albopictus* Females in Northern Italy". en. In: *Vector-Borne and Zoonotic Diseases* 10.8 (Oct. 2010), pp. 811–816. ISSN: 1530-3667, 1557-7759. DOI: 10.1089/vbz.2009.0098. URL: https://www.liebertpub.com/doi/10.1089/vbz.2009.0098 (visited on 04/04/2024).

[12] Roberto Vallorani et al. "Temperature Characterization of Different Urban Microhabitats of *Aedes albopictus* (Diptera Culicidae) in Central–Northern Italy". en. In: *Environmental Entomology* 44.4 (Aug. 2015), pp. 1182–1192. ISSN: 0046-225X, 1938-2936. DOI: 10.1093/ee/nvv067. URL: https://academic.oup.com/ee/article-lookup/doi/10.1093/ee/nvv067 (visited on 04/05/2024).

[13] S. Metelmann et al. "The UK's suitability for *Aedes albopictus* in current and future climates". en. In: *Journal of The Royal Society Interface* 16.152 (Mar. 2019), p. 20180761. ISSN: 1742-5689, 1742-5662. DOI: 10.1098/rsif.2018.0761. URL: https://royalsocietypublishing.org/doi/10.1098/rsif.2018.0761 (visited on 11/28/2023).

[14] Moritz Ug Kraemer et al. "The global distribution of the arbovirus vectors Aedes aegypti and Ae. albopictus". en. In: *eLife* 4 (June 2015), e08347. ISSN: 2050-084X. DOI: 10.7554/eLife.08347. URL: https://elifesciences.org/articles/08347 (visited on 07/06/2024).

[15] *Aedes albopictus (Skuse, 1894) in GBIF Secretariat (2023). GBIF Backbone Taxonomy. Checklist dataset https://doi.org/10.15468/39omei accessed via GBIF.org on 2024-03-04.*

[16] Darryl I. Mackenzie. "WAS IT THERE? DEALING WITH IMPERFECT DETECTION FOR SPECIES PRESENCE/ABSENCE DATA †". en. In: *Australian & New Zealand Journal of Statistics* 47.1 (Mar. 2005), pp. 65–74. ISSN: 1369-1473, 1467-842X. DOI: 10.1111/j.1467-842X.2005.00372.x. URL: https://onlinelibrary.wiley.com/doi/10.1111/j.1467-842X.2005.00372.x (visited on 08/15/2024).

4

The role of climatic variability on *Anopheles gambiae s.s.* populations

4.1 Introduction

Malaria is a mosquito-borne infectious disease caused by 5 *Plasmodium* [1] species, from which *Plasmodium falciparum* is the deadliest [84]. The former is transmitted through the bite of an *Anopheles* mosquito. The species *Anopheles gambiae s.s.* (*sensu stricto*) (hereafter *An. gambiae*) is widespread across most sub-Saharan Africa [85] and, given its antropophilic bitting behaviour, constitutes one of the most important malaria vectors in the continent [86]. As with other ectothermic arthropods, the life cycle of this mosquito is shaped by climatic factors and, consequently, climate-aware models can be used to study some aspects of its behaviour [80]. In this chapter we explore how air temperature variability at two-metre heigh, or two-metre air temperature variability, affects the population of the mosquito *An. gambiae*.

The underlying idea is that any given time series of this variable, $T_{2m}(t)$, is a composition of processes acting on different time scales. On top of the anthropogenically-driven trending background (climate change) [87] we find: changes in Earth's physical processes that manifest over periods of $\sim$ 1-10 years, driven by, *e.g.,* changes in Solar activity [88], volcanic eruptions [89, 90] or ocean-atmosphere interactions, such as El Niño [91, 92] ; processes with sub-daily time scales, like the diurnal cycle, convective processes or frontal systems. By suppressing the signal's variability for the desired time scale we aim to understand its effect on the population of the mosquito.

[1] A genus of eukaryote obligate parasites of vertebrates and insects.

The layout of this study is broad and unfinished. From the aforementioned time scales we here present some explorations of the effect of daily variability. Ultimately, the goal of this study is to gain insights on how climatic changes, at different time scales, affect the population of *An. gambiae* and, consequently, malaria dynamics.

4.2 Objectives

The objective of this study is thus one:

1.- Knock out experiment: In order to understand the impact of two-metre air temperature variability we perform a knock out experiment, namely a simulation where the variable of interest, in our case T_{2m}, lacks variability in the targeted time scale. The resulting signal is then compared against a *control* counterpart, *i.e.,* a simulation where no modifications have been made to the temperature series. Both experiments are performed with linearly detrended air temperature time series.

4.3 Methods

4.3.1 Model

We will here use the uncalibrated VECTRI model. In this study the model is set to describe the ecology of *An. gambiae* [53, 61, 68]. The main differences with respect to the description of *Ae. albopictus* rely on the temperature-dependent mortality scheme for adult vectors, larvae and eggs, the development rates and the preferred breeding sites. The mathematical structure describing the dynamics is however the same.

The usage coefficients for permanent and urban-related ponds, r_{perm} and r_{urbn}, respectively, are set to a very low number (10^{-6}), establishing the focus on rainfall-related temporary ponds.

4.3.2 Daily variability: knock out experiment

Time filters

It is our objective here to split a stochastic process, $X(t)$, into certain components characterized by distinct time scales, *e.g.,* fast (F) and slow (S),

$$X(t) = X(t)^F + X(t)^S \ . \tag{4.1}$$

This is the general purpose of **time filters**, where an input signal, $X(t)$, is transformed into an output with, ideally, the required suppressed variability, $Y(t)$. We will focus on linear filters, which are operators of the type

$$Y(t) = \sum_{k=-\infty}^{\infty} a_k X_{t+k} \ , \ a_k \in \mathbb{R} \ , \tag{4.2}$$

with $\sum_{k=-\infty}^{\infty} |a_k| < \infty$. Particularly, since in practice one works with a finite time series,

$$Y(t) = \sum_{k=-K}^{K} a_k X_{t+k} \ . \tag{4.3}$$

The weights, a_k, are free parameters that can be chosen so that the signal retains the desired time scales, filtering out the rest. Filters that retain high, short and intermediate time scales are typically known as *short-*, *high-* and *band-pass* filters. The notions of high, short and intermediate depend on the problem at hand. It is important to understand the effect filters have on the spectral density of our signal. For the case of filter (4.3), the input and output spectral densities are related by

$$\Gamma_{yy}(w) = |c(w)|^2 \, \Gamma_{xx}(w), \tag{4.4}$$

(see section 4.A) where $c(w)$ is the so-called frequency response function

$$c(w) = \sum_{k=-K}^{K} a_k e^{2\pi i k w} \ . \tag{4.5}$$

On a side note, a perfect filter that suppresses all frequencies above (below) a certain threshold, ω_0, would have a box-shaped frequency response function, equal to unity below (above) that threshold, $c(w) = 1$ for $\omega < \omega_0$ ($> \omega_0$), and zero otherwise. It would also require infinitely non-zero weights and thus one has to compromise with a less abrupt cut-off that has a finite number of weights.

The structure of $c(w)$ will therefore determine the effect and quality of our filter. For a more extended discussion we refer the reader to [93].

The "Running Mean" filter

The *running mean* or moving average is a simple filter used to suppress high-frequency variability. This time filter has weights

$$a_k = \frac{1}{2K+1} \ , \ -K \leq k \leq K \ , \tag{4.6}$$

is symmetric ($a_k = a_{-k}$) and preserves the mean of the signal, since

$$a_0 + 2\sum_{k=1}^{K} a_k = 1 \ . \tag{4.7}$$

A linear filter with weights (4.6) is commonly known as *centred* running mean, as opposed to *forward* or *backward* where the weights would be on either side of the time stamp. The response function of this filter is

$$c(\omega) = \sum_{k=-K}^{K} \frac{1}{2K+1} \cdot e^{2\pi i k \omega} \ . \tag{4.8}$$

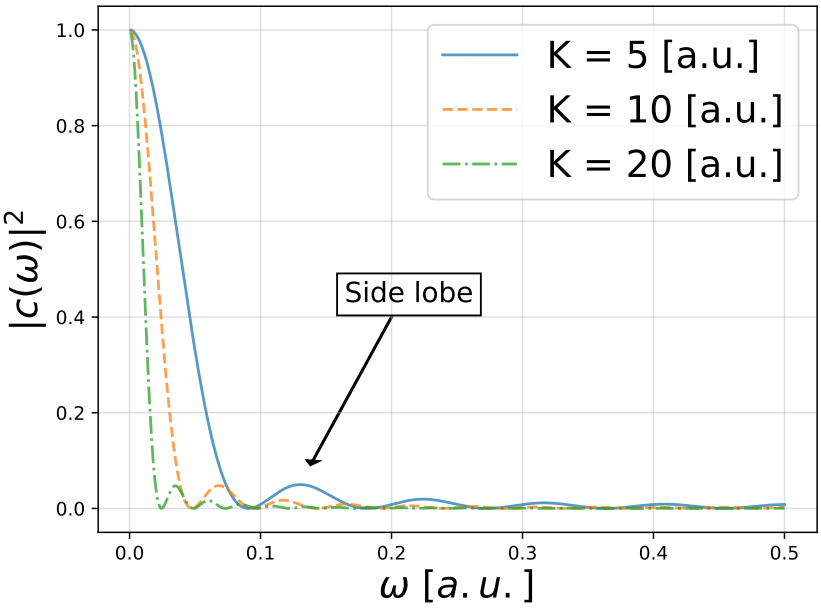

Figure 4.1: Modulus of the running mean's response function for three filter lengths, $2K + 1$.

This low-pass filter is far from perfect, since the response function has strong side lobes that allow for some high frequency leakage (Fig. 4.1). Our knock out experiment will be a **two-week centred running mean** applied to the two-meter air temperature time series, $T_{2m}(t)$, *i.e.,*

$$T_{2m}^{rm}(t_l) \equiv \sum_{k=-7}^{7} \frac{1}{15} \cdot T_{2m}(t_{l+k}) \; . \tag{4.9}$$

Example on a real time series

Let us now look at the effect of filter (4.9) on an archetypical $T_{2m}(t)$ time series. We first linearly detrend the process, accounting for the linear increase caused by global warming. On the resulting series we apply a centred two-week running mean (Fig. 4.2). We use a periodogram as estimator of the spectral density. The effect of the linear filter is obtained by multiplying the spectral density estimation with the modulus of the response function, $|c(\omega)|^2$ (Fig. 4.2). As expected, higher frequencies are damped with clearly visible side lobes remaining.

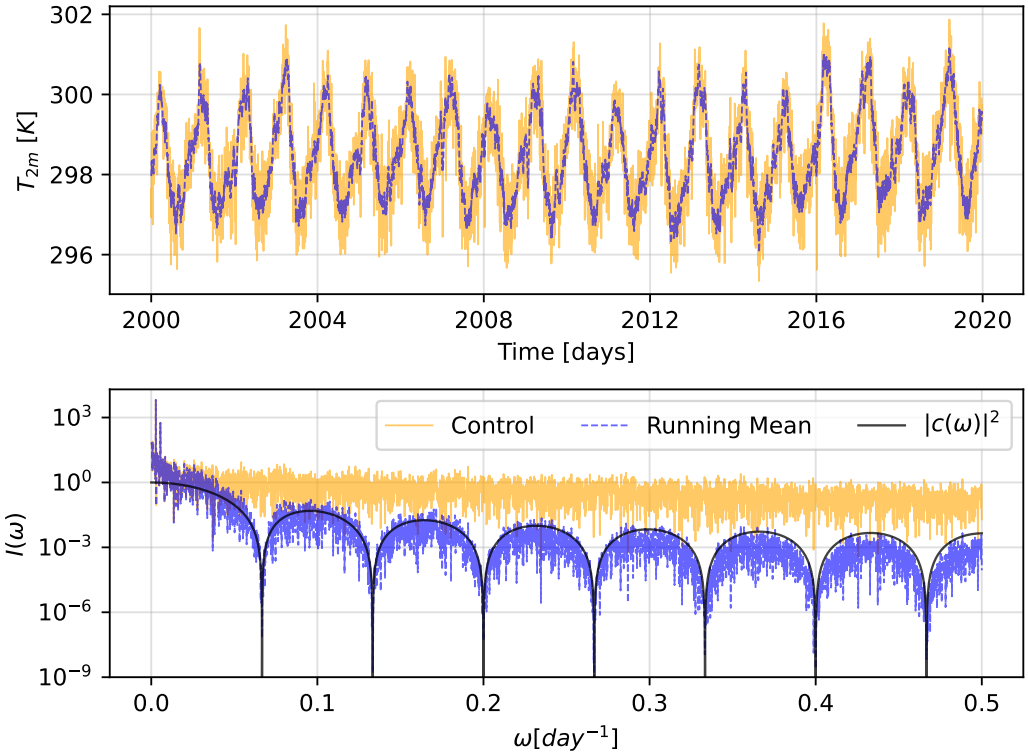

Figure 4.2: Upper panel: *control* versus *running mean* linearly detrended two-metre air temperature in Sierra Leone, $(\lambda, \phi) = (12.5^{\circ}\ W, 8^{\circ}\ N)$ (see section 4.3.3 for input data). Lower panel: periodogram of either series and modulus of the response function.

4.3.3 Input data

Daily two-metre air temperature and rainfall values are obtained from the ERA5 global reanalysis data set [94]. We used data for the years 1990-2019. The region of study is a highly populated area in sub-Saharan Africa (Fig. 4.3). Particularly: Senegal, Gambia, Guinea-Bissau, Guinea, Sierra Leone, Liberia, Ivory Coast, Burkina Faso, Mali, Ghana, Togo, Benin and Nigeria. Human population density estimates, necessary in VECTRI, are obtained from the *Gridded Population of the World GPwv4* project [71] and interpolated to the climate grid using a conservative interpolation method with the CDO software [72].

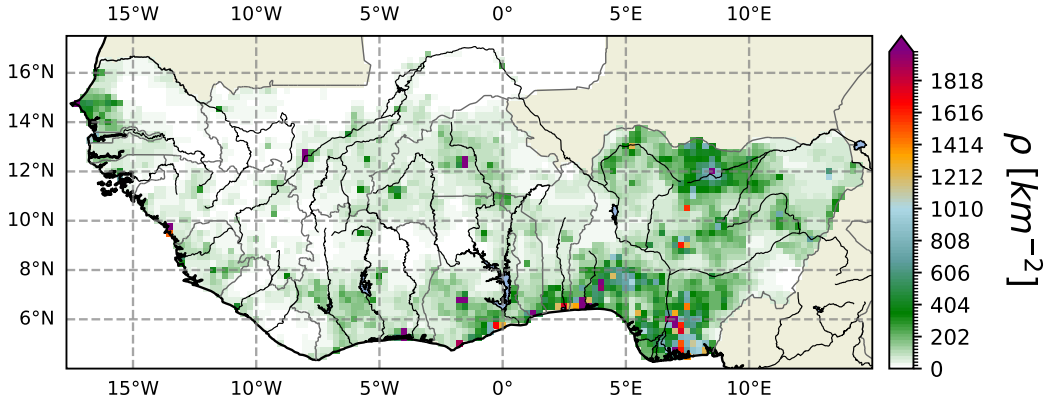

Figure 4.3: Human population density across the region of study.

4.4 Results

4.4.1 Control run

Long-term average behaviour

Let us denote $\overline{\square}$ as the average over the total time period (1990-2019) and $\langle \square \rangle_\tau$ as the τ-*climatological* operator, *i.e.,* a multi-year operation over the subset τ within each year [2]. Before comparing both experiments let us first look at the *control*'s average behaviour. Sub-Saharan Africa is a region where, temperature wise, conditions are suitable for year-round mosquito activity [3]. Consequently, rainfall, necessary for the creation of temporary breeding sites, represents the main driver controlling the spatial distribution of the arthropod's activity. In our simulations, mean vector populations, as expected, are mainly driven by rainfall occurrence (Fig. 4.4).

Seasonality

[2] If τ is, *e.g., day*-climatological *mean*, then by this we mean an average over all 1st of January, 2nd, ... and so on for all days in the year, using all years (in our case from 1990 until 2019) to compute each average. If we instead had a *day*-climatological *median* we would then calculate the $50th$ percentile over a same-day $30y$ sample.

[3] In VECTRI, temperature thresholds for *An. gambiae* larval and egg development are $12.16\ ^\circ C$ and $7.7\ ^\circ C$, respectively. The minimum air temperature in the ERA5 dataset for the studied region from 1990-2019 is $11.05\ ^\circ C$ and $13.56\ ^\circ C$ in the *running mean* experiment. The minimum water temperature is, therefore, $9.05\ ^\circ C$.

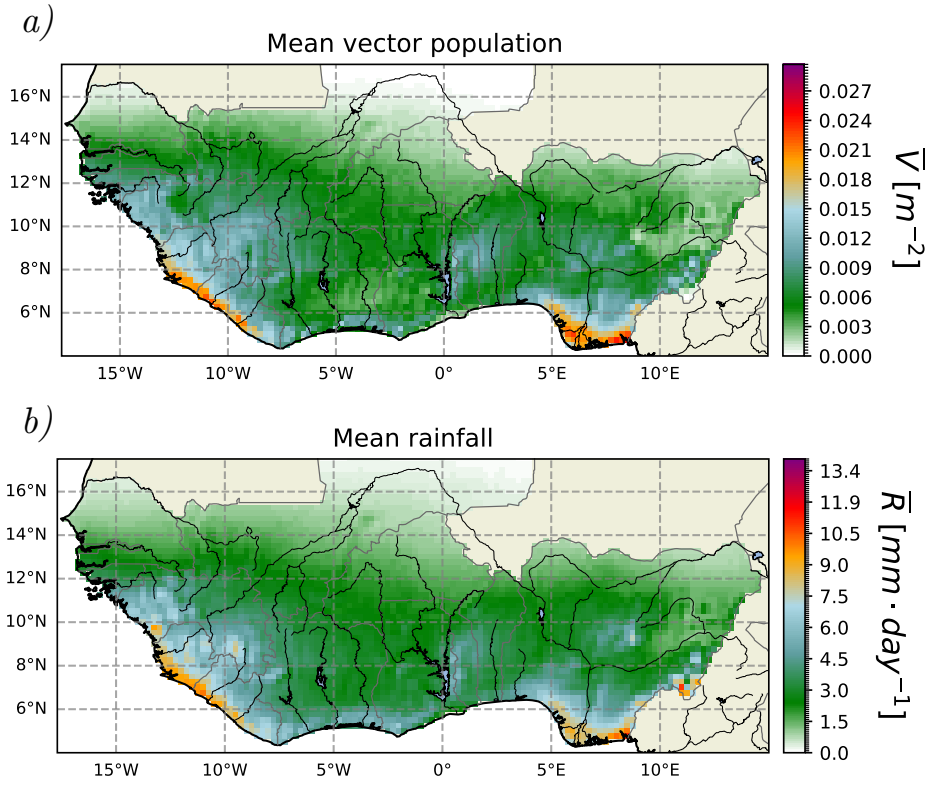

Figure 4.4: Time average of $a)$ the vector population density and $b)$ rainfall.

As a phenomenon partly driven by rainfall, the simulated population of *An. gambiae* shows a pronounced seasonality, with high values coinciding with the rainy season (Fig. 4.5 & 4.6). Simulated hotspots are located in the western coast, covering Senegal, Gambia, Guinea-Bissau, Guinea and Sierra Leone, as well as the coastal areas of Nigeria. Inland hotspots include the southernmost region of Mali and a western area of Nigeria. This is, however, not a risk estimate, since it lacks a description of the vectorial capacity [4].

4.4.2 Daily variability

Seasonality

The effect of daily two-metre air temperature variability on the average population of the mosquito is highly seasonal as well (Fig. 4.7). Averaged differences between *control* and *running mean* (*rm* hereafter) experiments yield values one to two orders of magnitude below absolute numbers. Month-climatological

[4] Understood as "*the number of potential new malaria cases originating per day from each existing malaria case, owing to transmission by a particular vector species*" [86, 95].

mean temperatures, $\langle T_{2m} \rangle_{month}$, seem to be a good proxy to estimate the geographical areas where this variability will have either a positive or a negative effect on the mosquito population. When these temperatures are too high or too low daily variability acts to the detriment of the mosquito, whereas temperatures around $297.5\ K$ seem to be a sweet spot for positive effects, *i.e.,* increased populations (Fig. 4.8a). These temperature-delimited regions are heterogenously spread across the study area (Fig. 4.8b). To test whether the month-climatological mean is a good diagnostic tool to delineate the regions where $\Delta V > 0$ on a monthly basis, we compare it against all individual monthly means in the 30-year time series. This is performed by quantifying their spatial overlap in terms of the number of grid points where both ΔV's are positive, or the number of true positives (TP), the number of grid points where both ΔV's are negative, or the number of true negatives (TN), and so on. Each individual month in the 30-year time series can then be reduced to one number (if we look at the TPs), each month of the year (January, February, ...) to a mean (calculated with 30 values) with standard deviation and the 30 years of data to a simple time series (4.8c) that allows us to ascertain the goodness of $\langle T_{2m} \rangle_{month}$ as a good diagnostic tool.

Season length

Warm heat events and cold snaps, acting on daily to weekly time scales and, therefore, damped in the *rm* experiment, have the potential to either benefit or impair vector populations, potentially anticipating or delaying the mosquito season. Temperature wise, the region of study is suitable for vector activity all year-round and, consequently, this effect might only be visible with the advent of the rainy season. We count active vector days, τ_V, as the number of days the vector density remains above $1.5 \cdot 10^{-4}\ m^{-2}$ (threshold selection was discussed in the Supplementary material of the manuscript of the previous chapter). The month-climatological mean of the difference, $\langle \Delta\tau_V \rangle_{month} = \langle \tau_V^{cntl} - \tau_V^{rm} \rangle_{month}$, marks regions where variability typically increases or decreases activity duration. The *rm* experiment presents a higher number of active days and a negative boundary appears and moves northward, following the rain (Fig. 4.9). Some regions present a positive value. Both positive and negative cases are related to a low population of the vector (Fig. 4.10, top and middle) and these effects are highly asymmetric in time, namely activity differences appear mainly at the beginning of the vector season and not at the end (Fig. 4.9 & 4.10, top). In Fig. 4.10, middle and bottom, we

show how the positive ($\Delta V > 0$) and negative effects ($\Delta V < 0$), discussed in the previous section, alternate as the system moves in and out of distinct temperature regimes.

4.5 Discussion

At this point, we have studied a few traits of the sensitivity of the uncalibrated VECTRI model against two-metre air temperature daily variability. We started by looking at the average behaviour of the vector and understood its pronounced rain-driven seasonality. The effect of variability on *An. gambiae* populations is highly seasonal as well, with net effect and location well described by the monthly temperature climatology. Furthermore, variability is also shown to affect the number of days of vector activity, mainly in areas of low vector density at the start of the rainy season.

Future prospects

This project is in its starting phase and further inquiries are required for a complete view.

1. **Mechanistic understanding**: one of the advantages of using a dynamical model is the possibility to give a mechanistic interpretation to the observed behaviour. Ultimately, we should formulate links between the observed model behaviour and the vector, larval and egg temperature-dependent mortality schemes as well as the larval breeding site model, where rainfall plays a crucial role.

2. **Extremes**: beyond the average behaviour one should also address the frequency and magnitude of variability-driven "extremes", since these might have a higher importance for vector forecasting and risk assessment.

3. **Variability over a trending climate**: by re-introducing the background linear temperature trend onto the two-metre air temperature series one would progressively move the seasonal cycle and daily-weekly fluctuations towards different temperature intervals, potentially altering the

net effect of these fluctuations. This more realistic scenario should be studied once the aforementioned points are fully understood.

4. **Risk estimates**: it is important to notice that our vector maps report the population density instead of the so-called *vectorial capacity*. Despite being a more realistic risk estimate, its complexity and dependence on traits such as host preference or vector competence make it accessible only under further model development. Future development should, therefore, focus on building a metric with this "epidemiological" dimension if one is to relate changes in vector population to potential changes in malaria dynamics.

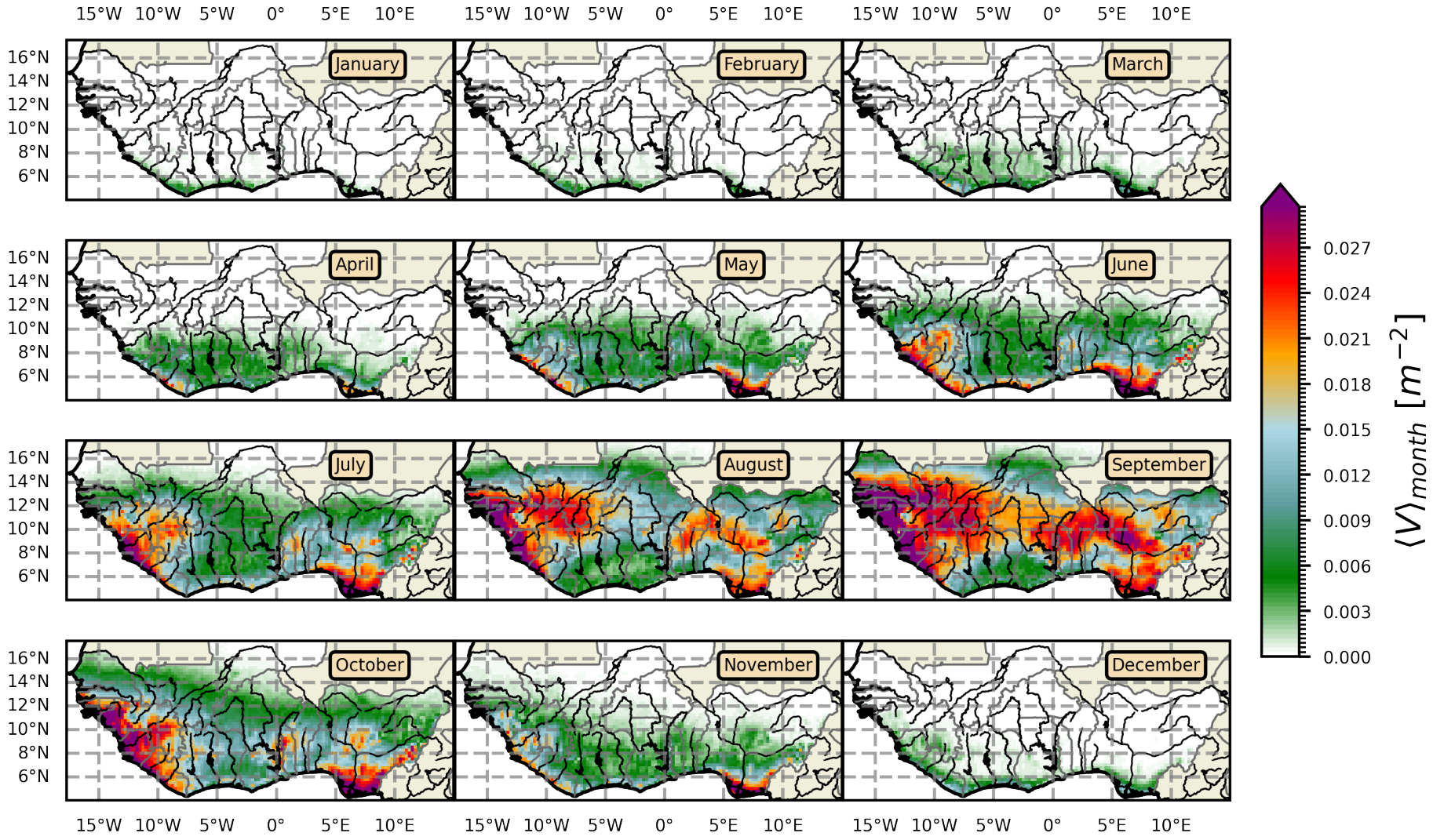

Figure 4.5: Month-climatological mean of the *control*'s vector population density.

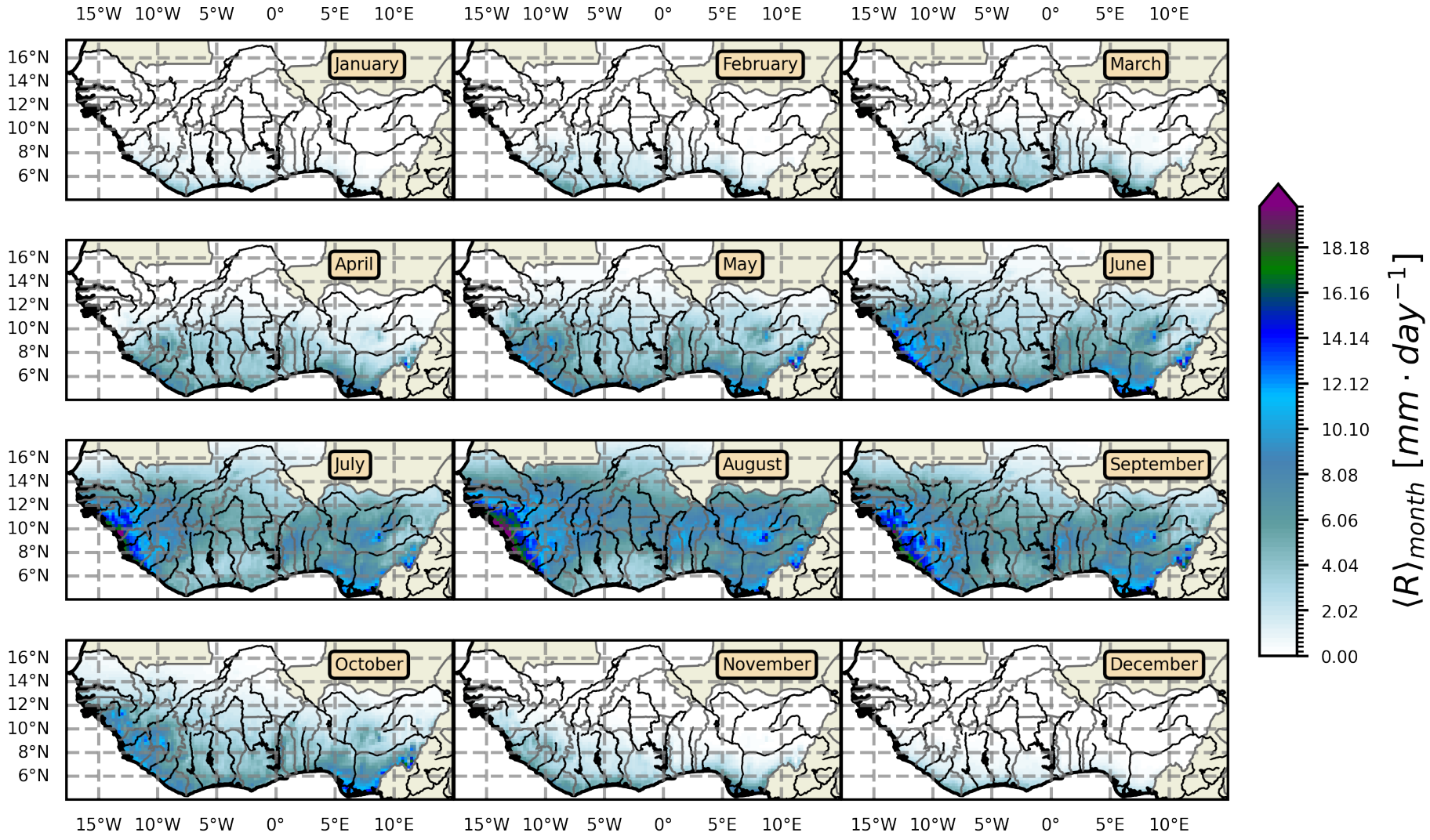

Figure 4.6: Rainfall month-climatological mean.

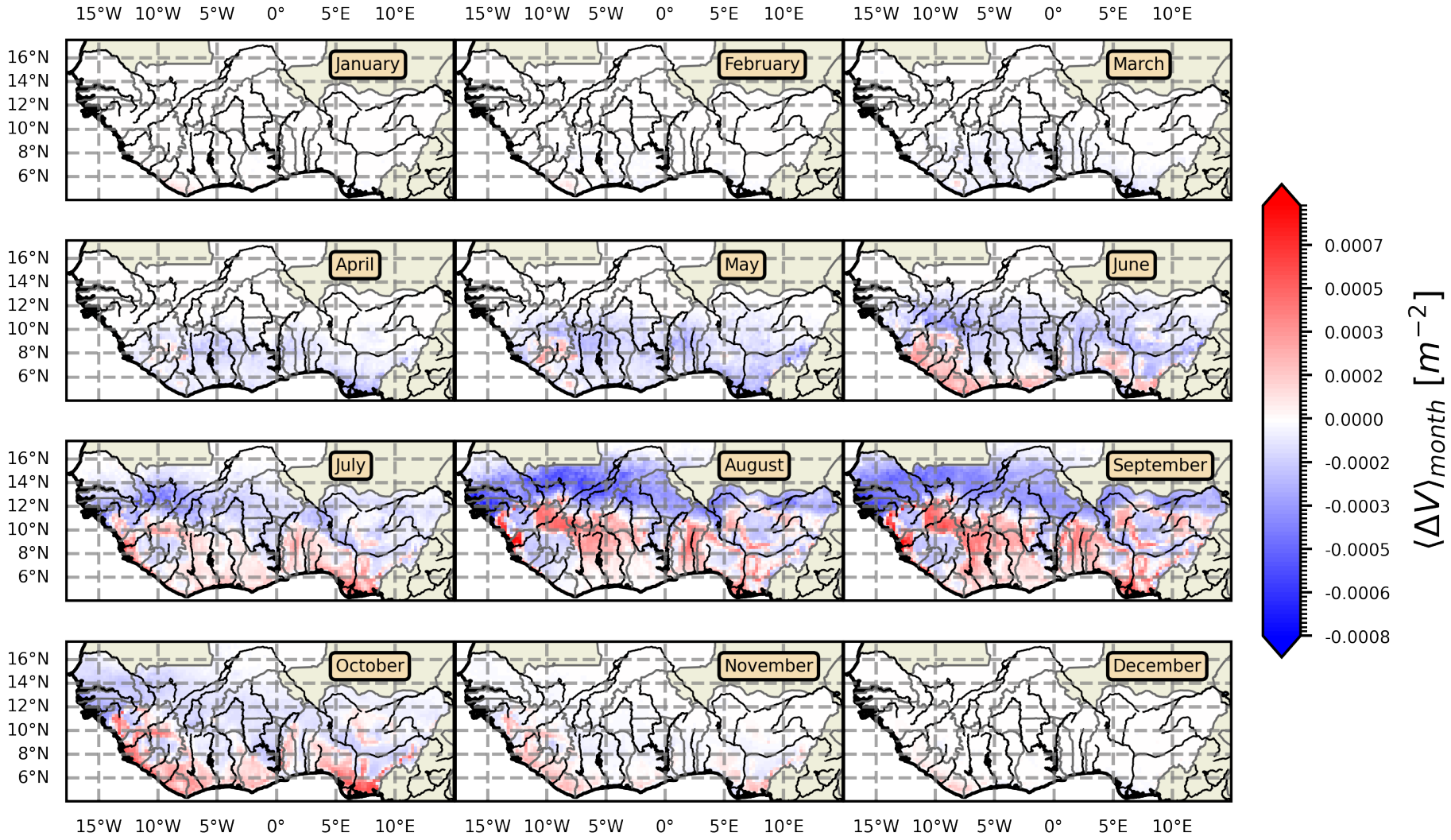

Figure 4.7: Month-climatological mean of the difference between *control* and *rm* experiments.

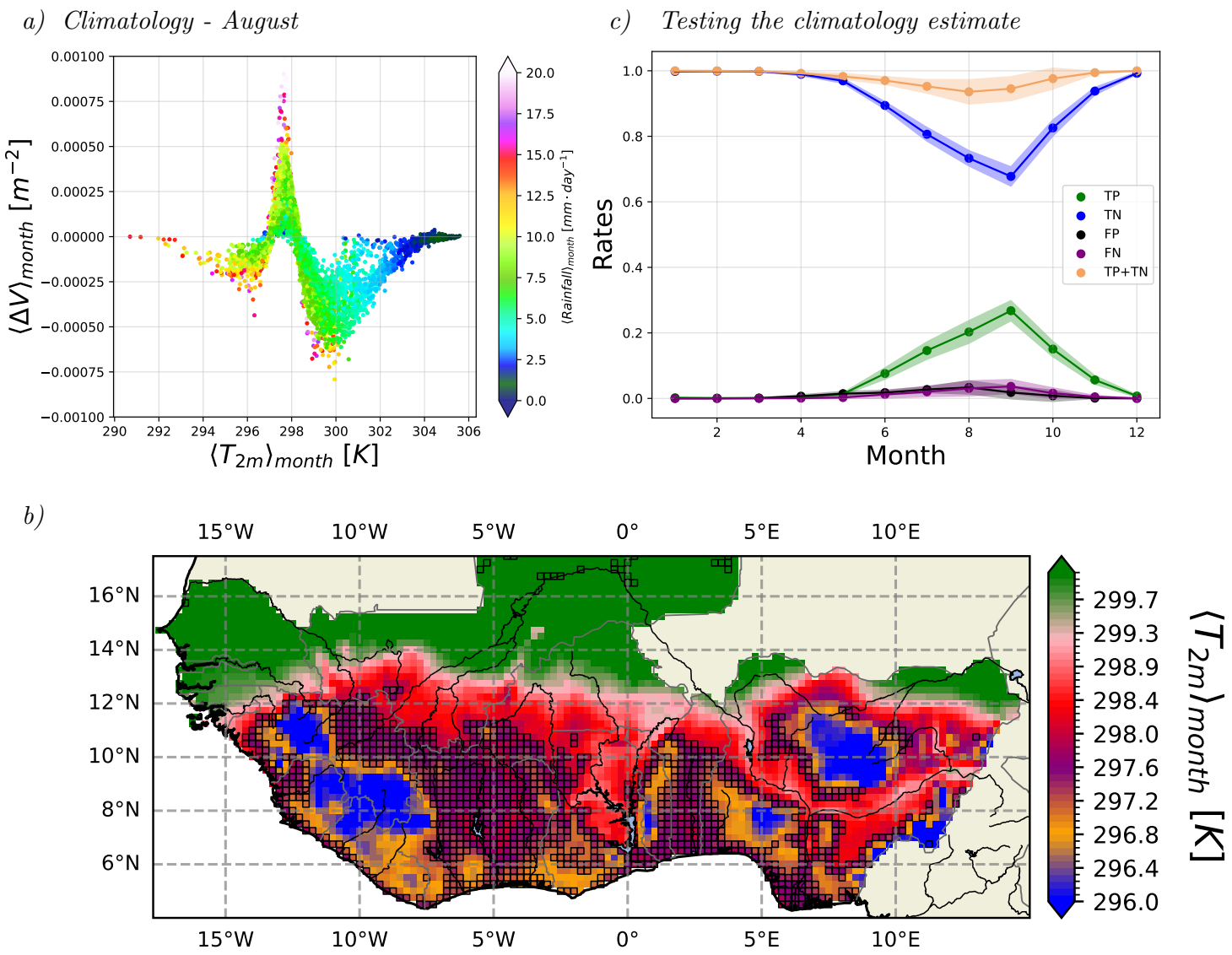

Figure 4.8: *a*) Month-climatological mean of the difference in vector density (*control−rm)* for August *b*) Spatial spread of the regions where $\Delta V > 0$, marked with empty black boxes over a temperature map *c*) True positive (TP), true negative (TN), their sum (TP+TN), false positive (FP) and false negative (FN) rates as a function of the month of the year.

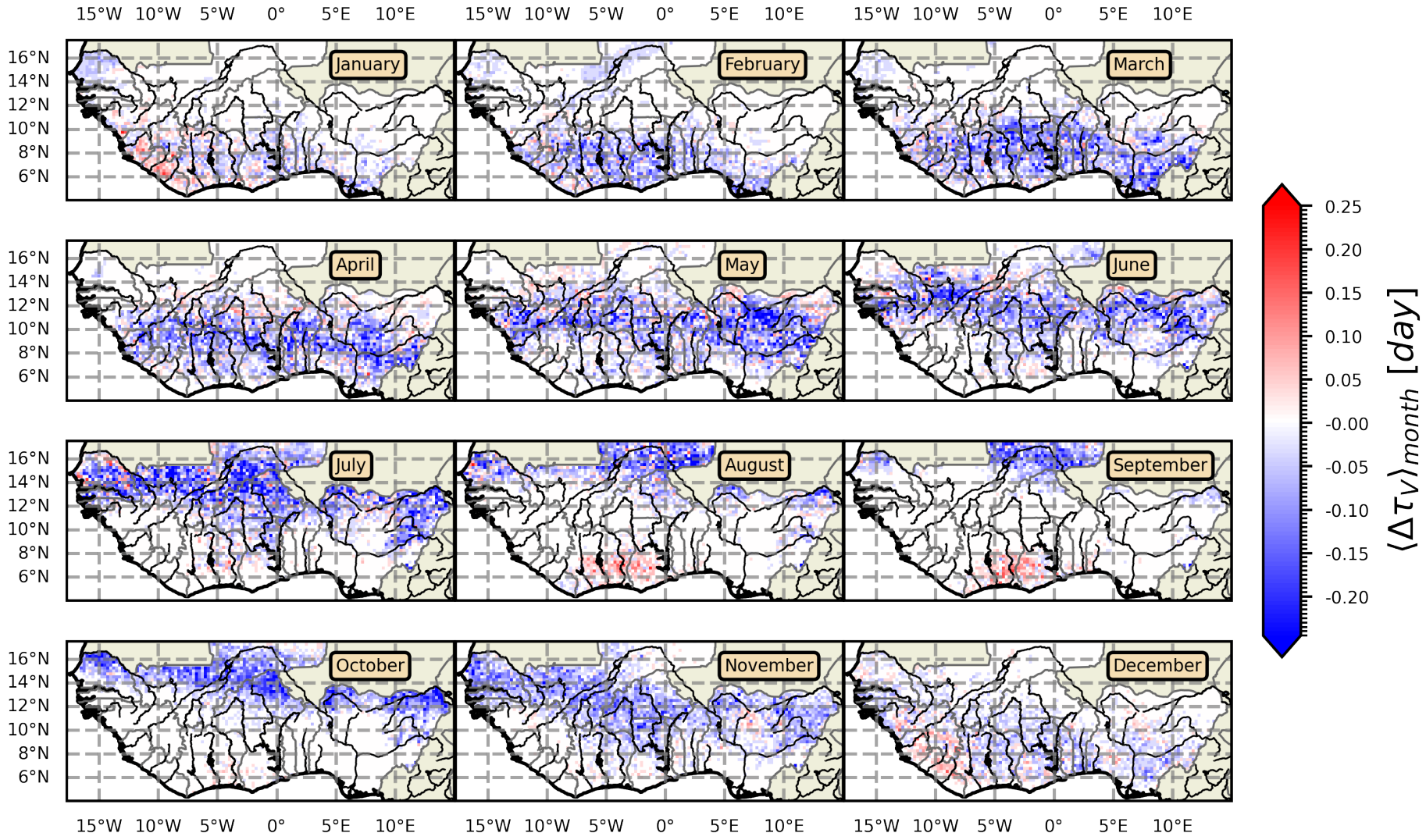

Figure 4.9: Month-climatological mean of the season length difference between *control* and *rm* experiments.

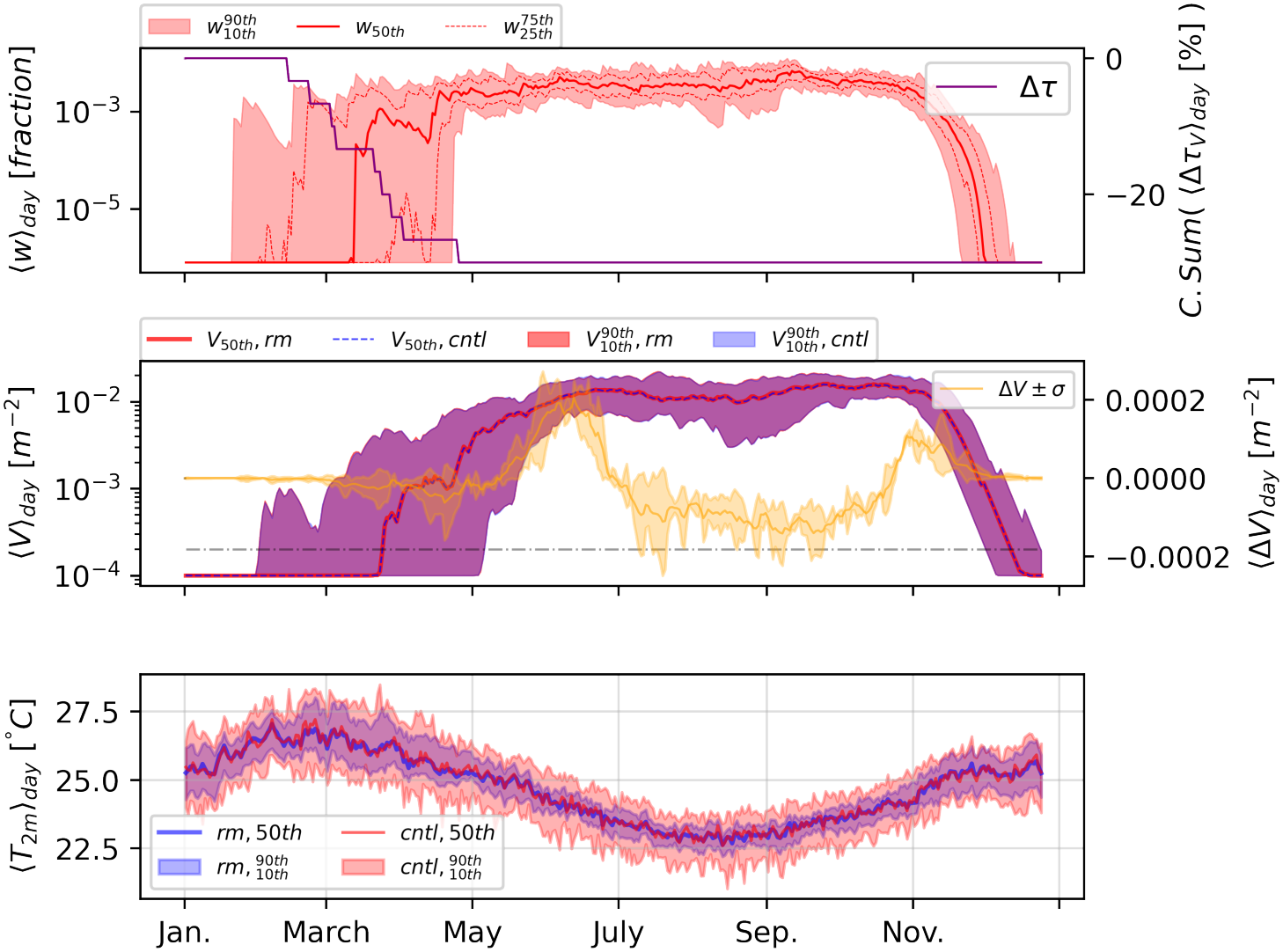

Figure 4.10: Top. Day-climatological median of the fractional coverage of potential breeding sites, $\langle w_{50th} \rangle_{day}$ wrapped by its $10th$ and $90th$ percentiles and the day-climatological cumulative sum of the difference in season length expressed as a percentage, $\langle \Delta\tau_V[\%] \rangle_{day}$. Middle. Day-climatological median of absolute vector densities for *cntl* and *rm* experiments with the $10th$ and $90th$ percentiles as envelope and the day-climatological mean difference $\langle \Delta V \rangle_{day}$. Bottom. Two-metre air temperature time series of the day-climatological median for the *cnlt* and *rm* experiments.

4.A Appendix: Relating spectral densities

It is straight forward to prove (4.4). We express the output's spectral density in terms of its auto-covariance function, $\gamma_{yy}(\tau)$ [93],

$$\Gamma_{yy}(w) = \sum_{\tau=-\infty}^{\infty} \gamma_{yy}(\tau) e^{-2\pi i \tau \omega} \ . \tag{4.10}$$

The auto-covariance function of the output can in turn be expressed in terms of that of the input

$$\gamma_{yy}(\tau) = \texttt{Cov}\left(Y(t), Y(t+\tau)\right) = \tag{4.11}$$

$$= \texttt{Cov}\left(\sum_{k=-K}^{K} a_k X(t+k), \sum_{l=-K}^{K} a_k X(t+\tau-l)\right) = \tag{4.12}$$

$$= \sum_{k=-K}^{K} \sum_{l=-K}^{K} a_k a_l \cdot \texttt{Cov}\left(X(t+k), X(t+\tau-l)\right) = \tag{4.13}$$

$$= \sum_{k=-K}^{K} \sum_{l=-K}^{K} a_k a_l \cdot \gamma_{xx}(\tau+k-l) \ . \tag{4.14}$$

Substituting (4.14) into (4.10) we obtain the desired result

$$\Gamma_{yy}(w) = \sum_{\tau=-\infty}^{\infty} \left(\sum_{k=-K}^{K} \sum_{l=-K}^{K} a_k a_l \gamma_{xx}(\tau+k-l) \right) e^{-2\pi i \tau \omega} = \tag{4.15}$$

$$= \sum_{k=-K}^{K} a_k e^{2\pi i k w} \sum_{l=-K}^{K} a_l e^{-2\pi i l w} \sum_{\tau=-\infty}^{\infty} \gamma_{xx}(\tau+k-l) e^{2\pi i (\tau+k-l) w} = \tag{4.16}$$

$$= |c(\omega)|^2 \Gamma_{xx}(\omega) \qquad q.e.d. \tag{4.17}$$

5 Conclusion

This thesis has explored the implications of some atmospheric features on three distinct biological systems, ranging from a purely conceptual to an applied and empirically validated approach. Overall, the work presented here provides insights on the complex role of environmental conditions on species' diversity, abundance and distribution.

The role of stochastic dispersal on microbial diversity was investigated in Chapter 2. In Chapter 3 we switched focus to a particularly interesting mosquito species, *Aedes albopictus*, and the role that climate change and temperature extremes play in its life cycle and geographical distribution in Italy. Lastly, in Chapter 4, we investigated how air temperature variability affects *Anopheles gambiae s.s.* populations in a region of sub-Saharan Africa.

Collectively, the thesis contributes to a deeper understanding of how spatial structure, environmental variability and climatic factors influence the behaviour and distribution of relevant biological populations. The mathematical and simulation approaches developed and employed throughout this work offer valuable frameworks for further exploration of these biological systems.

Bibliography

6

1. Haeckel E. Generelle Morphologie der Organismen: Allgemeine Grundzüge der organischen Formen-Wissenschaft, mechanisch begründet durch die von Charles Darwin reformierte Descendenz-Theorie. Band 1: Allgemeine Anatomie. Band 2: Allgemeine Entwicklungsgeschichte. de Gruyter, 1866 (cit. on p. 1)
2. Egerton FN. A history of the ecological sciences: early Greek origins. Bulletin of the Ecological Society of America 2001; 82. Publisher: JSTOR:93–7. Available from: https://www.jstor.org/stable/20168519 (cit. on p. 1)
3. Tansley AG. The Use and Abuse of Vegetational Concepts and Terms. en. 1935; 16:284–307. Available from: https://www.jstor.org/stable/1930070 (cit. on p. 1)
4. The Ecological Society of America. What is Ecology? Available from: https://www.esa.org/about/what-does-ecology-have-to-do-with-me/ [Accessed on: 2024 Jun 24] (cit. on p. 2)
5. Rezza G. Aedes albopictus and the reemergence of Dengue. en. BMC Public Health 2012 Dec; 12:72. DOI: 10.1186/1471-2458-12-72. Available from: http://bmcpublichealth.biomedcentral.com/articles/10.1186/1471-2458-12-72 [Accessed on: 2023 Dec 3] (cit. on pp. 2, 34)
6. McKenzie BA, Wilson AE, and Zohdy S. Aedes albopictus is a competent vector of Zika virus: A meta-analysis. en. PLOS ONE 2019 May; 14. Ed. by Moreira LA:e0216794. DOI: 10.1371/journal.pone.0216794. Available from: https://dx.plos.org/10.1371/journal.pone.0216794 [Accessed on: 2024 Mar 20] (cit. on pp. 2, 34)
7. Lounibos LP and Kramer LD. Invasiveness of *Aedes aegypti* and *Aedes albopictus* and Vectorial Capacity for Chikungunya Virus. en. Journal of Infectious Diseases 2016 Dec; 214:S453–S458. DOI: 10.1093/infdis/

jiw285. Available from: https://academic.oup.com/jid/article-lookup/doi/10.1093/infdis/jiw285 [Accessed on: 2023 Dec 3] (cit. on pp. 2, 34)

8. Coetzee M. Distribution of the African malaria vectors of the *Anopheles gambiae* complex. en. The American Journal of Tropical Medicine and Hygiene 2004 Feb; 70:103–4. DOI: 10.4269/ajtmh.2004.70.103. Available from: https://ajtmh.org/doi/10.4269/ajtmh.2004.70.103 [Accessed on: 2024 Jul 8] (cit. on p. 2)

9. Whitman WB, Coleman DC, and Wiebe WJ. Prokaryotes: The unseen majority. en. Proceedings of the National Academy of Sciences 1998 Jun; 95:6578–83. DOI: 10.1073/pnas.95.12.6578. Available from: https://pnas.org/doi/full/10.1073/pnas.95.12.6578 [Accessed on: 2024 Jul 2] (cit. on p. 3)

10. Breitbart M and Rohwer F. Here a virus, there a virus, everywhere the same virus? en. Trends in Microbiology 2005 Jun; 13:278–84. DOI: 10.1016/j.tim.2005.04.003. Available from: https://linkinghub.elsevier.com/retrieve/pii/S0966842X05001083 [Accessed on: 2024 Jul 2] (cit. on p. 3)

11. Suttle CA. Marine viruses — major players in the global ecosystem. en. Nature Reviews Microbiology 2007 Oct; 5:801–12. DOI: 10.1038/nrmicro1750. Available from: https://www.nature.com/articles/nrmicro1750 [Accessed on: 2024 Jul 2] (cit. on p. 3)

12. Breitbart M, Bonnain C, Malki K, and Sawaya NA. Phage puppet masters of the marine microbial realm. en. Nature Microbiology 2018 Jun; 3:754–66. DOI: 10.1038/s41564-018-0166-y. Available from: https://www.nature.com/articles/s41564-018-0166-y [Accessed on: 2024 Jul 2] (cit. on p. 3)

13. Pomeroy L, Williams P leB., Azam F, and Hobbie J. The Microbial Loop. en. Oceanography 2007 Jun; 20:28–33. DOI: 10.5670/oceanog.2007.45. Available from: https://tos.org/oceanography/article/the-microbial-loop [Accessed on: 2024 Jul 3] (cit. on p. 3)

14. Weinbauer MG and Rassoulzadegan F. Are viruses driving microbial diversification and diversity? en. Environmental Microbiology 2004 Jan; 6:1–11. DOI: 10.1046/j.1462-2920.2003.00539.x. Available from: https://sfamjournals.onlinelibrary.wiley.com/doi/10.1046/j.1462-2920.2003.00539.x [Accessed on: 2024 Jul 3] (cit. on p. 3)

15. Hewson I, Winget DM, Williamson KE, Fuhrman JA, and Wommack KE. Viral and bacterial assemblage covariance in oligotrophic waters of the West Florida Shelf (Gulf of Mexico). en. Journal of the Marine Biological Association of the United Kingdom 2006 Jun; 86:591–603. DOI: 10.1017/S0025315406013506. Available from: https://www.cambridge.org/core/product/identifier/S0025315406013506/type/journal_article [Accessed on: 2024 Jul 3] (cit. on p. 3)

16. Thingstad TF. Elements of a theory for the mechanisms controlling abundance, diversity, and biogeochemical role of lytic bacterial viruses in aquatic systems. en. Limnology and Oceanography 2000 Sep; 45:1320–8. DOI: 10.4319/lo.2000.45.6.1320. Available from: https://aslopubs.onlinelibrary.wiley.com/doi/10.4319/lo.2000.45.6.1320 [Accessed on: 2024 Jul 3] (cit. on p. 3)

17. Haerter JO, Mitarai N, and Sneppen K. Phage and bacteria support mutual diversity in a narrowing staircase of coexistence. en. The ISME Journal 2014 Nov; 8:2317–26. DOI: 10.1038/ismej.2014.80. Available from: https://academic.oup.com/ismej/article/8/11/2317-2326/7582436 [Accessed on: 2024 Jul 3] (cit. on p. 3)

18. Howard-Varona C, Lindback MM, Bastien GE, *et al.* Phage-specific metabolic reprogramming of virocells. en. The ISME Journal 2020 Apr; 14:881–95. DOI: 10.1038/s41396-019-0580-z. Available from: https://academic.oup.com/ismej/article/14/4/881/7474831 [Accessed on: 2024 Jul 3] (cit. on p. 3)

19. Wommack KE and Colwell RR. Virioplankton: Viruses in Aquatic Ecosystems. en. Microbiology and Molecular Biology Reviews 2000 Mar; 64:69–114. DOI: 10.1128/MMBR.64.1.69-114.2000. Available from: https://journals.asm.org/doi/10.1128/MMBR.64.1.69-114.2000 [Accessed on: 2024 Jul 3] (cit. on p. 3)

20. Zimmerman AE, Howard-Varona C, Needham DM, John SG, Worden AZ, Sullivan MB, Waldbauer JR, and Coleman ML. Metabolic and biogeochemical consequences of viral infection in aquatic ecosystems. en. Nature Reviews Microbiology 2020 Jan; 18:21–34. DOI: 10.1038/s41579-019-0270-x. Available from: https://www.nature.com/articles/s41579-019-0270-x [Accessed on: 2024 Jul 3] (cit. on p. 3)

21. Rosenwasser S, Ziv C, Creveld SGV, and Vardi A. Virocell Metabolism: Metabolic Innovations During Host–Virus Interactions in the Ocean. en.

Trends in Microbiology 2016 Oct; 24:821–32. DOI: 10.1016/j.tim.2016.06.006. Available from: https://linkinghub.elsevier.com/retrieve/pii/S0966842X16300695 [Accessed on: 2024 Jul 3] (cit. on p. 3)

22. Fuhrman JA. Marine viruses and their biogeochemical and ecological effects. en. Nature 1999 Jun; 399:541–8. DOI: 10.1038/21119. Available from: https://www.nature.com/articles/21119 [Accessed on: 2024 Jul 3] (cit. on p. 3)

23. Wilhelm SW and Suttle CA. Viruses and Nutrient Cycles in the Sea. en. BioScience 1999; 49:781–8. DOI: 10.2307/1313569 (cit. on p. 3)

24. Middelboe M and Jørgensen NO. Viral lysis of bacteria: an important source of dissolved amino acids and cell wall compounds. en. Journal of the Marine Biological Association of the United Kingdom 2006 Jun; 86:605–12. DOI: 10.1017/S0025315406013518. Available from: https://www.cambridge.org/core/product/identifier/S0025315406013518/type/journal_article [Accessed on: 2024 Jul 3] (cit. on p. 3)

25. Lønborg C, Middelboe M, and Brussaard CPD. Viral lysis of Micromonas pusilla: impacts on dissolved organic matter production and composition. en. Biogeochemistry 2013 Dec; 116:231–40. DOI: 10.1007/s10533-013-9853-1. Available from: http://link.springer.com/10.1007/s10533-013-9853-1 [Accessed on: 2024 Jul 3] (cit. on p. 3)

26. Shelford E, Middelboe M, Møller E, and Suttle C. Virus-driven nitrogen cycling enhances phytoplankton growth. en. Aquatic Microbial Ecology 2012 Mar; 66:41–6. DOI: 10.3354/ame01553. Available from: http://www.int-res.com/abstracts/ame/v66/n1/p41-46/ [Accessed on: 2024 Jul 3] (cit. on p. 3)

27. Poorvin L, Rinta-Kanto JM, Hutchins DA, and Wilhelm SW. Viral release of iron and its bioavailability to marine plankton. en. Limnology and Oceanography 2004 Sep; 49:1734–41. DOI: 10.4319/lo.2004.49.5.1734. Available from: https://aslopubs.onlinelibrary.wiley.com/doi/10.4319/lo.2004.49.5.1734 [Accessed on: 2024 Jul 3] (cit. on p. 3)

28. Gobler CJ, Hutchins DA, Fisher NS, Cosper EM, and Saňudo-Wilhelmy SA. Release and bioavailability of C, N, P Se, and Fe following viral lysis of a marine chrysophyte. en. Limnology and Oceanography 1997 Nov; 42:1492–504. DOI: 10.4319/lo.1997.42.7.1492. Available from:

https://aslopubs.onlinelibrary.wiley.com/doi/10.4319/lo.1997.42.7.1492 [Accessed on: 2024 Jul 3] (cit. on p. 3)

29. Moebus K and Nattkemper H. Bacteriophage sensitivity patterns among bacteria isolated from marine waters. en. Helgoländer Meeresuntersuchungen 1981 Sep; 34:375–85. DOI: 10.1007/BF02074130. Available from: https://link.springer.com/10.1007/BF02074130 [Accessed on: 2024 Jul 3] (cit. on p. 3)

30. Flores CO, Valverde S, and Weitz JS. Multi-scale structure and geographic drivers of cross-infection within marine bacteria and phages. en. The ISME Journal 2013 Mar; 7:520–32. DOI: 10.1038/ismej.2012.135. Available from: https://academic.oup.com/ismej/article/7/3/520/7590132 [Accessed on: 2024 Jul 3] (cit. on p. 3)

31. Kauffman KM, Chang WK, Brown JM, Hussain FA, Yang J, Polz MF, and Kelly L. Resolving the structure of phage–bacteria interactions in the context of natural diversity. en. Nature Communications 2022 Jan; 13:372. DOI: 10.1038/s41467-021-27583-z. Available from: https://www.nature.com/articles/s41467-021-27583-z [Accessed on: 2024 Jul 3] (cit. on p. 3)

32. Hardin G. The Competitive Exclusion Principle. en. 1960; 131:1292–7. DOI: 10.1126/science.131.3409.1292 (cit. on p. 3)

33. Tilman D. Competition and Biodiversity in Spatially Structured Habitats. en. Ecology 1994 Jan; 75:2–16. DOI: 10.2307/1939377. Available from: https://esajournals.onlinelibrary.wiley.com/doi/10.2307/1939377 [Accessed on: 2024 Jul 3] (cit. on p. 3)

34. Holyoak M and Lawler SP. Persistence of an Extinction-Prone Predator-Prey Interaction Through Metapopulation Dynamics. en. Ecology 1996 Sep; 77:1867–79. DOI: 10.2307/2265790. Available from: https://esajournals.onlinelibrary.wiley.com/doi/10.2307/2265790 [Accessed on: 2024 Jul 3] (cit. on p. 3)

35. Bonsall MB, French DR, and Hassell MP. Metapopulation structures affect persistence of predator–prey interactions. en. Journal of Animal Ecology 2002 Nov; 71:1075–84. DOI: 10.1046/j.1365-2656.2002.00670.x. Available from: https://besjournals.onlinelibrary.wiley.com/doi/10.1046/j.1365-2656.2002.00670.x [Accessed on: 2024 Jul 3] (cit. on p. 3)

36. Kellogg CA and Griffin DW. Aerobiology and the global transport of desert dust. en. Trends in Ecology & Evolution 2006 Nov; 21:638–44. DOI: 10.1016/j.tree.2006.07.004. Available from: https://linkinghub.elsevier.com/retrieve/pii/S0169534706002138 [Accessed on: 2024 Jul 3] (cit. on p. 4)

37. Griffin DW, Kellogg CA, Garrison VH, Lisle JT, Borden TC, and Shinn EA. Atmospheric microbiology in the northern Caribbean during African dust events. en. Aerobiologia 2003 Sep; 19:143–57. DOI: 10.1023/B:AERO.0000006530.32845.8d. Available from: http://link.springer.com/10.1023/B:AERO.0000006530.32845.8d [Accessed on: 2024 Jul 3] (cit. on p. 4)

38. Burrows SM, Butler T, Jöckel P, Tost H, Kerkweg A, Pöschl U, and Lawrence MG. Bacteria in the global atmosphere – Part 2: Modeling of emissions and transport between different ecosystems. en. Atmospheric Chemistry and Physics 2009 Dec; 9:9281–97. DOI: 10.5194/acp-9-9281-2009. Available from: https://acp.copernicus.org/articles/9/9281/2009/ [Accessed on: 2024 Jul 3] (cit. on p. 4)

39. Šantl-Temkiv T, Amato P, Casamayor EO, Lee PKH, and Pointing SB. Microbial ecology of the atmosphere. en. FEMS Microbiology Reviews 2022 Jul; 46:fuac009. DOI: 10.1093/femsre/fuac009. Available from: https://academic.oup.com/femsre/article/doi/10.1093/femsre/fuac009/6524182 [Accessed on: 2024 Jul 3] (cit. on p. 4)

40. Michaud JM, Thompson LR, Kaul D, *et al.* Taxon-specific aerosolization of bacteria and viruses in an experimental ocean-atmosphere mesocosm. en. Nature Communications 2018 May; 9:2017. DOI: 10.1038/s41467-018-04409-z. Available from: https://www.nature.com/articles/s41467-018-04409-z [Accessed on: 2024 Jul 3] (cit. on p. 4)

41. Rastelli E, Corinaldesi C, Dell'Anno A, Lo Martire M, Greco S, Cristina Facchini M, Rinaldi M, O'Dowd C, Ceburnis D, and Danovaro R. Transfer of labile organic matter and microbes from the ocean surface to the marine aerosol: an experimental approach. en. Scientific Reports 2017 Sep; 7:11475. DOI: 10.1038/s41598-017-10563-z. Available from: https://www.nature.com/articles/s41598-017-10563-z [Accessed on: 2024 Jul 3] (cit. on p. 4)

42. Reche I, D'Orta G, Mladenov N, Winget DM, and Suttle CA. Deposition rates of viruses and bacteria above the atmospheric boundary layer. en.

The ISME Journal 2018 Apr; 12:1154–62. DOI: 10.1038/s41396-017-0042-4. Available from: https://academic.oup.com/ismej/article/12/4/1154-1162/7475436 [Accessed on: 2024 Jul 3] (cit. on p. 4)

43. Woo C and Yamamoto N. Falling bacterial communities from the atmosphere. en. Environmental Microbiome 2020 Dec; 15:22. DOI: 10.1186/s40793-020-00369-4. Available from: https://environmentalmicrobiome.biomedcentral.com/articles/10.1186/s40793-020-00369-4 [Accessed on: 2024 Jul 3] (cit. on p. 4)

44. Moore RA, Hanlon R, Powers C, Schmale DG, and Christner BC. Scavenging of Sub-Micron to Micron-Sized Microbial Aerosols during Simulated Rainfall. en. Atmosphere 2020 Jan; 11:80. DOI: 10.3390/atmos11010080. Available from: https://www.mdpi.com/2073-4433/11/1/80 [Accessed on: 2024 Jul 3] (cit. on p. 4)

45. Després VR, Huffman JA, Burrows SM, *et al.* Primary biological aerosol particles in the atmosphere: a review. en. Tellus B: Chemical and Physical Meteorology 2012 Jan; 64:15598. DOI: 10.3402/tellusb.v64i0.15598. Available from: https://b.tellusjournals.se/article/10.3402/tellusb.v64i0.15598/ [Accessed on: 2024 Jul 3] (cit. on p. 4)

46. Levin BR, Stewart FM, and Chao L. Resource-Limited Growth, Competition, and Predation: A Model and Experimental Studies with Bacteria and Bacteriophage. en. The American Naturalist 1977 Jan; 111:3–24. DOI: 10.1086/283134. Available from: https://www.journals.uchicago.edu/doi/10.1086/283134 [Accessed on: 2024 Jul 3] (cit. on p. 5)

47. McKane AJ and Newman TJ. Predator-Prey Cycles from Resonant Amplification of Demographic Stochasticity. en. Physical Review Letters 2005 Jun; 94:218102. DOI: 10.1103/PhysRevLett.94.218102. Available from: https://link.aps.org/doi/10.1103/PhysRevLett.94.218102 [Accessed on: 2024 Jul 3] (cit. on p. 6)

48. Clements AN and Clements AN. The biology of mosquitoes. en. 1st ed. Vol. 1. London ; New York: Chapman & Hall, 1992 (cit. on p. 33)

49. Koenraadt CJM and Takken W. Cannibalism and predation among larvae of the *Anopheles gambiae* complex. en. Medical and Veterinary Entomology 2003 Mar; 17:61–6. DOI: 10.1046/j.1365-2915.2003.00409.x. Available from: https://resjournals.onlinelibrary.wiley.com/doi/10.1046/j.1365-2915.2003.00409.x [Accessed on: 2024 Mar 26] (cit. on p. 33)

50. Porretta D, Mastrantonio V, Crasta G, Bellini R, Comandatore F, Rossi P, Favia G, Bandi C, and Urbanelli S. Intra-instar larval cannibalism in Anopheles gambiae (s.s.) and Anopheles stephensi (Diptera: Culicidae). en. Parasites & Vectors 2016 Dec; 9:566. DOI: 10.1186/s13071-016-1850-5. Available from: http://parasitesandvectors.biomedcentral.com/articles/10.1186/s13071-016-1850-5 [Accessed on: 2024 Mar 26] (cit. on p. 33)

51. Denlinger DL and Armbruster PA. Mosquito Diapause. en. Annual Review of Entomology 2014 Jan; 59:73–93. DOI: 10.1146/annurev-ento-011613-162023. Available from: https://www.annualreviews.org/doi/10.1146/annurev-ento-011613-162023 [Accessed on: 2024 Jul 6] (cit. on p. 33)

52. Metelmann S, Caminade C, Jones AE, Medlock JM, Baylis M, and Morse AP. The UK's suitability for *Aedes albopictus* in current and future climates. en. Journal of The Royal Society Interface 2019 Mar; 16:20180761. DOI: 10.1098/rsif.2018.0761. Available from: https://royalsocietypublishing.org/doi/10.1098/rsif.2018.0761 [Accessed on: 2023 Nov 28] (cit. on pp. 33, 34, 38, 44)

53. Tompkins AM and Ermert V. A regional-scale, high resolution dynamical malaria model that accounts for population density, climate and surface hydrology. en. Malaria Journal 2013 Dec; 12:65. DOI: 10.1186/1475-2875-12-65. Available from: https://malariajournal.biomedcentral.com/articles/10.1186/1475-2875-12-65 [Accessed on: 2023 Nov 30] (cit. on pp. 34, 36, 39, 80)

54. Tran A, L'Ambert G, Lacour G, Benoît R, Demarchi M, Cros M, Cailly P, Aubry-Kientz M, Balenghien T, and Ezanno P. A Rainfall- and Temperature-Driven Abundance Model for Aedes albopictus Populations. en. International Journal of Environmental Research and Public Health 2013 Apr; 10:1698–719. DOI: 10.3390/ijerph10051698. Available from: http://www.mdpi.com/1660-4601/10/5/1698 [Accessed on: 2024 Apr 4] (cit. on p. 34)

55. Bomblies A, Duchemin JB, and Eltahir EA. A mechanistic approach for accurate simulation of village scale malaria transmission. en. Malaria Journal 2009 Dec; 8:223. DOI: 10.1186/1475-2875-8-223. Available from: https://malariajournal.biomedcentral.com/articles/10.1186/1475-2875-8-223 [Accessed on: 2024 Apr 4] (cit. on p. 34)

56. Cox FE. History of the discovery of the malaria parasites and their vectors. en. Parasites & Vectors 2010; 3:5. DOI: 10.1186/1756-3305-3-5. Available from: http://parasitesandvectors.biomedcentral.com/articles/10.1186/1756-3305-3-5 [Accessed on: 2023 Jun 27] (cit. on p. 34)

57. Lounibos LP. Invasions by Insect Vectors of Human Disease. en. Annual Review of Entomology 2002 Jan; 47:233–66. DOI: 10.1146/annurev.ento.47.091201.145206. Available from: https://www.annualreviews.org/doi/10.1146/annurev.ento.47.091201.145206 [Accessed on: 2023 Dec 3] (cit. on p. 34)

58. Kraemer MUG, Sinka ME, Duda KA, Mylne A, Shearer FM, Brady OJ, *et al.* The global compendium of Aedes aegypti and Ae. albopictus occurrence. en. Scientific Data 2015 Jul; 2:150035. DOI: 10.1038/sdata.2015.35. Available from: https://www.nature.com/articles/sdata201535 [Accessed on: 2024 Jan 9] (cit. on p. 34)

59. Reiter P and Sprenger D. The used tire trade: a mechanism for the worldwide dispersal of container breeding mosquitoes. J. Am. Mosq. Control. Assoc 1987; 3:494–501 (cit. on p. 34)

60. European Centre for Disease Prevention and Control and European Food Safety Authority. Mosquito maps. Stockholm, 2023. Available from: https://ecdc.europa.eu/en/disease-vectors/surveillance-and-disease-data/mosquito-maps (cit. on p. 34)

61. Tompkins AM and Thomson MC. Uncertainty in malaria simulations in the highlands of Kenya: Relative contributions of model parameter setting, driving climate and initial condition errors. en. PLOS ONE 2018 Sep; 13. Ed. by Arez AP:e0200638. DOI: 10.1371/journal.pone.0200638. Available from: https://dx.plos.org/10.1371/journal.pone.0200638 [Accessed on: 2023 Nov 30] (cit. on pp. 35, 44, 80)

62. Carrieri M, Albieri A, Angelini P, Baldacchini F, Venturelli C, Zeo SM, and Bellini R. Surveillance of the chikungunya vector Aedes albopictus (Skuse) in Emilia-Romagna (northern Italy): organizational and technical aspects of a large scale monitoring system. en. Journal of Vector Ecology 2011 Jun; 36:108–16. DOI: 10.1111/j.1948-7134.2011.00147.x. Available from: http://doi.wiley.com/10.1111/j.1948-7134.2011.00147.x [Accessed on: 2024 Feb 26] (cit. on p. 35)

63. Carrieri M, Albieri A, Urbanelli S, Angelini P, Venturelli C, Matrangolo C, and Bellini R. Quality control and data validation procedure in large-scale quantitative monitoring of mosquito density: the case of *Aedes albopictus* in Emilia-Romagna region, Italy. en. Pathogens and Global Health 2017 Feb; 111:83–90. DOI: 10.1080/20477724.2017.1292992. Available from: https://www.tandfonline.com/doi/full/10.1080/20477724.2017.1292992 [Accessed on: 2024 Feb 26] (cit. on p. 35)

64. Carrieri M, Albieri A, Gentili L, *et al.* Egg data validation in quantitative monitoring of *Aedes albopictus* in Emilia-Romagna region, Italy. en. Pathogens and Global Health 2021 Feb; 115:125–31. DOI: 10.1080/20477724.2020.1866375. Available from: https://www.tandfonline.com/doi/full/10.1080/20477724.2020.1866375 [Accessed on: 2024 Feb 26] (cit. on p. 35)

65. Kraemer MU, Sinka ME, Duda KA, Mylne AQ, Shearer FM, Barker CM, *et al.* The global distribution of the arbovirus vectors Aedes aegypti and Ae. albopictus. en. eLife 2015 Jun; 4:e08347. DOI: 10.7554/eLife.08347. Available from: https://elifesciences.org/articles/08347 [Accessed on: 2024 Jul 6] (cit. on p. 35)

66. Aedes albopictus (Skuse, 1894) in GBIF Secretariat (2023). GBIF Backbone Taxonomy. Checklist dataset https://doi.org/10.15468/39omei accessed via GBIF.org on 2024-03-04. (Cit. on p. 35)

67. Caminade C, Kovats S, Rocklov J, Tompkins AM, Morse AP, Colón-González FJ, Stenlund H, Martens P, and Lloyd SJ. Impact of climate change on global malaria distribution. en. Proceedings of the National Academy of Sciences 2014 Mar; 111:3286–91. DOI: 10.1073/pnas.1302089111. Available from: https://pnas.org/doi/full/10.1073/pnas.1302089111 [Accessed on: 2023 Jun 26] (cit. on p. 36)

68. Tompkins AM and Di Giuseppe F. Potential Predictability of Malaria in Africa Using ECMWF Monthly and Seasonal Climate Forecasts. en. Journal of Applied Meteorology and Climatology 2015 Mar; 54:521–40. DOI: 10.1175/JAMC-D-14-0156.1. Available from: https://journals.ametsoc.org/view/journals/apme/54/3/jamc-d-14-0156.1.xml [Accessed on: 2023 Jun 26] (cit. on pp. 36, 80)

69. Chemison A, Ramstein G, Tompkins AM, Defrance D, Camus G, Charra M, and Caminade C. Impact of an accelerated melting of Greenland on malaria distribution over Africa. en. Nature Communications 2021

Jun; 12:3971. DOI: 10.1038/s41467-021-24134-4. Available from: https://www.nature.com/articles/s41467-021-24134-4 [Accessed on: 2023 Jun 26] (cit. on p. 36)

70. Cornes RC, Van Der Schrier G, Van Den Besselaar EJM, and Jones PD. An Ensemble Version of the E-OBS Temperature and Precipitation Data Sets. en. Journal of Geophysical Research: Atmospheres 2018 Sep; 123:9391–409. DOI: 10.1029/2017JD028200. Available from: https://agupubs.onlinelibrary.wiley.com/doi/10.1029/2017JD028200 [Accessed on: 2024 Feb 25] (cit. on p. 37)

71. Center for International Earth Science Information Network - CIESIN - Columbia University. Gridded Population of the World, Version 4 (GPWv4): Population Density, Revision 11. Palisades, New York, 2018. Available from: https://doi.org/10.7927/H49C6VHW (cit. on pp. 37, 84)

72. Schulzweida U. CDO User Guide. Version Number: 2.3.0. 2023 Oct. DOI: 10.5281/zenodo.10020800. Available from: https://doi.org/10.5281/zenodo.10020800 (cit. on pp. 37, 84)

73. Delatte H, Gimonneau G, Triboire A, and Fontenille D. Influence of Temperature on Immature Development, Survival, Longevity, Fecundity, and Gonotrophic Cycles of *Aedes albopictus* , Vector of Chikungunya and Dengue in the Indian Ocean. en. Journal of Medical Entomology 2009 Jan; 46:33–41. DOI: 10.1603/033.046.0105. Available from: https://academic.oup.com/jme/article-lookup/doi/10.1603/033.046.0105 [Accessed on: 2024 Feb 1] (cit. on p. 38)

74. Paaijmans KP, Wandago MO, Githeko AK, and Takken W. Unexpected High Losses of Anopheles gambiae Larvae Due to Rainfall. en. PLoS ONE 2007 Nov; 2. Ed. by Carter D:e1146. DOI: 10.1371/journal.pone.0001146. Available from: https://dx.plos.org/10.1371/journal.pone.0001146 [Accessed on: 2024 Jul 6] (cit. on p. 39)

75. White G. Anopheles gambiae complex and disease transmission in Africa. en. Transactions of the Royal Society of Tropical Medicine and Hygiene 1974 Jan; 68:278–98. DOI: 10.1016/0035-9203(74)90035-2. Available from: https://academic.oup.com/trstmh/article-lookup/doi/10.1016/0035-9203(74)90035-2 [Accessed on: 2024 Jul 6] (cit. on p. 39)

76. Paupy C, Delatte H, Bagny L, Corbel V, and Fontenille D. Aedes albopictus, an arbovirus vector: From the darkness to the light. en. Microbes and Infection 2009 Dec; 11:1177–85. DOI: 10.1016/j.micinf.2009.05.005.

Available from: https://linkinghub.elsevier.com/retrieve/pii/S1286457909001051 [Accessed on: 2023 Nov 15] (cit. on p. 39)

77. Asare EO, Tompkins AM, and Bomblies A. A Regional Model for Malaria Vector Developmental Habitats Evaluated Using Explicit, Pond-Resolving Surface Hydrology Simulations. en. PLOS ONE 2016 Mar; 11. Ed. by Pappalardo F:e0150626. DOI: 10.1371/journal.pone.0150626. Available from: https://dx.plos.org/10.1371/journal.pone.0150626 [Accessed on: 2023 Dec 31] (cit. on p. 40)

78. Asare EO, Tompkins AM, Amekudzi LK, and Ermert V. A breeding site model for regional, dynamical malaria simulations evaluated using in situ temporary ponds observations. en. Geospatial Health 2016 Mar; 11. DOI: 10.4081/gh.2016.390. Available from: http://www.geospatialhealth.net/index.php/gh/article/view/390 [Accessed on: 2024 Aug 23] (cit. on p. 40)

79. Detinova TS, Bertram DS, and World Health Organization. Age-grouping methods in Diptera of medical importance, with special reference to some vectors of malaria. World Health Organization, 1962 (cit. on p. 42)

80. Eikenberry SE and Gumel AB. Mathematical modeling of climate change and malaria transmission dynamics: a historical review. en. Journal of Mathematical Biology 2018 Oct; 77:857–933. DOI: 10.1007/s00285-018-1229-7. Available from: http://link.springer.com/10.1007/s00285-018-1229-7 [Accessed on: 2023 Jun 26] (cit. on pp. 42, 79)

81. Lyimo EO, Takken W, and Koella J. Effect of rearing temperature and larval density on larval survival, age at pupation and adult size of Anopheles gambiae. Entomologia experimentalis et applicata 1992; 63. Publisher: Wiley Online Library:265–71 (cit. on p. 43)

82. Bayoh M and Lindsay S. Effect of temperature on the development of the aquatic stages of *Anopheles gambiae* sensu stricto (Diptera: Culicidae). en. Bulletin of Entomological Research 2003 Sep; 93:375–81. DOI: 10.1079/BER2003259. Available from: https://www.cambridge.org/core/product/identifier/S0007485303000440/type/journal_article [Accessed on: 2024 Jul 8] (cit. on p. 43)

83. Lacour G, Vernichon F, Cadilhac N, Boyer S, Lagneau C, and Hance T. When mothers anticipate: Effects of the prediapause stage on embryo development time and of maternal photoperiod on eggs of a temperate and a tropical strains of Aedes albopictus (Diptera: Culicidae). en. Journal

of Insect Physiology 2014 Dec; 71:87–96. DOI: 10.1016/j.jinsphys.2014.10.008. Available from: https://linkinghub.elsevier.com/retrieve/pii/S0022191014002030 [Accessed on: 2024 Aug 26] (cit. on p. 46)

84. World Health Organization, Malaria, fact sheet. 2023 Dec. Available from: https://www.who.int/news-room/fact-sheets/detail/malaria (cit. on p. 79)

85. Sinka ME, Bangs MJ, Manguin S, *et al.* The dominant Anopheles vectors of human malaria in Africa, Europe and the Middle East: occurrence data, distribution maps and bionomic précis. en. Parasites & Vectors 2010 Dec; 3:117. DOI: 10.1186/1756-3305-3-117. Available from: https://parasitesandvectors.biomedcentral.com/articles/10.1186/1756-3305-3-117 [Accessed on: 2024 Jul 18] (cit. on p. 79)

86. White BJ, Collins FH, and Besansky NJ. Evolution of *Anopheles gambiae* in Relation to Humans and Malaria. en. Annual Review of Ecology, Evolution, and Systematics 2011 Dec; 42:111–32. DOI: 10.1146/annurev-ecolsys-102710-145028. Available from: https://www.annualreviews.org/doi/10.1146/annurev-ecolsys-102710-145028 [Accessed on: 2024 Jul 18] (cit. on pp. 79, 86)

87. Calvin K, Dasgupta D, Krinner G, *et al.* IPCC, 2023: Climate Change 2023: Synthesis Report. Contribution of Working Groups I, II and III to the Sixth Assessment Report of the Intergovernmental Panel on Climate Change [Core Writing Team, H. Lee and J. Romero (eds.)]. IPCC, Geneva, Switzerland. en. Tech. rep. Edition: First. Intergovernmental Panel on Climate Change (IPCC), 2023 Jul. DOI: 10.59327/IPCC/AR6-9789291691647. Available from: https://www.ipcc.ch/report/ar6/syr/ [Accessed on: 2023 Dec 8] (cit. on p. 79)

88. Gray LJ, Beer J, Geller M, *et al.* Solar influences on climate. en. Reviews of Geophysics 2010 Oct; 48:RG4001. DOI: 10.1029/2009RG000282. Available from: http://doi.wiley.com/10.1029/2009RG000282 [Accessed on: 2024 Jul 5] (cit. on p. 79)

89. Robock A. Volcanic eruptions and climate. en. Reviews of Geophysics 2000 May; 38:191–219. DOI: 10.1029/1998RG000054. Available from: https://agupubs.onlinelibrary.wiley.com/doi/10.1029/1998RG000054 [Accessed on: 2024 Jul 5] (cit. on p. 79)

90. Wang T, Otterå OH, Gao Y, and Wang H. The response of the North Pacific Decadal Variability to strong tropical volcanic eruptions. Climate Dynamics 2012 Dec; 39:2917–36. DOI: 10.1007/s00382-012-1373-5. Available from: https://doi.org/10.1007/s00382-012-1373-5 (cit. on p. 79)

91. Wang B. Interdecadal Changes in El Niño Onset in the Last Four Decades. English. Journal of Climate 1995 Feb; 8. Place: Boston MA, USA Publisher: American Meteorological Society:267–85. DOI: 10.1175/1520-0442(1995)008<0267:ICIENO>2.0.CO;2. Available from: https://journals.ametsoc.org/view/journals/clim/8/2/1520-0442_1995_008_0267_icieno_2_0_co_2.xml (cit. on p. 79)

92. Li J, Xie SP, Cook ER, Huang G, D'Arrigo R, Liu F, Ma J, and Zheng XT. Interdecadal modulation of El Niño amplitude during the past millennium. en. Nature Climate Change 2011 May; 1:114–8. DOI: 10.1038/nclimate1086. Available from: https://www.nature.com/articles/nclimate1086 [Accessed on: 2024 Jul 11] (cit. on p. 79)

93. Storch HV and Zwiers FW. Statistical Analysis in Climate Research. en. 1st ed. Cambridge University Press, 1984 Feb. DOI: 10.1017/CBO9780511612336. Available from: https://www.cambridge.org/core/product/identifier/9780511612336/type/book [Accessed on: 2024 May 20] (cit. on pp. 82, 96)

94. Hersbach H, Bell B, Berrisford P, *et al.* The ERA5 global reanalysis. en. Quarterly Journal of the Royal Meteorological Society 2020 Jul; 146:1999–2049. DOI: 10.1002/qj.3803. Available from: https://rmets.onlinelibrary.wiley.com/doi/10.1002/qj.3803 [Accessed on: 2024 Jul 19] (cit. on p. 84)

95. Garrett-Jones C, Ferreira Neto JA, and World Health Organization. The prognosis for interruption of malaria transmission through assessment of the mosquito' s vectorial capacity / by C. Garrett-Jones. en. 1964. Available from: https://iris.who.int/handle/10665/65229 (cit. on p. 86)